

# Confinement Effects For Efficient Macrocyclization Reactions With Supported Cationic Molybdenum Imido Alkylidene *N*-Heterocyclic Carbene Complexes

Felix Ziegler<sup>†</sup>, Hamzeh Kraus<sup>||</sup>, Mathis J. Benedikter<sup>†</sup>, Dongren Wang<sup>†</sup>, Johanna R. Bruckner<sup>‡</sup>, Michal Nowakowski<sup>§</sup>, Kilian Weißer<sup>†</sup>, Helena Solodenko<sup>⊖</sup>, Guido Schmitz<sup>⊖</sup>, Matthias Bauer<sup>§</sup>, Niels Hansen<sup>||</sup> and Michael R. Buchmeiser<sup>\*†</sup>

<sup>†</sup>Institute of Polymer Chemistry, University of Stuttgart, Pfaffenwaldring 55, D-70569 Stuttgart, Germany

<sup>||</sup>Institute of Thermodynamics and Thermal Process Engineering, University of Stuttgart, Pfaffenwaldring 9, D-70569 Stuttgart, Germany

<sup>‡</sup>Institute of Physical Chemistry, University of Stuttgart, Pfaffenwaldring 55, D-70569 Stuttgart, Germany

<sup>§</sup>Department of Chemistry and Center for Sustainable Systems Design (CSSD), University of Paderborn, Warburger Str. 100, D-33098 Paderborn, Germany

<sup>⊖</sup>Institute for Materials Science, University of Stuttgart, Heisenbergstraße 3, 70569 Stuttgart, Germany

Email: michael.buchmeiser@ipoc.uni-stuttgart.de

## Table of Contents

<b>1. General</b> .....	<b>3</b>
<i>Equipment and Chemicals</i> .....	3
<b>2. Procedures</b> .....	<b>5</b>
<b>3. Catalyst Syntheses</b> .....	<b>6</b>
<b>4. Synthesis of Substrates for RCM</b> .....	<b>11</b>
<i>General Procedure for the Synthesis of Ester-Based <math>\alpha,\omega</math>-Dienes (GP-1)</i> .....	11
<i>General Procedure for the RCM of <math>\alpha,\omega</math>-Dienes (GP-2)</i> .....	11
<i>Dec-9-en-1-yl undec-10-enoate 1</i> .....	11
<i>tert-Butyldimethyl(nonadeca-1,18-dien-10-yloxy)silane 2</i> .....	12
<i>1,2-Bis(undec-10-enyloxy)benzene 3</i> .....	13
<i>Dodecane-1,12-diyl bis(undec-10-enoate) 4</i> .....	13
<i>(E)-Oxacycloicos-11-en-2-one (E)-5</i> .....	14
<i>(Z)-Oxacycloicos-11-en-2-one (Z)-5</i> .....	14
<i>(E)+(Z)-tert-Butyl(cycloheptadec-9-en-1-yloxy)dimethylsilane 6</i> .....	15
<i>E/Z-1,4-Dioxacyclotetracosine 7</i> .....	16
<i>E/Z-1,7-Dioxacycloheptacos-17-ene-8,27-dione 8</i> .....	16

5.	Synthesis of Ordered Mesoporous Silica (OMS <sub>25Å</sub> ) .....	17
6.	Modification of Mesoporous Silica .....	17
7.	Transmission Electron Micrographs of OMS <sub>25Å</sub> , SBA-15 <sub>50Å</sub> and SBA-15 <sub>62Å</sub> .....	21
8.	Macrocyclization Reactions .....	28
9.	MALDI-TOF Measurements .....	44
10.	Spectra of Relevant Compounds .....	45
11.	Molecular Dynamics Simulations.....	70
12.	EXAFS.....	76
13.	References .....	78

## 1. General

### Equipment and Chemicals

All reactions were performed under the exclusion of air and moisture in a N<sub>2</sub>-filled glove box (MBraun Labmaster) unless noted otherwise. Chemicals were purchased from ABCR, Acros Organics, Alfa Aesar, Sigma Aldrich, Fluka and TCI. Mesoporous silica SBA-15 was purchased from Glantreo: SBA-15 (50 Å, <100 µm particle size, hexagonal pore morphology), SBA-15 (62 Å, <100 µm particle size, hexagonal pore morphology). Poly(ethylene glycol)-*b*-poly(propylene glycol)-*b*-poly(ethylene glycol) (PEG-PPG-PEG, Pluronic® P-123), dodecylethyldimethylammonium bromide (≥ 98%), tetramethyl orthosilicate (98%, TMOS) and 1,2-dichlorobenzene (anhydrous) were purchased from Sigma Aldrich. CH<sub>2</sub>Cl<sub>2</sub>, diethyl ether, *n*-pentane and toluene were dried using an MBraun SPS-800 solvent purification system and stored over 4 Å molecular sieves. Deuterated solvents were stored over activated alumina and 4 Å molecular sieves for a minimum of 24 h prior to use. NMR spectra were recorded on a Bruker Avance III 400 spectrometer. NMR spectra were internally calibrated to solvent signals.<sup>1</sup> Abbreviations for multiplicities: s (singlet), bs (broad singlet), d (doublet), t (triplet), q (quartet), hept (heptet), m (multiplet). GC-MS analyses were performed on an Agilent Technologies 5975C inert MSD device consisting of a triple-axis detector, a 7693 autosampler and a 7890A GC system equipped with an SPB-5 fused silica column (34.13 m×0.25 mm×0.25 µm film thickness). GC data were plotted in Excel (Microsoft). Elemental analyses were measured on a Perkin Elmer 240 device at the Institute of Inorganic Chemistry, University of Stuttgart, Germany. High performance liquid chromatography (HPLC) was performed at the Institute of Organic Chemistry, University of Stuttgart, Germany using a Knauer K-501 pump, Knauer RI-detector K 2400 and a Macherey&Nagel VP250/21 Nucleodur 100-5 column. Argon adsorption analyses were performed at 87 K on a Quantachrome Instruments Autosorb iQ MP automatic volumetric instrument. SBA-15 samples were degassed for 16 h at 110 °C under vacuum prior to the gas adsorption studies. Surface areas were evaluated using the Brunauer-Emmett-Teller (BET) model applied between  $p/p_0$  values of  $9.1 \cdot 10^{-6}$  and 0.9 for microporous/mesoporous SBA-15. Pore size distributions were calculated using the non-local Density Functional Theory (NLDFT) cylindrical adsorption pores for zeolites/silica implemented in the ASiQwin software version 3.01. ICP-OES data were recorded on a Spectro Acros 160 CCD equipped with a Cetec ASX-260 autosampler. Analysis of the samples was carried out with the Software Smart Analyzer Vision

4.02.0834. Samples for small-angle X-ray scattering experiments were carefully pestled, filled into Hilgenberg quartz glass mark-tubes with an outer diameter of 0.9 mm and investigated at 25 °C with the Anton Paar SAXSess mc<sup>2</sup>. Cu K $\alpha$  radiation ( $\lambda$  = 1.5406 Å) was generated by an ID3003 X-ray generator from Seifert (40 kV, 40 mA). For detection of the scattered intensity, the 1D CMOS detector Mythen 1K from Dectris was used and the sample to detector distance was calibrated with a sample of cholesteryl palmitate. The scattering data was background corrected and deconvolved with respect to the line collimated beam profile using the associated software SAXSquant.

SBA-15 samples for TEM analysis were prepared by a lift-out procedure with a focused ion beam (FIB) instrument (FEI FIB Scios Dual beam, equipped with a Ga source). Powder particles of suitable size (approximately 50  $\mu$ m in diameter) were directly attached to a copper TEM lift-out grid. The particles were consecutively thinned to a thickness of less than 100 nm by applying ion currents of 500 pA to 50 pA at 30 kV beam voltage. The resulting TEM lamella was then treated with a low voltage cleaning step at 5 kV and 48 pA to reduce Ga beam damage.

TEM samples of the OMS were prepared by further grinding the powder and adding a few drops of pure ethanol. Then one droplet of the powder-ethanol solution was carefully placed on a standard TEM grid. The ethanol evaporated and therefore left a thin layer of powder particles on the grid. This procedure was chosen, since FIB lift-out resulted in an unfavorable orientation of the particles, where no pores were visible. TEM bright field images were recorded on a Philips CM-200 FEG TEM operated at 200 kV acceleration voltage for all samples.

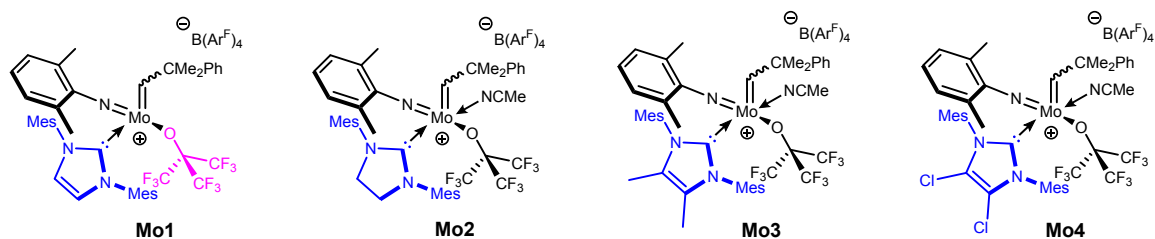
Positive ion MALDI-TOF (matrix-assisted laser desorption ionization time-of-flight) measurements were performed on a Bruker Autoflex III with smart beam. Measurements were carried out in the reflector mode. Samples were prepared from a THF solution by mixing dihydroxybenzoic acid (10 mg/mL), the sample (5 mg/mL) and sodium trifluoromethanesulfonate (17 mg/mL) in a ratio of 20:5:2 (wt).

### **Determination of the metal loading via ICP-OES**

Quantitative analysis of the Mo-loading of each silica sample was determined by ICP-OES.<sup>2</sup> For analysis, the corresponding silica (30-50 mg, Table S1) was mixed with KOH (0.38 g, 6.77 mmol) and KNO<sub>3</sub> (0.65 g, 6.42 mmol). The mixture was heated to 450 °C and the temperature was held for 3 hours. After cooling to room temperature,

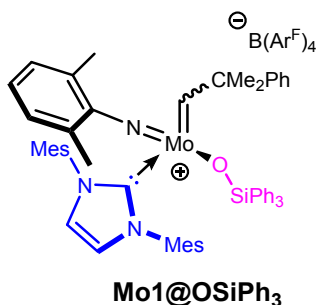
$K_2S_2O_8$  (50.0 mg, 0.18 mmol) was added. The colorless solid was dissolved in a minimum amount of deionized water and 1 M KOH (2 mL) was added. The suspension was filtered, transferred into a 10 mL volumetric flask and filled to the mark with deionized water. The solution was slowly added to a 25 mL volumetric flask with concentrated HCl (5 mL) and filled to the mark with deionized water. This solution was analyzed by ICP-OES for Mo. Mo was measured at  $\lambda = 202.095$  nm; the background was measured at  $\lambda = 203.76$  nm - 203.79 nm and  $\lambda = 203.97$  nm - 204.02 nm, respectively. The limit of detection (LOD) was 0.0001 mg. L<sup>-1</sup>. For calibration, aqueous Mo-standards with Mo concentration of 0.000, 0.100, 0.500, 1.000, 2.500 and 5.000 mg L<sup>-1</sup> were used. A reference, containing the same amount of KOH, KNO<sub>3</sub>, HCl and deionized water was subjected to the same treatment for comparison.

## 2. Procedures



IMes<sup>2</sup>, IMesMe<sub>2</sub><sup>3</sup>, IMesCl<sub>2</sub><sup>4</sup>, IMesH<sub>2</sub><sup>5</sup>, [Mo(N-2,6-Me<sub>2</sub>-C<sub>6</sub>H<sub>3</sub>)(CHCMe<sub>2</sub>Ph)(IMes)(OC(CF<sub>3</sub>)<sub>3</sub>)] [B(Ar<sup>F</sup>)<sub>4</sub>] **Mo1**<sup>6</sup>, [Mo(N-2,6-Me<sub>2</sub>-C<sub>6</sub>H<sub>3</sub>)(CHCMe<sub>2</sub>Ph)(IMesH<sub>2</sub>)(OC(CF<sub>3</sub>)<sub>3</sub>)] [B(Ar<sup>F</sup>)<sub>4</sub>] · MeCN **Mo2**<sup>7</sup>, [Mo(N-2,6-Me<sub>2</sub>-C<sub>6</sub>H<sub>3</sub>)(CHCMe<sub>2</sub>Ph)(IMesMe<sub>2</sub>)(OC(CF<sub>3</sub>)<sub>3</sub>)] [B(Ar<sup>F</sup>)<sub>4</sub>] · MeCN **Mo3**<sup>7</sup>, [Mo(N-2,6-Me<sub>2</sub>-C<sub>6</sub>H<sub>3</sub>)(CHCMe<sub>2</sub>Ph)(IMesCl<sub>2</sub>)(OC(CF<sub>3</sub>)<sub>3</sub>)] [B(Ar<sup>F</sup>)<sub>4</sub>] · MeCN **Mo4**<sup>7</sup>, Mo(N-2,6-Me<sub>2</sub>-C<sub>6</sub>H<sub>3</sub>)(C\*HCMe<sub>3</sub>)(IMes\*)(OTf)<sub>2</sub><sup>8</sup>, (E)+(Z)-cycloheptadec-9-en-1-ol<sup>9</sup> were synthesized according to the literature.

### 3. Catalyst Syntheses



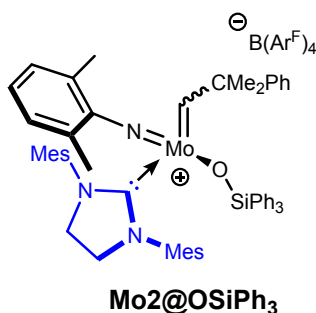
**[Mo(N-2,6-Me<sub>2</sub>-C<sub>6</sub>H<sub>3</sub>)(CHCMe<sub>2</sub>Ph)(IMes)(OSiPh<sub>3</sub>)] [B(Ar<sup>F</sup>)<sub>4</sub>]** **Mo1@OSiPh<sub>3</sub>**: **Mo1** (200 mg, 0.112 mmol) was dissolved in CH<sub>2</sub>Cl<sub>2</sub> (3 mL). HOSiPh<sub>3</sub> (31.9 mg, 0.111 mmol, 1 equiv.) in CH<sub>2</sub>Cl<sub>2</sub> (3 mL) was added dropwise to the solution and the reaction mixture was stirred for three hours at room temperature. Then the solvent was removed *in vacuo* to yield **Mo1@OSiPh<sub>3</sub>** as yellow/orange powder. Since this compound exhibits very broad signals in NMR, the alkylidene and carbene signals in <sup>13</sup>C NMR are not visible.

**Yield:** 200 mg (98%); **<sup>1</sup>H-NMR** (CDCl<sub>3</sub>) δ 12.20 (s, 1H), 7.78 – 7.66 (m, 8H), 7.45 – 7.42 (m, 4H), 7.42 – 7.36 (m, 3H), 7.27 – 7.24 (m, 11H), 7.18 (s, 2H), 6.98 – 6.91 (m, 4H), 6.84 – 6.80 (m, 2H), 6.78 – 6.75 (m, 2H), 6.67 – 6.62 (m, 2H), 6.52 (s, 2H), 2.15 (s, 6H), 1.98 – 1.86 (m, 6H), 1.82 (s, 6H), 1.64 (s, 6H), 1.46 (s, 3H), 0.90 (s, 3H) ppm; **<sup>19</sup>F-NMR** (CDCl<sub>3</sub>) δ 62.42 (s, 24F) ppm; **<sup>13</sup>C-NMR** (CDCl<sub>3</sub>) δ 161.7 (q, <sup>1</sup>J<sub>BC</sub> = 49.8 Hz), 155.1, 147.2, 141.4, 135.2, 134.8, 134.6, 134.3, 133.8, 130.6, 130.3, 129.8, 129.5, 128.9 (qq, <sup>2</sup>J<sub>CF</sub> = 31.4, <sup>3</sup>J<sub>CB</sub> = 2.7 Hz), 128.6, 128.3, 128.1, 127.8, 126.6, 126.0, 125.9, 125.3, 123.2, 120.5, 117.4, 54.9, 30.3, 29.6, 21.0, 19.6, 17.9, 17.7. ppm. **Elemental analysis** calcd. for C<sub>89</sub>H<sub>72</sub>BF<sub>24</sub>MoN<sub>3</sub>OSi: C, 59.71; H, 4.05; N, 2.35. found: C: 59.70; H, 4.115; N, 2.48.

After the addition of one drop of deuterated acetonitrile the alkylidene and carbene signals became visible. Acetonitrile is loosely coordinated and can be removed by applying vacuum.

**<sup>1</sup>H-NMR** (CDCl<sub>3</sub>+CD<sub>3</sub>CN) δ 13.69 (s, 1H), 7.94 – 7.82 (m, 8H), 7.56 – 7.51 (m, 4H), 7.42 – 7.35 (m, 3H), 7.33 – 7.17 (m, 15H), 7.10 (m, 2H), 7.06 – 6.94 (m, 4H), 6.94 – 6.80 (m, 2H), 6.70 – 6.34 (bs, 2H), 2.64 (s, 3H), 2.28 (s, 6H), 1.96 (s, 6H), 1.85 (s, 3H), 1.81 – 1.61 (m, 12H), 0.94 (s, 3H) ppm; **<sup>19</sup>F-NMR** (CDCl<sub>3</sub>) δ 62.38 (s, 24F) ppm; **<sup>13</sup>C-NMR** (CDCl<sub>3</sub>) δ 321.9, 183.9, 160.5 (q, <sup>1</sup>J<sub>BC</sub> = 49.7 Hz), 152.2, 145.8, 139.5, 135.9, 135.2, 134.4, 134.2, 133.9, 128.8, 128.5, 128.1, 127.7 (qq, <sup>2</sup>J<sub>CF</sub> = 31.4, <sup>3</sup>J<sub>CB</sub> = 2.7 Hz),

127.4, 127.3, 126.0, 125.4, 124.5, 124.4, 123.6, 122.0, 119.3, 116.3, 54.8, 28.7, 27.6, 19.5, 19.4, 17.5, 17.4. ppm.



**[Mo(N-2,6-Me-C<sub>6</sub>H<sub>3</sub>)(CHC(PhMe<sub>2</sub>))(SIMes)(OSiPh<sub>3</sub>)] [B(ArF)<sub>4</sub>]** **Mo2@OSiPh<sub>3</sub>**: **Mo2** (200 mg, 0.112 mmol) was dissolved in CH<sub>2</sub>Cl<sub>2</sub> (3 mL). HOSiPh<sub>3</sub> (31.9 mg, 0.111 mmol, 1 equiv.) in CH<sub>2</sub>Cl<sub>2</sub> (3 mL) was added dropwise to the solution and the reaction mixture was stirred for three hours at room temperature. Then the solvent was removed *in vacuo* to yield **Mo2@OSiPh<sub>3</sub>** as yellow/orange powder. Since this compound exhibits very broad signals in NMR, the alkylidene and carbene signals in <sup>13</sup>C NMR are not visible.

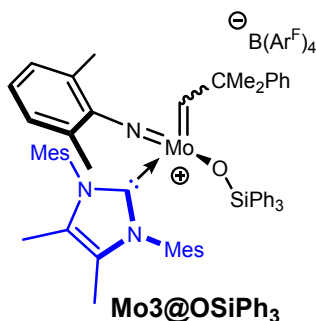
**<sup>1</sup>H-NMR** (CDCl<sub>3</sub>) δ 13.12 (bs, 1H), 7.73 – 7.67 (m, 8H), 7.53 – 7.49 (m, 4H), 7.44 – 7.38 (m, 3H), 7.36 – 7.31 (m, 7H), 7.30 – 7.24 (m, 4H), 7.15 – 7.07 (m, 3H), 7.04 – 6.96 (m, 2H), 6.94 – 6.87 (m, 2H), 6.87 – 6.77 (m, 4H), 6.05 (bs, 2H), 3.94 (s, 4H), 2.22 – 2.12 (m, 15H), 1.98 (bs, 6H), 1.69 (s, 3H), 1.02 (bs, 3H), 0.90 (s, 3H) ppm; **<sup>19</sup>F-NMR** (CDCl<sub>3</sub>) δ 62.40 (s, 24F) ppm; **<sup>13</sup>C-NMR** (CDCl<sub>3</sub>) δ 160.5 (q, <sup>1</sup>J<sub>BC</sub> = 49.8 Hz), 152.6, 145.7, 138.8, 135.1, 134.7, 134.3, 134.1, 133.6, 132.9, 129.3, 129.2, 128.8, 128.7, 127.6 (qq, <sup>2</sup>J<sub>CF</sub> = 31.4, <sup>3</sup>J<sub>CB</sub> = 2.7 Hz), 127.4, 127.2, 126.7, 126.6, 125.4, 124.7, 124.3, 122.0, 119.3, 116.2, 53.8, 50.5, 28.6, 27.8, 19.6, 19.2, 17.5, 17.2, 12.9 ppm.

**Elemental analysis** calcd. for C<sub>89</sub>H<sub>72</sub>BF<sub>24</sub>MoN<sub>3</sub>OSi: C, 59.64; H, 4.16; N, 2.34. found: C: 59.29; H, 4.252; N, 2.52.

After the addition of one drop of deuterated acetonitrile the alkylidene and carbene carbon signals became visible. Acetonitrile is loosely coordinated and can be removed by applying vacuum.

**<sup>1</sup>H-NMR** (CDCl<sub>3</sub>) δ 13.54 (s, 1H), 7.73 – 7.67 (m, 8H), 7.53 – 7.49 (m, 4H), 7.42 – 7.36 (m, 3H), 7.37 – 7.32 (m, 7H), 7.06 – 6.97 (m, 3H), 6.92 – 6.88 (m, 3H), 6.88 – 6.77 (m, 3H), 3.91 (s, 4H), 2.72 (s, 3H), 2.27 – 2.13 (m, 12H), 2.07 – 1.86 (m, 6H), 1.80 (s, 3H), 1.62 (bs, 3H), 0.86 (s, 3H) ppm; **<sup>19</sup>F-NMR** (CDCl<sub>3</sub>) δ 62.43 (s, 24F) ppm; **<sup>13</sup>C-NMR** (CDCl<sub>3</sub>) δ 322.4, 207.8, 160.3 (q, <sup>1</sup>J<sub>BC</sub> = 49.8 Hz), 151.9, 145.5, 138.4, 135.9, 134.8,

134.3, 134.0, 133.4, 133.0, 129.1, 129.0, 128.4, 127.5 (qq,  $^2J_{CF} = 31.4$ ,  $^3J_{CB} = 2.7$  Hz), 127.3, 127.1, 126.4, 125.2, 124.5, 124.2, 121.8, 119.1, 116.1, 53.6, 50.4, 28.3, 27.3, 19.5, 19.3, 17.7, 17.4, 12.7 ppm.



**[Mo(N-2,6-Me-C<sub>6</sub>H<sub>3</sub>)(CHC(PhMe<sub>2</sub>))(IMesMe<sub>2</sub>)(OSiPh<sub>3</sub>)]<sup>+</sup>[B(ArF)<sub>4</sub>]<sup>-</sup> Mo3@OSiPh<sub>3</sub>:**

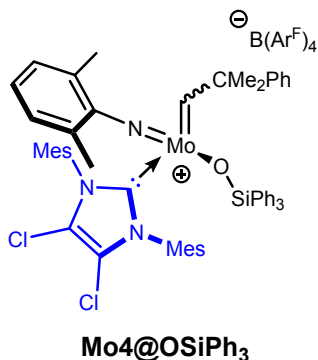
**Mo3** (200 mg, 0.112 mmol) was dissolved in CH<sub>2</sub>Cl<sub>2</sub> (3 mL). HOSiPh<sub>3</sub> (31.9 mg, 0.111 mmol, 1 equiv.) in CH<sub>2</sub>Cl<sub>2</sub> (3 mL) was added dropwise to the solution and the reaction mixture was stirred for three hours at room temperature. The solvent was removed *in vacuo* to yield **Mo3@OSiPh<sub>3</sub>** as yellow/orange powder. Since this compound exhibits very broad signals in NMR, the alkyldiene signal in <sup>13</sup>C NMR is not visible.

**<sup>1</sup>H-NMR** (CDCl<sub>3</sub>) δ 11.92 (bs, 1H), 7.73 – 7.67 (m, 8H), 7.53 – 7.48 (m, 4H), 7.48 – 7.44 (m, 3H), 7.41 – 7.36 (m, 1H), 7.34 – 7.30 (m, 11H), 7.05 (t, 1H), 7.00 – 6.94 (m, 2H), 6.92 – 6.89 (m, 2H), 6.87 (bs, 2H), 6.69 – 6.65 (m, 2H), 6.62 (bs, 2H), 2.24 (s, 6H), 2.10 – 1.88 (m, 6H), 1.82 (s, 3H), 1.80 (s, 3H), 1.63 (s, 3H), 1.50 (s, 3H), 0.97 (s, 3H) ppm; **<sup>19</sup>F-NMR** (CDCl<sub>3</sub>) δ 62.44 (s, 24F) ppm; **<sup>13</sup>C-NMR** (CDCl<sub>3</sub>) δ 176.4, 161.7 (q,  $^1J_{BC} = 49.8$  Hz), 155.3, 147.4, 141.3, 135.2, 134.8, 134.8, 134.7, 134.2, 132.0, 130.6, 130.5, 129.9, 129.4, 128.9 (qq,  $^2J_{CF} = 31.4$ ,  $^3J_{CB} = 2.7$  Hz), 128.6, 128.2, 128.1, 127.8, 126.5, 125.9, 125.2, 123.2, 120.5, 117.4, 54.8, 30.4, 29.6, 21.0, 19.5, 17.8, 17.5, 9.2 ppm. **Elemental analysis** calcd. for C<sub>89</sub>H<sub>72</sub>BF<sub>24</sub>MoN<sub>3</sub>OSi: C, 60.11; H, 4.21; N, 2.31. found: C: 59.83; H, 4.327; N, 2.53.

After the addition of one drop of deuterated acetonitrile the alkyldiene and carbene carbon signal became visible. Acetonitrile is loosely coordinated and can be removed by applying vacuum.

**<sup>1</sup>H-NMR** (CDCl<sub>3</sub>) δ 13.59 (s, 1H), 7.75 – 7.68 (m, 8H), 7.55 – 7.50 (m, 4H), 7.40 – 7.33 (m, 3H), 7.33 – 7.25 (m, 6H), 7.25 – 7.16 (m, 8H), 7.05 – 6.98 (m, 2H), 6.98 – 6.79 (m, 5H), 6.58 (bs, 1H), 2.65 (bs, 3H), 2.29 (s, 6H), 1.89 (s, 6H), 1.86 (s, 3H), 1.84 (s, 3H), 1.79 – 1.62 (m, 12H), 0.97 (s, 3H) ppm; **<sup>19</sup>F-NMR** (CDCl<sub>3</sub>) δ 62.43 (s, 24F) ppm; **<sup>13</sup>C-NMR** (CDCl<sub>3</sub>) δ 320.8, 180.7, 160.4 (q,  $^1J_{BC} = 49.8$  Hz), 152.2, 146.1, 139.2, 136.1,

134.7, 134.2, 134.1, 133.6, 132.4, 131.0, 128.9, 128.4, 128.3, 127.7 (qq,  $^2J_{CF} = 31.4$ ,  $^3J_{CB} = 2.7$  Hz), 127.4, 127.2, 126.8, 126.7, 126.5, 125.3, 124.7, 124.3, 122.0, 116.2, 53.7, 32.9, 28.6, 27.6, 21.1, 19.7, 17.6, 17.3, 8.0 ppm.



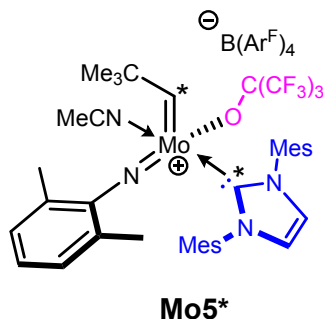
**[Mo(N-2,6-Me-C<sub>6</sub>H<sub>3</sub>)(CHC(PhMe<sub>2</sub>))(IMesCl<sub>2</sub>)(OSiPh<sub>3</sub>)[B(ArF)<sub>4</sub>] Mo4@OSiPh<sub>3</sub>:** Mo4 (200 mg, 0.112 mmol) was dissolved in CH<sub>2</sub>Cl<sub>2</sub> (3 mL). HOSiPh<sub>3</sub> (31.9 mg, 0.111 mmol, 1 equiv.) in CH<sub>2</sub>Cl<sub>2</sub> (3 mL) was added dropwise to the solution. The reaction mixture was stirred for three hours at room temperature. The solvent was removed *in vacuo* to yield **Mo4@OSiPh<sub>3</sub>** as yellow/orange powder. Since this compound exhibits very broad signals in NMR, the alkyldiene and carbene signals in <sup>13</sup>C NMR are not visible.

**<sup>1</sup>H-NMR** (CDCl<sub>3</sub>) δ 13.39 (bs, 1H), 7.73 – 7.68 (m, 8H), 7.53 – 7.49 (m, 4H), 7.43 – 7.36 (m, 3H), 7.31 – 7.22 (m, 1H), 7.17 – 7.13 (m, 11H), 7.01 (t, 1H), 6.93 – 6.85 (m, 2H), 6.59 (bs, 2H), 2.28 (s, 6H), 2.14 – 1.59 (bs, 3H), 1.93 (s, 6H), 1.76 (s, 9H), 0.99 (s, 3H), 0.96 (s, 3H) ppm; **<sup>19</sup>F-NMR** (CDCl<sub>3</sub>) δ 62.38 (s, 24F) ppm; **<sup>13</sup>C-NMR** (CDCl<sub>3</sub>) δ 183.2, 160.5 (q,  $^1J_{BC} = 49.8$  Hz), 152.6, 145.5, 140.8, 135.2, 135.1, 134.4, 134.1, 133.6, 130.8, 129.1, 128.5, 127.9, 127.7 (qq,  $^2J_{CF} = 31.4$ ,  $^3J_{CB} = 2.7$  Hz), 127.3, 126.7, 126.5, 125.5, 124.7, 124.3, 122.0, 120.1, 119.3, 116.3.5, 54.1, 28.7, 27.8, 19.9, 19.8, 19.2, 17.4, 17.1 ppm.

After the addition of one drop of deuterated acetonitrile the alkyldiene and carbene carbon signal were visible.

**<sup>1</sup>H-NMR** (CDCl<sub>3</sub>) δ 14.42 (s, 1H), 7.75 – 7.68 (m, 8H), 7.55 – 7.50 (m, 4H), 7.42 – 7.35 (m, 3H), 7.31 – 7.17 (m, 15H), 7.06 – 7.00 (m, 3H), 6.95 – 6.91 (m, 3H), 6.88 – 6.82 (m, 1H), 6.20 (bs, 1H), 2.65 (bs, 3H), 2.30 (bs, 6H), 1.95 (bs, 6H), 1.83 (s, 3H), 1.69 (s, 3H), 1.62 (bs, 3H), 0.96(s, 3H) ppm; **<sup>19</sup>F-NMR** (CDCl<sub>3</sub>) δ 62.44 (s, 24F) ppm; **<sup>13</sup>C-NMR** (CDCl<sub>3</sub>) δ 324.3, 184.5, 160.4 (q,  $^1J_{BC} = 49.8$  Hz), 152.1, 145.4, 140.4, 139.0, 136.1, 135.1, 134.1, 133.5, 130.1, 131.0, 128.5, 128.4, 128.3, 127.7 (qq,  $^2J_{CF} = 31.4$ ,  $^3J_{CB} = 2.7$  Hz), 127.3, 127.2, 126.9, 126.6, 126.5, 126.4, 125.4, 124.6, 124.2, 121.9,

119.5, 119.2, 116.2, 54.4, 27.4, 28.6, 27.6, 21.1, 19.7, 19.1, 17.3 ppm. **Elemental analysis** calcd. for  $C_{91}H_{73}BCl_2F_{24}MoN_4OSi$ : C, 57.52; H, 3.87; N, 2.95. found: C: 57.23; H, 3.870; N, 2.70.



**[Mo(N-2,6-Me<sub>2</sub>-C<sub>6</sub>H<sub>3</sub>)(C\*HCMe<sub>3</sub>)(IMes\*)(OC(CF<sub>3</sub>)<sub>3</sub>)] [B(Ar<sup>F</sup>)<sub>4</sub>] Mo5\***. To a solution of Mo(N-2,6-Me<sub>2</sub>-C<sub>6</sub>H<sub>3</sub>)(C\*HCMe<sub>3</sub>)(IMes\*)(OTf)<sub>2</sub> (200 mg, 0.225 mmol) in CH<sub>2</sub>Cl<sub>2</sub> (3 mL) was added solid Na(BAr<sup>F</sup>)<sub>4</sub> (200 mg, 0.225 mmol, 1 equiv.). The mixture was stirred at room temperature for three hours. The suspension was filtered and Li(OC(CF<sub>3</sub>)<sub>3</sub>) (109 mg, 0.451 mmol, 2 equiv.), dissolved in CH<sub>2</sub>Cl<sub>2</sub> (3 mL), and a few drops of acetonitrile were added. The mixture was stirred for three hours, then the solvent was removed under reduced pressure and the remaining oil was again dissolved in CH<sub>2</sub>Cl<sub>2</sub>. The suspension was filtered and the solvent was evaporated. The residue was triturated with *n*-pentane to form a yellow suspension. *n*-Pentane was decanted, and the solid was dried *in vacuo*. The solid was treated with CH<sub>2</sub>Cl<sub>2</sub>, diethyl ether and *n*-pentane. The solution was kept at -35 °C overnight; during this time, yellow crystals formed.

**Yield:** 320 mg (82%). **<sup>1</sup>H-NMR** (CDCl<sub>3</sub>) δ 12.77 (s, 1H, *syn*-isomer), 7.67 (s, 8H), 7.47 (s, 4H), 7.26 (s, 2H), 7.09 (t, *J* = 7.6 Hz, 1H), 7.01 – 6.93 (m, 4H), 6.71 (s, 2H), 2.25 (s, 6H), 2.21 – 1.90 (m, 9H), 1.85 (s, 6H), 0.76 (s, 9H) ppm.; **<sup>19</sup>F-NMR** (CDCl<sub>3</sub>) δ -62.45 (s, 24F), -72.73 (s, 9F) ppm; **<sup>13</sup>C-NMR** (CDCl<sub>3</sub>) δ 317.4, 178.1, 159.6 (q, <sup>1</sup>J<sub>BC</sub> = 50.7 Hz), 139.8, 132.8, 132.8, 132.7, 131.5, 126.8 (qq, <sup>2</sup>J<sub>CF</sub> = 31.9 Hz, <sup>3</sup>J<sub>CB</sub> = 2.5 Hz), 126.1, 124.1, 122.5 (q, <sup>1</sup>J<sub>CF</sub> = 272.5 Hz) 120.0, 117.1, 115.4, 115.4, 115.3, 115.3, 115.2, 75.2, 74.9, 74.6, 48.4, 27.8, 18.8, 18.8, 17.1, 15.4 ppm. **Elemental analysis** calcd. for C<sub>72</sub>H<sub>58</sub>F<sub>33</sub>MoN<sub>4</sub>O: C, 50.02; H, 3.38; N, 3.24. found: C: 49.83; H, 3.505; N, 2.97.

#### 4. Synthesis of Substrates for RCM

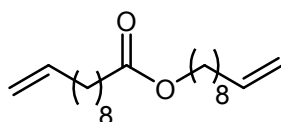
##### General Procedure for the Synthesis of Ester-Based $\alpha,\omega$ -Dienes (GP-1).

To a stirred solution of the carboxylic acid chloride (21.0 mmol) in  $\text{CH}_2\text{Cl}_2$  (40 mL) were subsequently added pyridine (1.7 mL, 21.0 mmol) and the corresponding alcohol (9.5 mmol/19 mmol) at 0 °C. After stirring for 4 hours at room temperature, the reaction mixture was washed with 1.0 M aq. HCl solution (40 mL), sat. aq.  $\text{NaHCO}_3$  solution (40 mL), brine (40 mL), dried over anhydrous  $\text{Na}_2\text{SO}_4$ , filtered, and evaporated. The obtained crude product was purified by column chromatography on  $\text{SiO}_2$  to obtain the corresponding ester.

##### General Procedure for the RCM of $\alpha,\omega$ -Dienes (GP-2).

To a stirred solution of the diene (0.75 mmol) in  $\text{CH}_2\text{Cl}_2$  (200 mL) was added the 2<sup>nd</sup>-generation Grubbs catalyst  $\text{RuCl}_2(\text{IMes})(\text{PCy}_3)(\text{CHPh})$  (31.8 mg, 0.0375 mmol, 5 mol-%) at room temperature. After stirring for 14 hours under reflux and under  $\text{N}_2$ , the reaction mixture was cooled to room temperature and ethyl vinyl ether (5 mL, 70 eq) was added. The mixture was stirred for a further 2 hours at room temperature. All volatiles were removed under reduced pressure and the obtained crude product was purified via column chromatography on  $\text{SiO}_2$  to obtain the corresponding macrocyclic product, whose *E/Z* isomers were separated by semi-preparative HPLC.

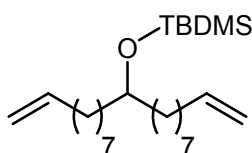
##### Dec-9-en-1-yl undec-10-enoate **1**



The compound was prepared following the general procedure **GP-1**. Undec-10-enoyl chloride (4.5 mL, 21.0 mmol) was dissolved in  $\text{CH}_2\text{Cl}_2$  (40 mL), treated with pyridine (1.7 mL, 21.0 mmol) and dec-9-en-1-ol (3.39 mL, 19.0 mmol) to yield the corresponding ester **1** after column chromatography on  $\text{SiO}_2$  (*n*-pentane:diethyl ether – 20:1). Spectral data were in agreement with previous reports.<sup>9, 10</sup> **Yield:** 5.76 g (17.9 mmol, 85.0%). **Physical State:** colorless liquid. **<sup>1</sup>H NMR** ( $\text{CDCl}_3$ )  $\delta$  5.74 (ddt,  $J = 17.0, 10.3, 6.7$  Hz, 2H), 4.89 – 4.95 (m, 2H), 4.86 (ddt,  $J = 10.2, 2.3, 1.1$  Hz, 2H), 3.98 (t,  $J = 6.7$  Hz, 2H), 2.22 (t,  $J = 7.5$  Hz, 2H), 1.94 – 2.00 (m, 4H), 1.53 – 1.58 (m, 4H), 1.22 – 1.32 (m, 20H) ppm; **<sup>13</sup>C NMR** ( $\text{CDCl}_3$ )  $\delta$  174.2, 139.3, 139.3, 114.3, 114.3, 64.5, 34.5, 33.9, 29.5, 29.4, 29.4, 29.3, 29.3, 29.2, 29.2, 29.0, 28.8, 26.1, 25.2 ppm.

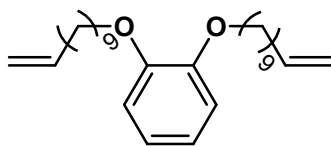
Two carbons were not observed due to incidental equivalence. **<sup>1</sup>H NMR** (C<sub>6</sub>D<sub>6</sub>) δ 5.80 (ddt, *J* = 17.0, 10.3, 6.7 Hz, 1H), 5.80 (ddt, *J* = 17.0, 10.3, 6.7 Hz, 1H), 5.02 – 5.08 (m, 2H), 4.98 – 5.02 (m, 2H), 4.07 (t, *J* = 6.7 Hz, 2H), 2.20 (t, *J* = 7.4 Hz, 2H), 1.95 – 2.02 (m, 4H), 1.58 – 1.65 (m, 2H), 1.45 – 1.53 (m, 2H), 1.27 – 1.32 (m, 4H), 1.13 – 1.25 (m, 16H) ppm; **<sup>13</sup>C NMR** (C<sub>6</sub>D<sub>6</sub>) δ 173.1, 139.3, 139.2, 114.6, 114.5, 64.3, 34.5, 34.2, 29.8, 29.7, 29.6, 29.6, 29.5, 29.4, 29.4, 29.3, 29.2, 26.3, 25.4 ppm. 2 carbons were not observed due to incidental equivalence. **DOSY NMR** (C<sub>6</sub>D<sub>6</sub>): *D* = 8.3 · 10<sup>-10</sup> m<sup>2</sup>/s; **IR** (ATR, in C<sub>6</sub>D<sub>6</sub>) ν 3077 (w), 2976 (w), 2925 (s), 2854 (m), 1737 (s), 1640 (w), 1464 (w), 1417 (w), 1390 (w), 1353 (w), 1239 (w), 1171 (m), 1115 (w) cm<sup>-1</sup>.

### ***tert*-Butyldimethyl(nonadeca-1,18-dien-10-yloxy)silane 2**



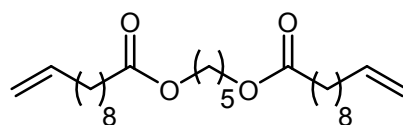
The compound was prepared according to the literature.<sup>9</sup> To a stirred solution of nonadeca-1,18-dien-10-ol (420.8 mg, 1.5 mmol) in DMF (5 mL) was added imidazole (306.4 mg, 4.5 mmol) and TBDMSCl (339.1 mg, 2.25 mmol). After stirring at room temperature for four hours, H<sub>2</sub>O (15 mL) was added and the aqueous phase was extracted with *n*-pentane (4x 10 mL). The combined organic layers were dried over anhydrous Na<sub>2</sub>SO<sub>4</sub>, filtered and evaporated. The obtained crude product was purified by column chromatography over SiO<sub>2</sub> (*n*-pentane:diethyl ether – 20:1) to yield the corresponding silyl ether **2**. Spectral data were in good agreement with previous reports.<sup>9, 10</sup> **Yield:** 430.2 mg (1.1 mmol, 73%). **Physical State:** colorless liquid. **<sup>1</sup>H NMR** (CDCl<sub>3</sub>) δ 5.81 (ddt, *J* = 17.0, 10.3, 6.7 Hz, 2H), 4.99 (ddt, *J* = 17.1, 2.1, 1.6 Hz, 2H), 4.92 (ddt, *J* = 10.2, 2.3, 1.1 Hz, 2H), 3.57 – 3.72 (m, 1H), 2.01 – 2.06 (m, 4H), 1.33 – 1.38 (m, 9H), 1.21 – 1.32 (m, 15H), 0.88 (s, 9H), 0.03 (s, 6H) ppm; **<sup>13</sup>C NMR** (CDCl<sub>3</sub>) δ 139.4, 114.2, 72.5, 37.3, 34.0, 30.0, 29.6, 29.2, 29.1, 26.1, 25.5, 18.3, -4.3 ppm; **<sup>1</sup>H NMR** (C<sub>6</sub>D<sub>6</sub>) δ 5.80 (ddt, *J* = 17.0, 10.3, 6.7 Hz, 2H), 5.06 (ddt, *J* = 17.1, 2.1, 1.6 Hz, 2H), 5.01 (ddt, *J* = 10.2, 2.3, 1.2 Hz, 2H), 3.66 – 3.72 (m, 1H), 1.98 – 2.03 (m, 4H), 1.49 – 1.57 (m, 4H), 1.28 – 1.48 (m, 20H) ppm; **<sup>13</sup>C NMR** (C<sub>6</sub>D<sub>6</sub>) δ 139.2, 114.6, 72.7, 37.7, 34.2, 30.3, 30.0, 29.5, 29.3, 26.2, 25.8, 18.4, -4.1 ppm; **DOSY NMR** (C<sub>6</sub>D<sub>6</sub>): *D* = 9.4 · 10<sup>-10</sup> m<sup>2</sup>/s; **IR** (ATR, in C<sub>6</sub>D<sub>6</sub>) ν 3077 (w), 2926 (s), 2855 (m), 1614 (w), 1463 (w), 1440 (w), 1414 (w), 1373 (w), 1361 (w), 1254 (m), 1053 (m), 1005 (m) cm<sup>-1</sup>.

### 1,2-Bis(undec-10-enyloxy)benzene **3**



The compound was prepared according to the literature.<sup>11</sup> To a stirred solution of 1,2-benzenediol (2.0 g, 18.2 mmol) in DMF (100 mL) were added NaOH (3.0 g, 75.0 mmol) and 11-bromo-1-undecene (12.0 g, 51.5 mmol). After stirring at 40 °C for 16 hours, H<sub>2</sub>O (100 mL) and diethyl ether (100 mL) were added and the aqueous phase was extracted with diethyl ether (200 mL). The combined organic layers were washed with brine, dried over anhydrous MgSO<sub>4</sub>, filtered and evaporated. The obtained crude product was purified by column chromatography over SiO<sub>2</sub> using *n*-pentane:diethyl ether – 20:1 as mobile phase to yield the corresponding aryl ether **3**. Spectral data were in good agreement with previous reports.<sup>11</sup> **Yield:** 6.0 g (14.6 mmol, 80%). **Physical State:** colorless solid. **<sup>1</sup>H NMR** (C<sub>6</sub>D<sub>6</sub>) δ 6.94 – 6.80 (m, 4H), 5.81 (ddt, *J* = 16.9, 10.1, 6.6 Hz, 2H), 5.06 (ddt, *J* = 17.1, 2.2, 1.6 Hz, 2H), 5.01 (ddt, *J* = 10.6, 2.3, 1.2 Hz, 2H), 3.79 (t, *J* = 6.2 Hz, 4H), 1.98 – 2.06 (m, 4H), 1.66 – 1.75 (m, 4H), 1.39 – 1.47 (m, 4H), 1.31 – 1.39 (m, 4H), 1.21 – 1.29 (m, 16H) ppm; **<sup>13</sup>C NMR** (C<sub>6</sub>D<sub>6</sub>) δ 150.2, 139.28, 121.33, 114.6, 114.5, 69.1, 30.0, 29.9, 29.9, 29.8, 29.5, 29.4, 26.6 ppm; **DOSY NMR** (C<sub>6</sub>D<sub>6</sub>): *D* = 7.3 · 10<sup>-10</sup> m<sup>2</sup>/s.

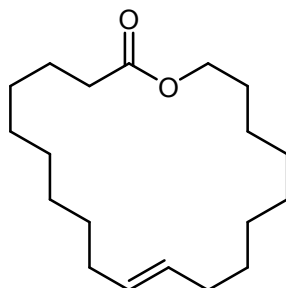
### Dodecane-1,12-diyl bis(undec-10-enoate) **4**



The compound was prepared following the general procedure **GP-1**. Undec-10-enoyl chloride (4.5 mL, 21.0 mmol) was dissolved in CH<sub>2</sub>Cl<sub>2</sub> (40 mL), treated with pyridine (2.0 mL, 25.0 mmol) and pentan-1,5-diol (2.0 g, 10.0 mmol) to yield the corresponding diester **2** after column chromatography over silica 60 (*n*-pentane:diethyl ether – 20:1 → 10:1). Spectroscopic data were in agreement with previous reports.<sup>9, 10</sup> **Yield:** 5.10 g (9.5 mmol, 95%). **Physical State:** white solid. **<sup>1</sup>H NMR** (CDCl<sub>3</sub>) δ 5.80 (ddt, *J* = 17.0, 10.3, 6.7 Hz, 2H), 4.98 (ddt, *J* = 17.1, 2.0, 1.6 Hz, 2H), 4.93 (ddt, *J* = 10.2, 2.3, 1.1 Hz, 2H), 4.05 (t, *J* = 6.7 Hz, 4H), 2.28 (t, *J* = 7.5 Hz, 4H), 2.00 – 2.06 (m, 4H), 1.57 – 1.64 (m, 9H), 1.25 – 1.38 (m, 35H) ppm; **<sup>13</sup>C NMR** (C<sub>6</sub>D<sub>6</sub>) δ 173.0, 139.2, 114.5, 63.9, 34.4, 34.2, 29.7, 29.6, 29.5, 29.4, 29.3, 28.7, 25.4, 22.8 ppm. **DOSY NMR** (C<sub>6</sub>D<sub>6</sub>): *D* = 6.8

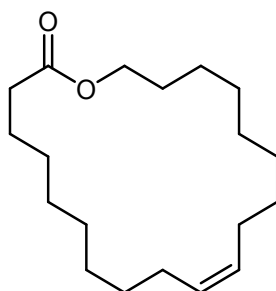
$\cdot 10^{-10} \text{ m}^2/\text{s}$ ; **IR** (ATR, in  $\text{C}_6\text{D}_6$ )  $\nu$  3077 (w), 2997 (w), 2925 (s), 2854 (m), 1736 (s), 1640 (s), 1463 (w), 1418 (w), 1390 (w), 1353 (w), 1239 (w), 1169 (w), 1116 (m), 1073 (w), 993 (w), 909 (w), 724 (w), 635 (w)  $\text{cm}^{-1}$ .

### **(E)-Oxacycloicos-11-en-2-one (E)-5**



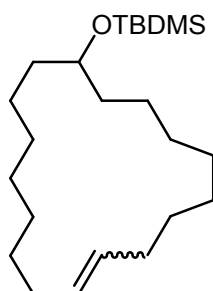
The compound was prepared according to **GP-2**. The  $\alpha,\omega$ -diene **1** (241.9 mg, 0.75 mmol) was dissolved in  $\text{CH}_2\text{Cl}_2$  (250 mL), treated with the 2<sup>nd</sup>-generation *Grubbs* catalyst (31.8 mg, 0.0375 mmol, 5 mol%) to yield the corresponding macrocycle **E-5** after column chromatography over  $\text{SiO}_2$  and semi-preparative HPLC (petroleum ether:ethyl acetate – 75:1). Spectral data were in good agreement with previous reports.<sup>9, 10</sup> **Physical State:** colorless liquid. **<sup>1</sup>H NMR** ( $\text{C}_6\text{D}_6$ )  $\delta$  5.31 – 5.41 (m, 2H), 4.00 – 4.05 (m, 2H), 2.15 (t,  $J = 6.6 \text{ Hz}$ , 2H), 1.99 – 2.07 (m, 4H), 1.54 – 1.61 (m, 2H), 1.38 – 1.44 (m, 2H), 1.18 – 1.37 (m, 20H) ppm; **<sup>13</sup>C NMR** ( $\text{C}_6\text{D}_6$ )  $\delta$  173.0, 131.1, 131.0, 64.0, 34.0, 32.3, 32.2, 29.7, 29.5, 29.3, 29.2, 29.1, 29.0, 28.9, 28.5, 28.0, 27.9, 26.4, 25.2 ppm; **IR** (ATR, in  $\text{C}_6\text{D}_6$ )  $\nu$  2922 (s), 2852 (m), 1734 (s), 1460 (w), 1440 (w), 1387 (w), 1348 (w), 1253 (m), 1236 (m), 1172 (m), 1119 (m), 1098 (m), 1061 (w), 1022 (w), 966 (m)  $\text{cm}^{-1}$ .

### **(Z)-Oxacycloicos-11-en-2-one (Z)-5**



The compound was prepared according to **GP-2**. The  $\alpha,\omega$ -diene **1** (241.9 mg, 0.75 mmol) was dissolved in  $\text{CH}_2\text{Cl}_2$  (250 mL), treated with the 2<sup>nd</sup>-generation *Grubbs* catalyst (31.8 mg, 0.0375 mmol, 5 mol%) to yield the corresponding macrocycle **Z-5** after column chromatography over  $\text{SiO}_2$  and semi-preparative HPLC (petroleum ether:ethyl acetate – 75:1). Spectral data were in good agreement with previous reports.<sup>9, 10</sup> **Physical State:** colorless liquid. **<sup>1</sup>H NMR** ( $\text{C}_6\text{D}_6$ )  $\delta$  5.40 – 5.50 (m, 2H), 4.05 (t,  $J = 5.7$  Hz, 2H), 2.17 (t,  $J = 6.8$  Hz, 2H), 2.02 – 2.09 (m, 4H), 1.51 – 1.58 (m, 2H), 1.32 – 1.43 (m, 6H), 1.20 – 1.30 (m, 16H) ppm; **<sup>13</sup>C NMR** ( $\text{C}_6\text{D}_6$ )  $\delta$  172.9, 130.4, 130.3, 64.0, 34.8, 29.7, 29.6, 29.4, 29.2, 29.2, 29.1, 29.0, 28.9, 28.8, 28.5, 26.9, 26.8, 26.6, 25.5 ppm; **IR** (ATR, in  $\text{C}_6\text{D}_6$ )  $\nu$  3002 (w), 2923 (s), 2853 (m), 1734 (s), 1461 (w), 1385 (w), 1345 (w), 1237 (m), 1173 (m), 1116 (w), 1093 (w), 1065 (w), 1018 (w)  $\text{cm}^{-1}$ .

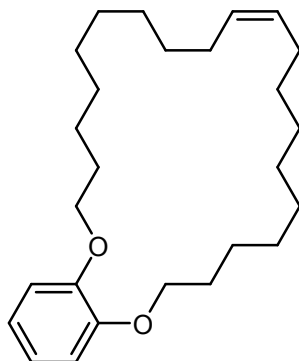
**(E)+(Z)-tert-Butyl(cycloheptadec-9-en-1-yloxy)dimethylsilane 6**



To a solution of *E/Z*-cycloheptadec-9-en-1-ol (12.6 mg, 0.05 mmol) in DMF (1 mL), were subsequently added imidazole (10.2 mg, 0.15 mmol) and TBDMSCI (11.3 mg, 0.075 mmol). After stirring overnight at room temperature, ethanol (1 mL) was added and the reaction mixture was stirred for a further 15 minutes. The mixture was then diluted with *n*-pentane (10 mL), washed with  $\text{H}_2\text{O}$  (15 mL) and brine (15 mL), dried over anhydrous  $\text{Na}_2\text{SO}_4$ , filtered and all volatiles were removed *in vacuo*. The obtained crude product was purified by column chromatography over  $\text{SiO}_2$  (*n*-pentane:diethyl ether – 100:0 → 100:1) to yield the corresponding macrocycle *E/Z-6* as an inseparable mixture. Spectral data were in agreement with previous reports.<sup>9, 10</sup> **Physical State:** colorless oil. **<sup>1</sup>H NMR** ( $\text{C}_6\text{D}_6$ )  $\delta$  5.39 – 5.43 (m, 0.21H), 5.31 – 5.37 (m, 1.79H), 3.75 – 3.81 (m, 1H), 2.00 – 2.10 (m, 4H), 1.50 – 1.63 (m, 4H), 1.26 – 1.43 (m, 20H), 1.03 (s, 9H), 0.12 (s, 6H) ppm; **<sup>13</sup>C NMR** ( $\text{C}_6\text{D}_6$ )  $\delta$  131.1, 130.4, 72.1, 71.6, 36.3, 36.1, 32.8, 29.5, 29.4, 29.2, 29.0, 28.5, 28.5, 28.2, 27.6, 27.3, 26.2, 23.8, 22.9, 18.4, -4.3, -4.4 ppm. Two carbons were not observed due to incidental equivalence; **IR** (ATR in  $\text{C}_6\text{D}_6$ )  $\nu$  3026 (w), 2925 (s), 2854 (s), 1472 (w), 1461 (w), 1443 (w), 1405 (w), 1388 (w), 1373

(w), 1360 (w), 1254 (m), 1211 (w), 1188 (w), 1101 (w), 1050 (m), 1005 (w), 966 (m)  $\text{cm}^{-1}$ .

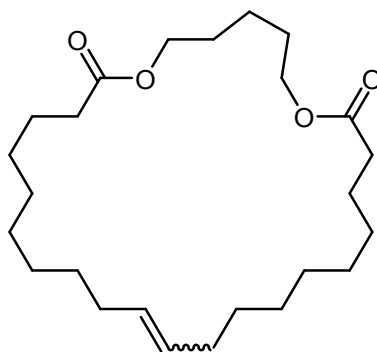
### ***E/Z*-1,4-Dioxacyclotetracosine 7**



The compound was prepared according to **GP-2**. The  $\alpha,\omega$ -diene **3** (300 mg, 0.72 mmol) was dissolved in  $\text{CH}_2\text{Cl}_2$  (350 mL) and treated with the 2<sup>nd</sup>-generation Grubbs catalyst (29.1 mg, 0.0361 mmol, 5 mol%) to yield the corresponding macrocycle *E/Z*-7 after column chromatography on  $\text{SiO}_2$  as an inseparable mixture.

**Physical State:** colorless oil. **<sup>1</sup>H NMR** ( $\text{C}_6\text{D}_6$ )  $\delta$  6.74 – 6.94 (m, 4H), 5.44 – 5.54 (m, 0.33H), 5.33 – 5.44 (m, 1.66H), 3.72 (t,  $J = 6.3$  Hz, 4H), 2.06 – 2.14 (m, 4H), 1.60 – 1.69 (m, 4H), 1.49 – 1.60 (m, 4H), 1.28 – 1.46 (m, 20H) ppm; **<sup>13</sup>C NMR** ( $\text{C}_6\text{D}_6$ )  $\delta$  150.3, 150.1, 131.3, 121.4, 121.1, 114.6, 113.8, 69.3, 68.8, 32.6, 30.6, 30.2, 30.2, 30.1, 29.8, 29.5, 28.9, 27.4, 27.2, 29.1. **HRMS** (ESI,  $m/z$ ) calcd. for  $\text{C}_{26}\text{H}_{42}\text{O}_2\text{Na}^+$ : 409.3077; found: 409.3077.

### ***E/Z*-1,7-Dioxacycloheptacos-17-ene-8,27-dione 8**



The compound was prepared following **GP-2**. The  $\alpha,\omega$ -diene **4** (327.5 mg, 0.75 mmol) was dissolved in  $\text{CH}_2\text{Cl}_2$  (250 mL) and treated with the 2<sup>nd</sup>-generation Grubbs catalyst

(31.8 mg, 0.0375 mmol, 5 mol%) to yield the corresponding macrocycle *E/Z*-8 after column chromatography over SiO<sub>2</sub> as an inseparable mixture. Spectral data were in good agreement with previous reports.<sup>10, 12</sup> **Physical State:** white solid. **<sup>1</sup>H NMR** (C<sub>6</sub>D<sub>6</sub>) δ 5.44 – 5.49 (m, 0.38H), 5.40 – 5.43 (m, 1.62H), 3.99 (t, *J* = 5.7 Hz, 4H), 2.18 (t, *J* = 7.3 Hz, 0.76H), 2.17 (t, *J* = 7.4 Hz, 3.24H), 2.03 – 2.10 (m, 4H), 1.56 – 1.62 (m, 4H), 1.19 – 1.39 (m, 26H) ppm; **<sup>13</sup>C NMR** (C<sub>6</sub>D<sub>6</sub>) δ 173.0, 173.0, 131.0, 130.4, 63.9, 63.8, 34.5, 32.7, 29.8, 29.5, 29.4, 29.4, 29.3, 29.2, 29.1, 28.7, 28.6, 27.3, 25.4, 23.2, 23.1 ppm. Five carbons were not observed due to incidental equivalence; **IR** (ATR, in C<sub>6</sub>D<sub>6</sub>) ν 2923 (s), 2853 (m), 1734 (s), 1457 (w), 1441 (w), 1420 (w), 1388 (w), 1357 (w), 1238 (m), 1173 (m), 1112 (w), 1094 (w), 1047 (w), 968 (w) cm<sup>-1</sup>; **HRMS** (EI) calcd. for C<sub>25</sub>H<sub>44</sub>O<sub>4</sub><sup>+</sup>: 408.3240; found: 408.3238.

## 5. Synthesis of Ordered Mesoporous Silica (OMS<sub>25A</sub>)

In general, the synthesis followed the procedure described in reference 13 with slight adaptations necessary due to the changed surfactant. 30.46 g of TMOS were added to 21.76 g of an aqueous 0.1 N HCl solution and stirred at room temperature for approximately 10 min while an underpressure or 120 mbar was applied to remove most of the formed methanol. This colloidal silica mixture was added to 14.995 g of dodecylethyldimethylammonium bromide and homogenized. The clear liquid was poured into a PTFA dish and was left at 80 °C for 48 hours to complete the polycondensation process. The now solid material was milled for 1 min with a ball mill (Spex 8000 Mixer/Mill, vial and balls made from stainless steel). Afterwards the powder was calcined by heating it to 550 °C with 1 °C·min<sup>-1</sup> in the presence of an air flow of 14.5 L·h<sup>-1</sup> and kept at this temperature for 6 h to remove all surfactant molecules.<sup>13</sup>

## 6. Modification of Mesoporous Silica

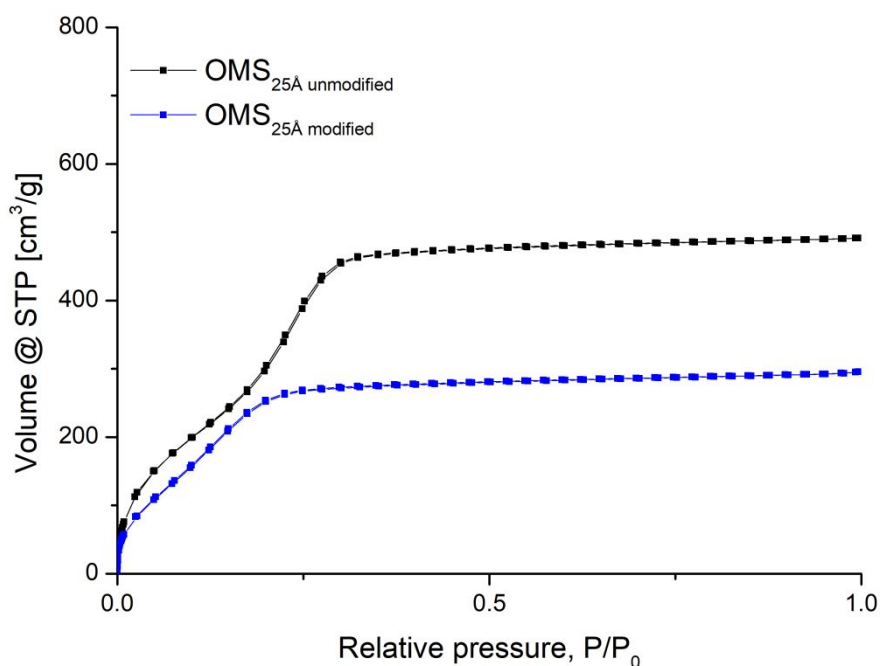
### General procedure for the multi-step modification of SBA-15 (GP-3).

**Refilling:** SBA-15/OMS (approx. 10 g) was added to a solution of P123 (40 g) in ethanol (150 mL). The mixture was stirred for 24 hours at room temperature. The suspension was filtered and dried *in vacuo* at 80 °C for 24 hours.

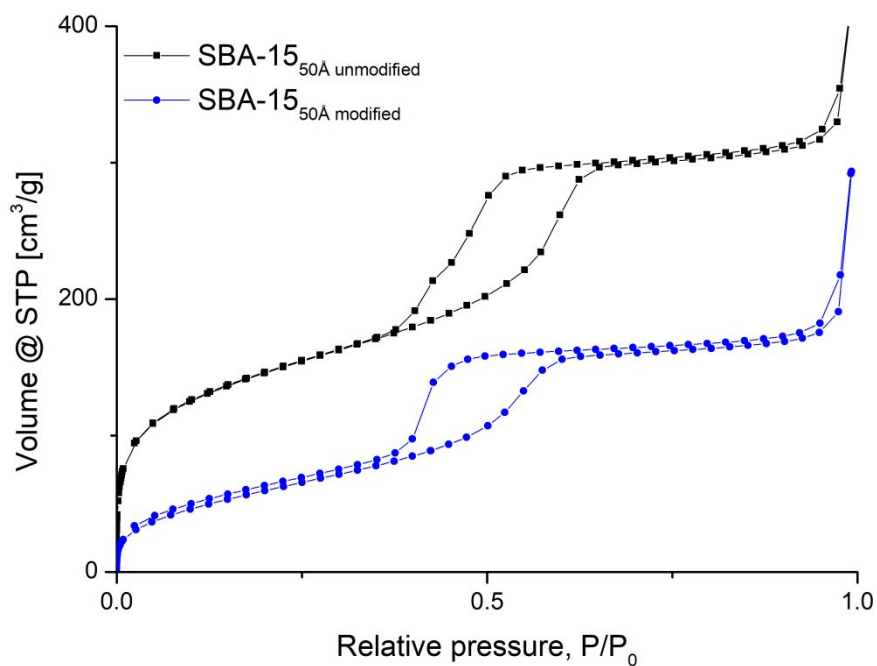
**Selective protection of silanol groups outside the mesopores:** The refilled SBA-15/OMS (approx. 15 g) was treated with hexamethyldisilazane (HMDS, 200 mL) for three hours at room temperature. Then the mixture was filtered and the silica was washed with hexane (500 mL).

**Removal of the surfactant:** The surfactant was removed by Soxhlet extraction with ethanol at 140 °C for seven days.

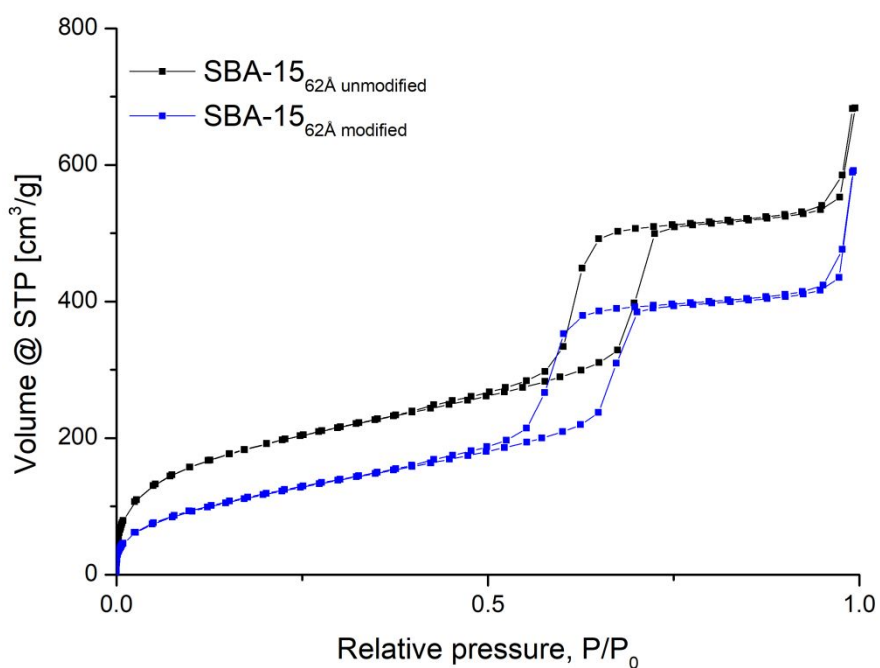
**Immobilization of the catalyst:** Refilled, selectively protected, and extracted silica (600 mg) was added to a solution of the catalyst (30 mg) in 1,2-dichlorobenzene (12 mL). For the removal of nitrogen in the pores, vacuum was applied. The suspension was stirred for three hours under vacuum at room temperature. Then, the suspension was filtered and the resulting silica containing the immobilized catalyst was washed with 1,2-dichlorobenzene (150 mL) and *n*-pentane (150 mL), dried under vacuum at room temperature for three hours and stored under inert atmosphere at -35 °C. Characterization of both the unmodified and modified SBA-15/OMS silica materials was carried out via Ar-sorption measurements (Figures S1-S3).



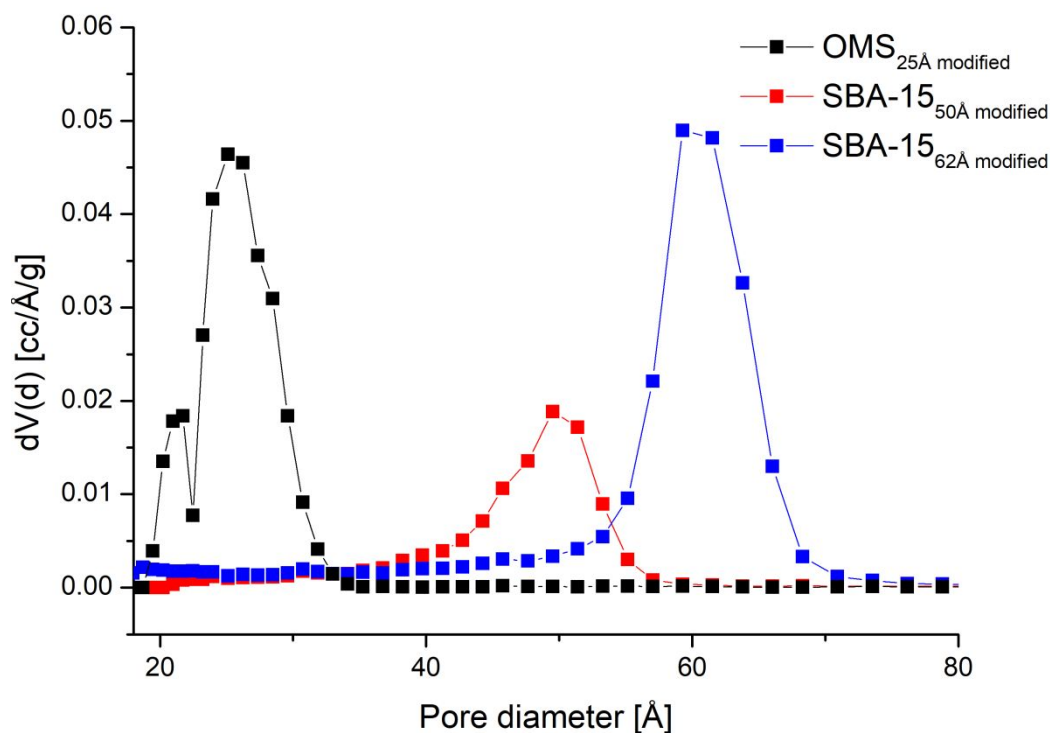
**Figure S1:** Ar-sorption isotherms of OMS<sub>25A</sub> unmodified and OMS<sub>25A</sub> modified (**OMS<sub>25A</sub>**).



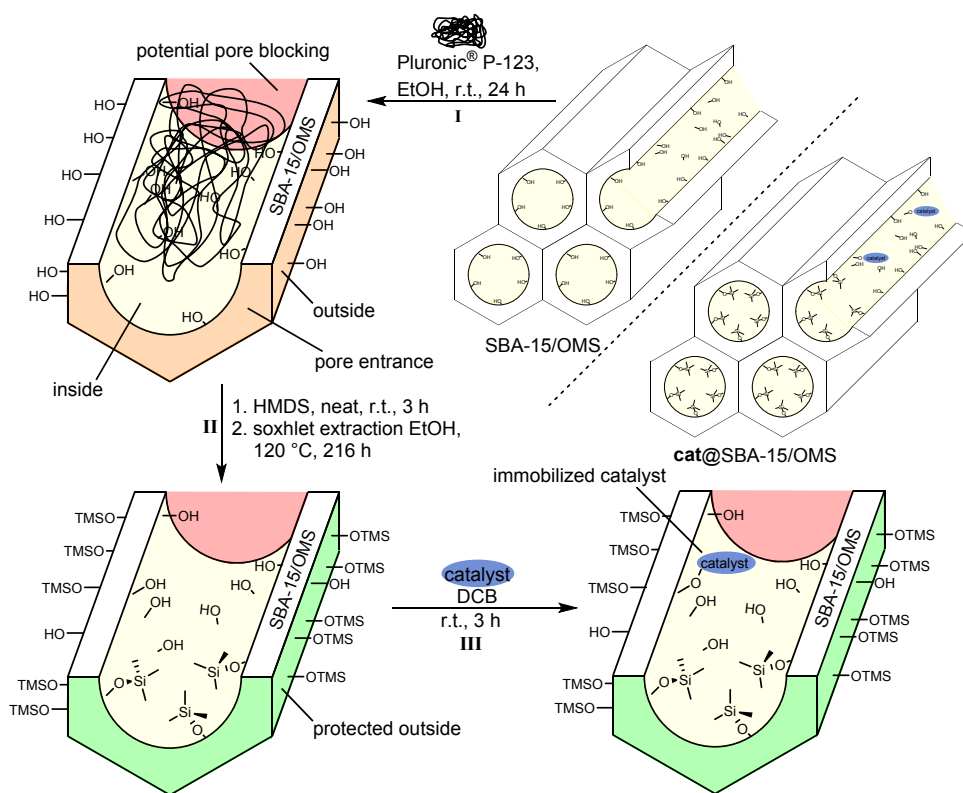
**Figure S2:** Ar-sorption isotherms of SBA-15<sub>50A</sub> unmodified and SBA-15<sub>50A</sub> modified (SBA-15<sub>50A</sub>).



**Figure S3:** Ar-sorption isotherms of SBA-15<sub>62A</sub> unmodified and SBA-15<sub>62A</sub> modified (SBA-15<sub>62A</sub>).



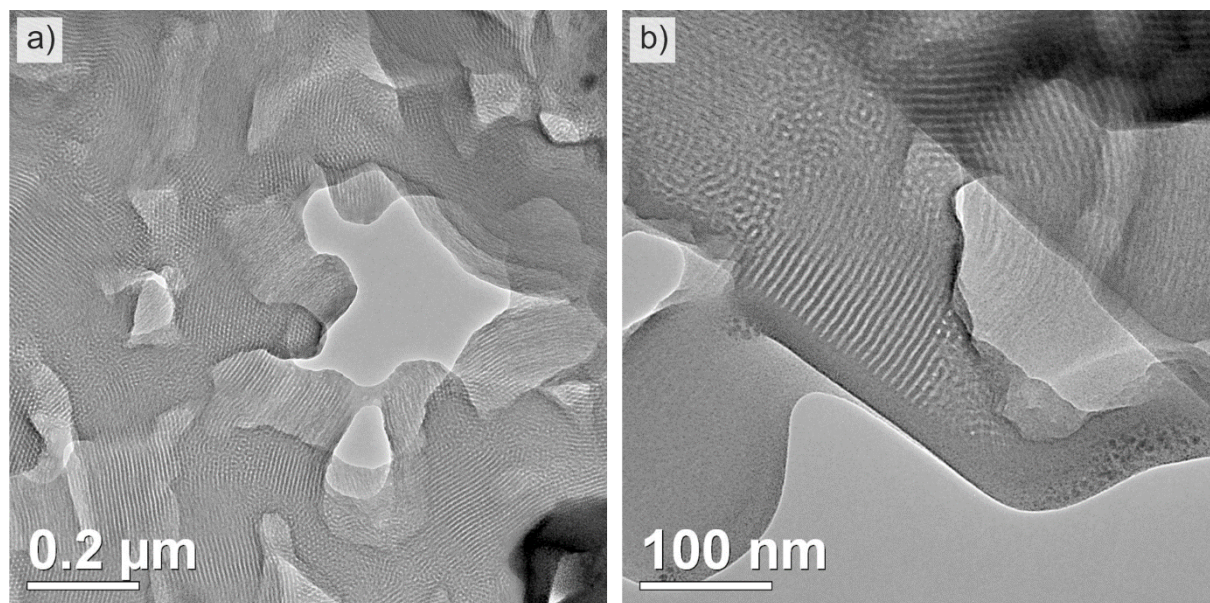
**Figure S4:** Pore distribution of OMS<sub>25Å</sub> modified (**OMS<sub>25Å</sub>**) SBA-15<sub>50Å</sub> modified (**SBA-15<sub>50Å</sub>**) and SBA-15<sub>62Å</sub> modified (**SBA-15<sub>62Å</sub>**) after Soxhlet extraction.



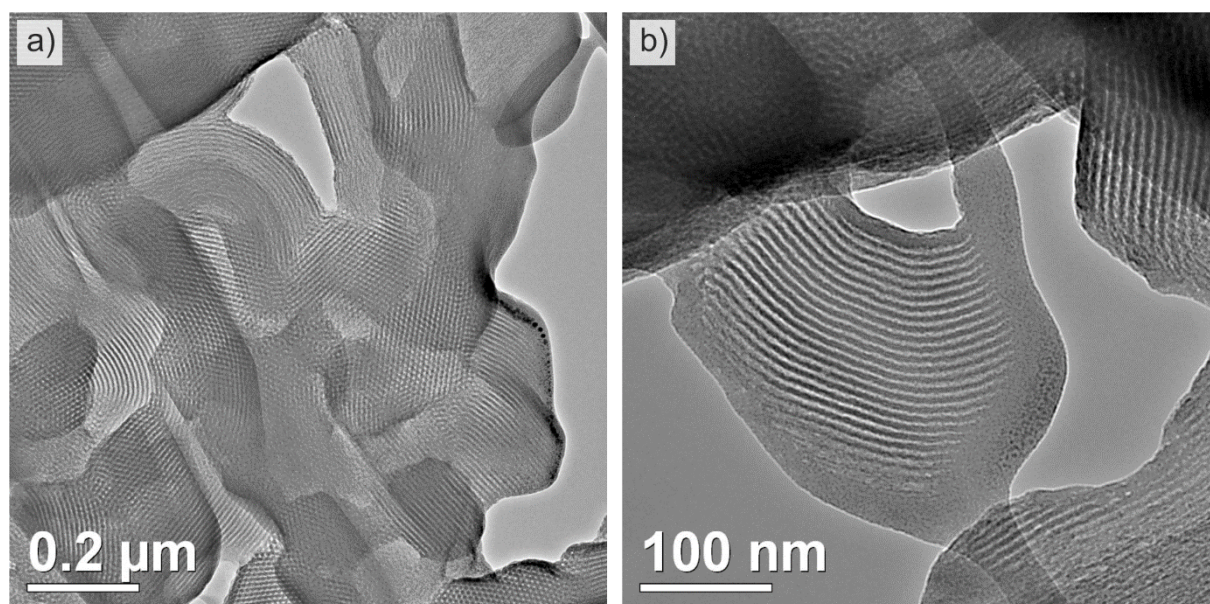
**Figure S5:** Multi-step modification of SBA-15/OMS for the pore-selective immobilization of the catalyst inside the mesopores.

## 7. Transmission Electron Micrographs of OMS<sub>25A</sub>, SBA-15<sub>50A</sub> and SBA-15<sub>62A</sub>

All three mesoporous materials were investigated by transmission electron microscopy (TEM) prior to their modification. Explicit differences between the pore structure of the purchased SBA-15 materials and the OMS material were observed.

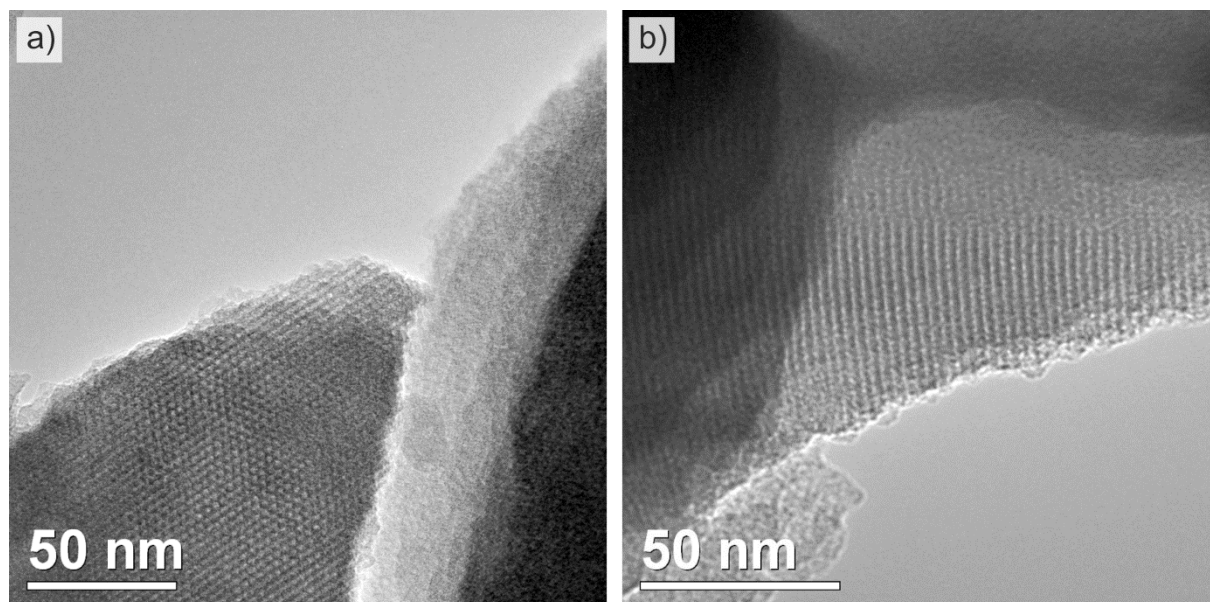


**Figure S6:** Transmission electron micrographs of SBA-15<sub>50A</sub> with two different magnifications. a) The pores follow the direction of the worm-like silica particles, which enables the visibility of different orientations in one micrograph. b) In numerous cases, we found that the pores were not open at the ends of the worm-like particles but blocked by a silica layer.

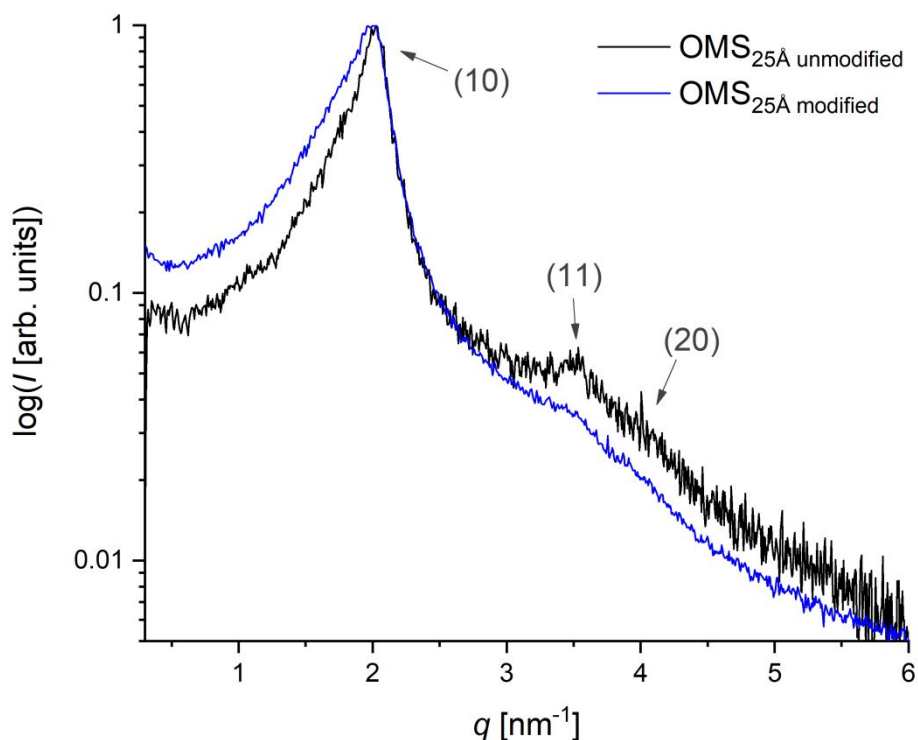


**Figure S7:** Transmission electron micrographs of SBA-15<sub>62A</sub> with two different magnifications. a) The pores follow the direction of the worm-like silica particles,

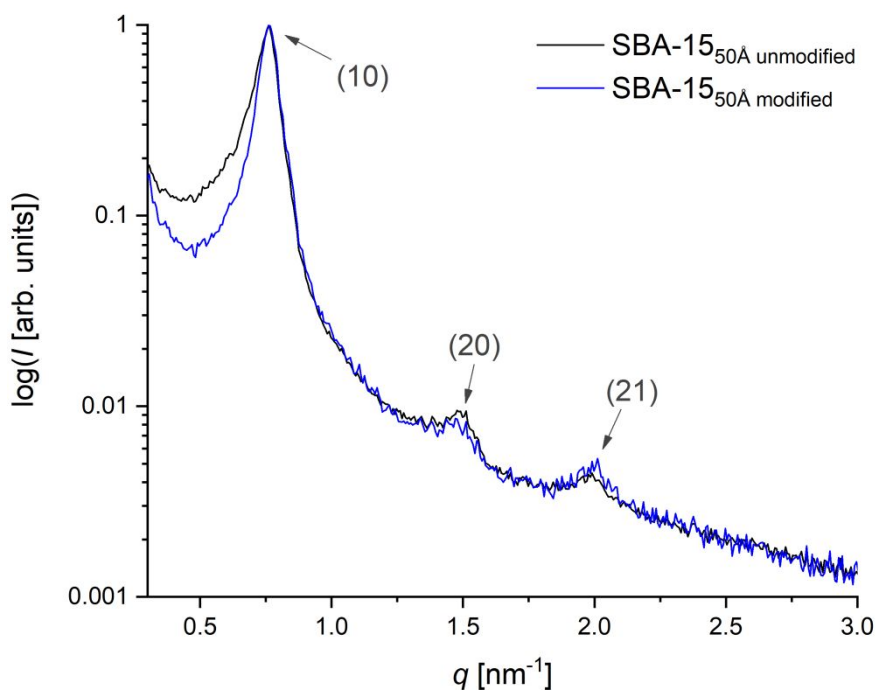
which enables the visibility of different orientations in one micrograph. b) In numerous cases, we found that the pores were not open at the ends of the worm-like particles but blocked by a silica layer.



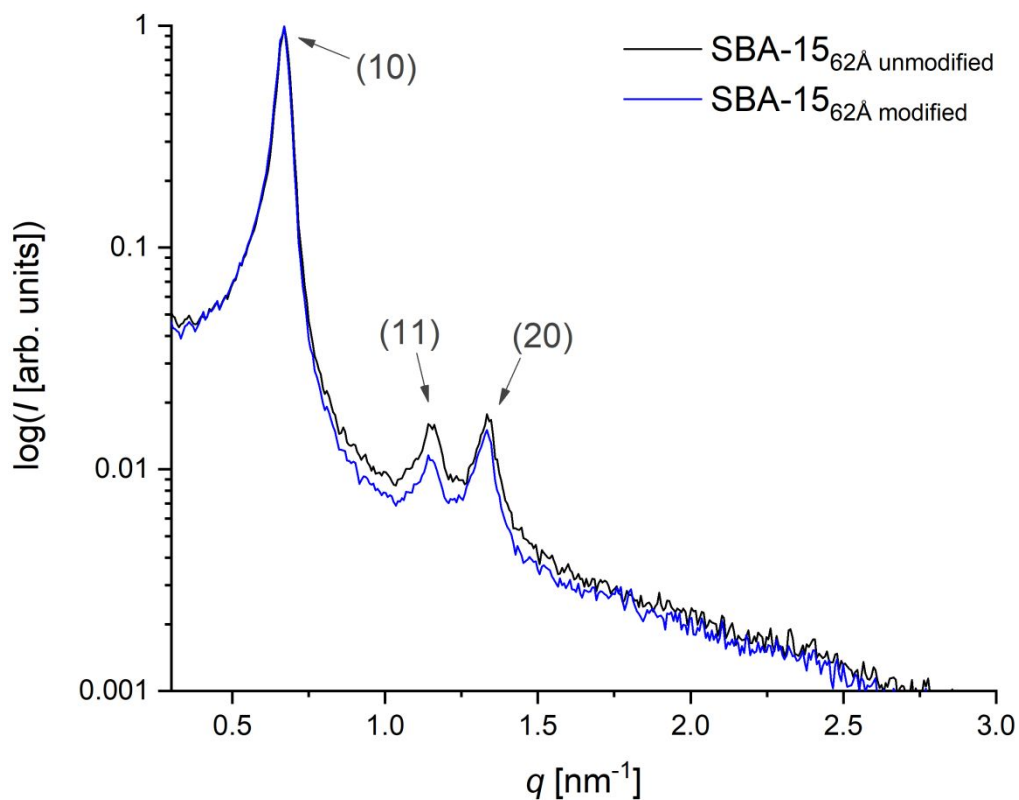
**Figure S8:** Transmission electron micrographs of OMS<sub>25A</sub> with the electron beam direction parallel to the pore direction (a) and perpendicular to the pores (b). Within one grain, the pores exhibit a uniform orientation and are open ended, allowing for a direct access of the pores by solutes.



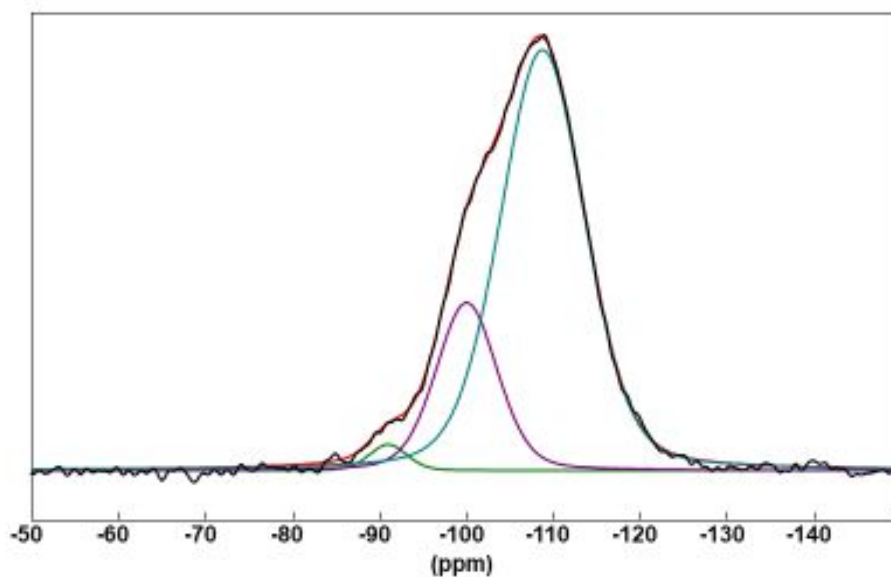
**Figure S9:** Diffractogram of OMS<sub>25Å</sub> unmodified and OMS<sub>25Å</sub> modified (**OMS<sub>25Å</sub>**) with assigned Miller indices ( $hk$ ). The hexagonal lattice parameter of OMS<sub>25Å</sub> was determined as 3.6 nm before modification and as 3.7 nm after modification. With respect to the rather broad scattering maxima and the thus occurring fitting difficulties, the lattice parameter seems to be unaffected by the modification.



**Figure S10:** Diffractogram of SBA-15<sub>50Å</sub> unmodified and SBA-15<sub>50Å</sub> modified (**SBA-15<sub>50Å</sub>**) with assigned Miller indices ( $hk$ ). The hexagonal lattice parameter of SBA-15<sub>50Å</sub> is 9.8 nm.



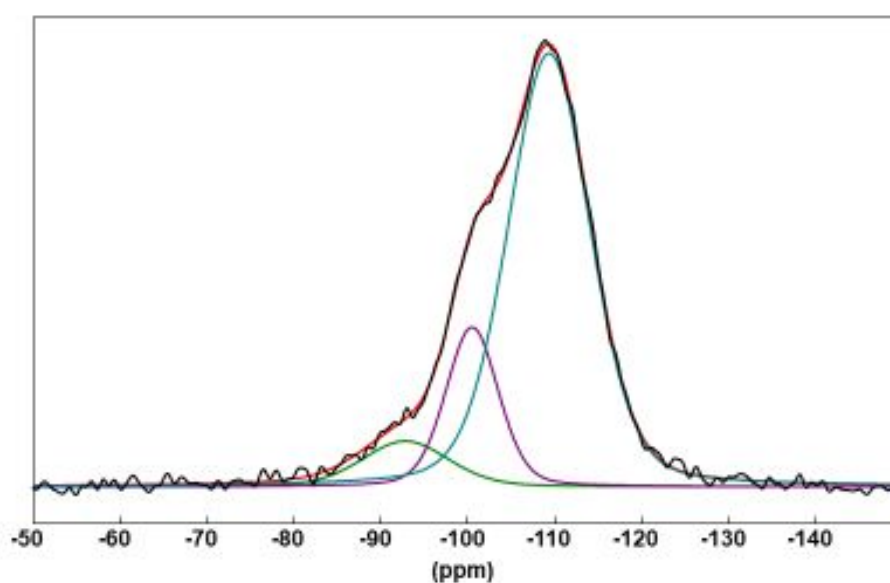
**Figure S11:** Diffractogram of SBA-15<sub>62Å</sub> unmodified and SBA-15<sub>62Å</sub> modified (**SBA-15<sub>62Å</sub>**) with assigned Miller indices ( $hk$ ). The hexagonal lattice parameter of SBA-15<sub>62Å</sub> is 10.7 nm.



**Figure S12:**  $^{29}\text{Si}$  NMR of  $\text{OMS}_{25\text{A}}$  and the allocation of the  $\text{Q}^2$  (green),  $\text{Q}^3$  (purple) and  $\text{Q}^4$  (blue) site on the NMR spectrum.

**Table S1:**  $\text{Q}^2$ ,  $\text{Q}^3$  and  $\text{Q}^4$  content of  $\text{OMS}_{25\text{A}}$ .

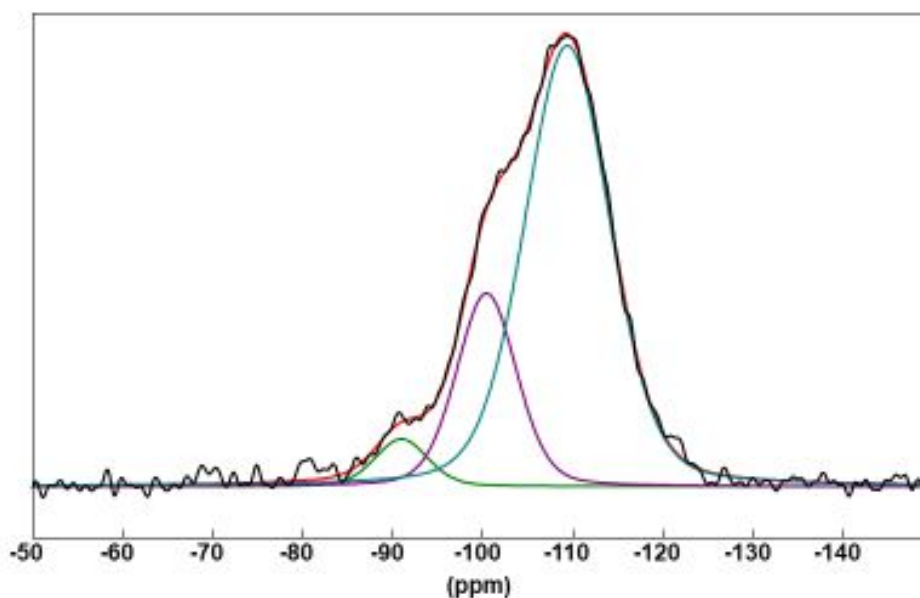
$^{29}\text{Si}$	amp	pos [ppm]	width [ppm]	Gaus/Lor	Integral [%]
$\text{Q}^2$	74593.51	-91.04	5.17	0.76	2.11
$\text{Q}^3$	482031.2	-100.08	8.29	0.76	21.91
$\text{Q}^4$	1204471	-108.82	11.49	0.76	75.97



**Figure S13:**  $^{29}\text{Si}$  NMR of  $\text{SBA-15}_{50\text{A}}$  and the allocation of the  $\text{Q}^2$  (green),  $\text{Q}^3$  (purple) and  $\text{Q}^4$  (blue) site on the NMR spectrum.

**Table S2:** Q<sup>2</sup>, Q<sup>3</sup> and Q<sup>4</sup> content of SBA-15<sub>50A</sub>.

<sup>29</sup> Si	ampl.	pos [ppm]	width [ppm]	Gaus/Lor	Integral [%]
Q <sup>2</sup>	97336.63	-92.94	11.79	0.76	8.22
Q <sup>3</sup>	341146.1	-100.61	7.13	0.76	17.44
Q <sup>4</sup>	929834.2	-109.46	11.14	0.76	74.34

**Figure S14:** <sup>29</sup>Si NMR of SBA-15<sub>62</sub> and the allocation of the Q<sup>2</sup> (green), Q<sup>3</sup> (purple) and Q<sup>4</sup> (blue) site on the NMR spectrum.**Table S3:** Q<sup>2</sup>, Q<sup>3</sup> and Q<sup>4</sup> content of SBA-15<sub>62A</sub>.

<sup>29</sup> Si	Ampl.	pos [ppm]	width [ppm]	Gaus/Lor	Integral [%]
Q <sup>2</sup>	73173.82	-91.07	6.91	0.76	4.76
Q <sup>3</sup>	302694	-100.51	7.85	0.76	22.4
Q <sup>4</sup>	690588.8	-109.48	11.18	0.76	72.84

To investigate whether the catalysis process compromised the structural integrity of the support material or not, we exemplarily investigated SBA-15<sub>50A</sub> modified after the catalysis and found no changes in the scattering pattern (Figure S16).

**Table S4:** Mo-content of different silica types (25 Å, 50 Å and 62 Å mesopore diameter) as determined by ICP-OES.

Mesopore size	silica used for quantification [mg]	c(Mo) in diluted sample [mg/L]	c(Mo) on silica [ $\mu\text{mol Mo/g silica}$ ]
<b>Mo1@SBA-15/OMS</b>			
25 Å	24.3	0.2	1.9
50 Å	38.2	1.3	8.9
62 Å	30.5	2.0	17.1
<b>Mo2@SBA-15/OMS</b>			
25 Å	33.2	0.4	3.0
50 Å	49.6	1.5	7.6
62 Å	49.1	3.0	15.9
<b>Mo3@SBA-15/OMS</b>			
25 Å	27.5	0.2	2.1
50 Å	28.0	0.9	8.5
62 Å	34.5	2.2	16.5
<b>Mo4@SBA-15/OMS</b>			
25 Å	23.0	0.3	3.7
50 Å	35.1	1.3	9.7
62 Å	33.8	2.4	18.5

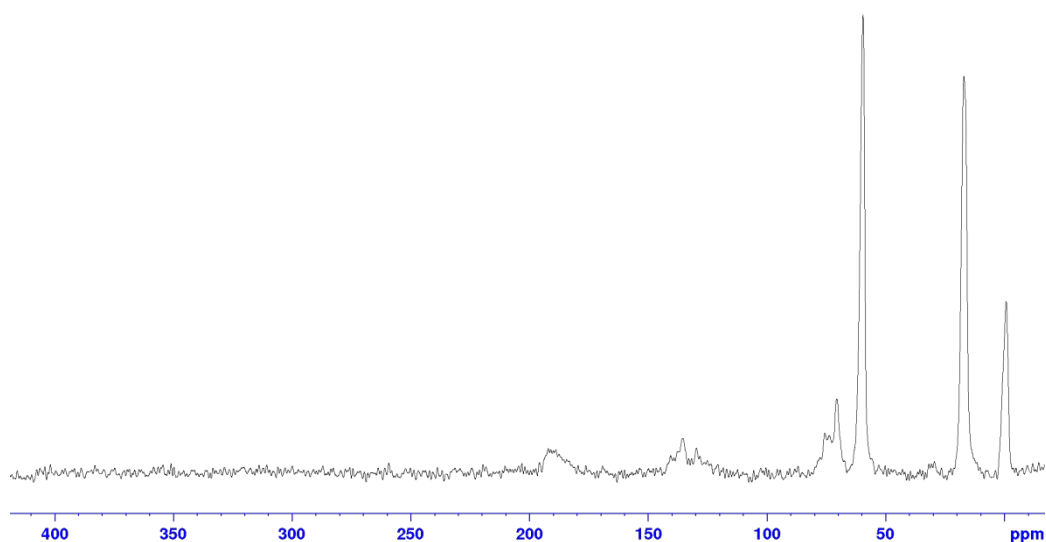


**Figure S15:**  $^{13}\text{C}$  CP/MAS NMR of **Mo5\*@SBA-15<sub>62A</sub>**.

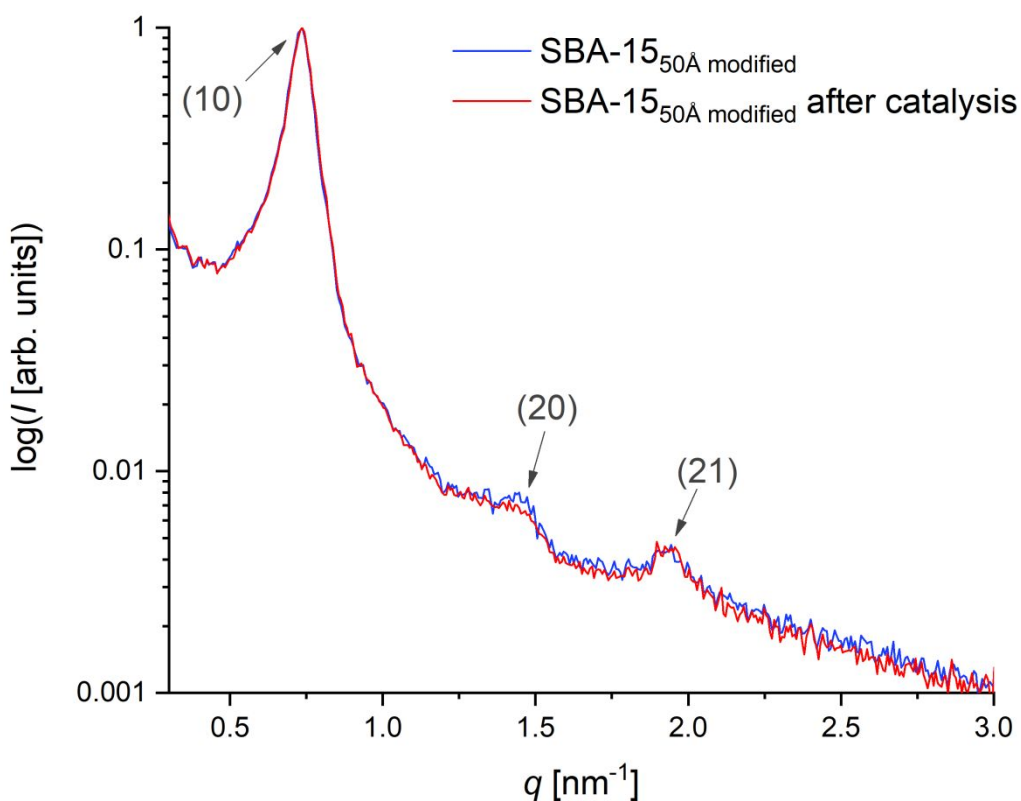


**Figure S16:** Diffractogram of OMS<sub>50Å unmodified</sub> before and after catalysis.

## 8. Macrocyclization Reactions

### Standard Reactions

For the correct determination of conversion by NMR, the deconvolution function of the MestReNova program (Version 12.0.0) was used. This was necessary because part of the signals for the terminal double bonds of the oligomers were covered by the signals of the starting material (see Figure S17).

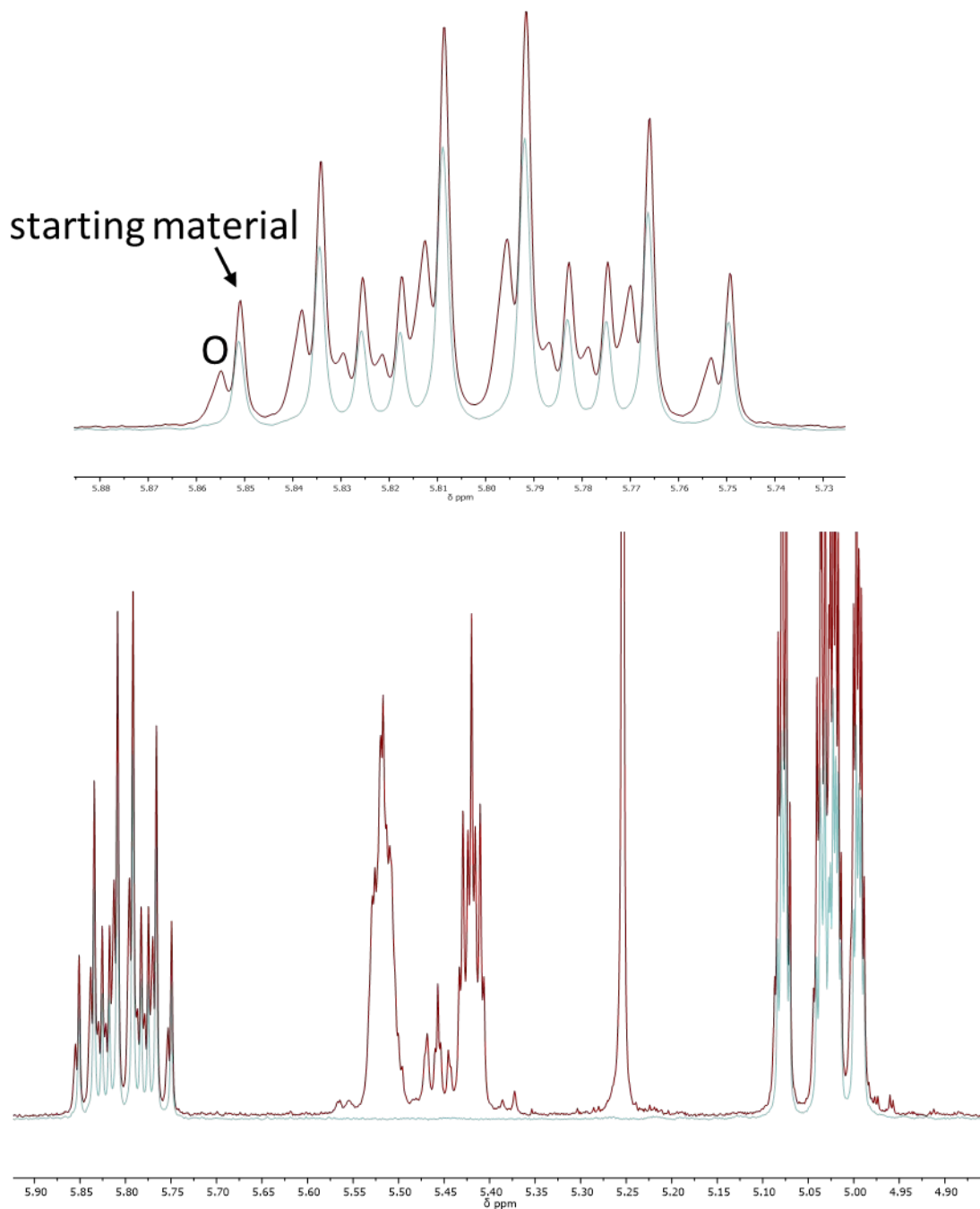


**Figure S17:** Stacked <sup>1</sup>H NMR spectrum of the starting material **4** (green) and the reaction mixture of the MMC reaction of **4** with the homogeneous catalyst **Mo1@OSiPh<sub>3</sub>** (red) in C<sub>6</sub>D<sub>6</sub>.

The determination of the MMC:O ratios by NMR is exemplified for substrate **4**. One needs to integrate the oligomer signal (O) around 5.525 ppm and the signals for the *E*- and *Z*-monomacrocycles (MMC) at 5.457 ppm and 5.429 ppm, respectively (see Figure S17). Note hereby, that the signals for the *E*- and *Z*-monomacrocycles are substrate-

specific. The ratio of the oligomer signal and the sum of the *E*- and *Z*-monomacrocycles yield the MMC:O value.

**General procedure for the RCM of  $\alpha,\omega$ -dienes (GP-4).** The substrate was dissolved in  $C_6D_6$  (1000  $\mu$ L) and the catalyst (stock solution) was added. After 16 hours,  $^1H$  NMR spectra were acquired. Conversion and MMC:O ratios were determined by integration of the corresponding signals.

**Example reaction with 0.5 mol% catalyst, MMC with Mo1@OSiPh<sub>3</sub>: 4** (10.9 mg, 0.025 mmol, 1 eq.) was dissolved in  $C_6D_6$  (965.2  $\mu$ L, 26.1 mM) and a stock solution of catalyst Mo1@OSiPh<sub>3</sub> (43.8  $\mu$ L, 2.9 mM; 0.5 mol-%) was added. The resulting mixture (substrate concentration 25 mM) was stirred for 16 hours and subjected to  $^1H$  NMR spectroscopy. Overall conversion: 74%. MMC:O = 0.99 (selectivity = 50%).

**Example reaction with 1 mol% catalyst, MMC with Mo1@OSiPh<sub>3</sub>: 4** (10.9 mg, 0.025 mmol, 1 eq.) was dissolved in  $C_6D_6$  (912.5  $\mu$ L, 27.4 mM) and a stock solution of catalyst Mo1@OSiPh<sub>3</sub> (87.5  $\mu$ L, 2.9 mM; 1.0 mol-%) was added. The resulting mixture (substrate concentration 25 mM) was stirred for 16 hours and subjected to  $^1H$  NMR spectroscopy. Overall conversion: 76%. MMC:O = 0.99 (selectivity = 50%).

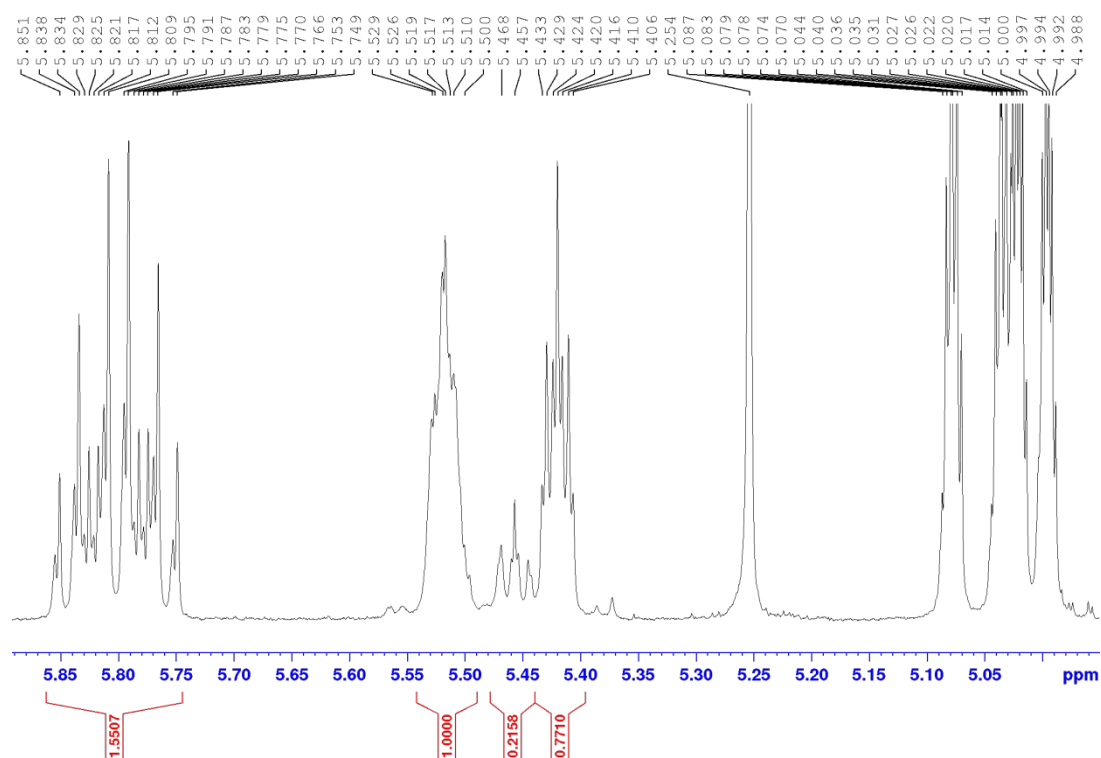


**Figure S18:**  $^1H$  NMR spectrum of the reaction mixture of the MMC of **4** with the homogeneous catalyst Mo1@OSiPh<sub>3</sub> in  $C_6D_6$ . Ratio of MMC to oligomerization MMC/O = 0.99 (selectivity = 50%).

**Table S5:** Conversion, MMC:O ratio, selectivity and Z/E ratio for the RCM of substrate **1** by the action of **Mo1@OSiPh<sub>3</sub>** – **Mo4@OSiPh<sub>3</sub>** as determined by NMR.

	Conversion [%]	MMC:O	Selectivity [%]	Z/E
<b>Mo1@OSiPh<sub>3</sub></b>				
0.5 mol%	71	0.97	49	0.45
1.0 mol%	69	0.92	48	0.52
<b>Mo2@OSiPh<sub>3</sub></b>				
0.5 mol%	64	1.29	56	0.43
1.0 mol%	71	0.88	47	0.52
<b>Mo3@OSiPh<sub>3</sub></b>				
0.5 mol%	72	0.83	45	0.51
1.0 mol%	71	0.85	46	0.54
<b>Mo4@OSiPh<sub>3</sub></b>				
0.5 mol%	71	0.94	49	0.51
1.0 mol%	72	0.88	47	0.50

**Table S6:** Conversion, MMC:O ratio, selectivity and Z/E ratio for the RCM of substrate **2** by the action of **Mo1@OSiPh<sub>3</sub>** – **Mo4@OSiPh<sub>3</sub>** as determined by NMR.

	Conversion [%]	MMC:O	Selectivity [%]	Z/E
<b>Mo1@OSiPh<sub>3</sub></b>				
0.5 mol%	79	0.45	31	0.23
1.0 mol%	75	0.41	29	0.23
<b>Mo2@OSiPh<sub>3</sub></b>				
0.5 mol%	76	0.43	30	0.23
1.0 mol%	77	0.42	29	0.25
<b>Mo3@OSiPh<sub>3</sub></b>				
0.5 mol%	71	0.43	30	0.23
1.0 mol%	79	0.40	29	0.24
<b>Mo4@OSiPh<sub>3</sub></b>				
0.5 mol%	71	0.46	31	0.24
1.0 mol%	77	0.41	29	0.24

**Table S7:** Conversion, MMC:O ratio, selectivity and Z/E ratio for the RCM of substrate **3** by the action of **Mo1@OSiPh<sub>3</sub>** – **Mo4@OSiPh<sub>3</sub>** as determined by NMR.

	Conversion [%]	MMC:O	Selectivity [%]	Z/E
<b>Mo1@OSiPh<sub>3</sub></b>				
0.5 mol%	78	4.23	81	0.23
1.0 mol%	76	4.56	82	0.17
<b>Mo2@OSiPh<sub>3</sub></b>				
0.5 mol%	79	4.29	81	0.23
1.0 mol%	77	4.56	82	0.21
<b>Mo3@OSiPh<sub>3</sub></b>				
0.5 mol%	79	3.92	80	0.24
1.0 mol%	79	4.56	82	0.20
<b>Mo4@OSiPh<sub>3</sub></b>				
0.5 mol%	79	4.04	80	0.24
1.0 mol%	79	4.07	80	0.23

**Table S8:** Conversion, MMC:O ratio, selectivity and Z/E ratio for the RCM of substrate **4** by the action of **Mo1@OSiPh<sub>3</sub>** – **Mo4@OSiPh<sub>3</sub>** as determined by NMR.

	Conversion [%]	MMC:O	Selectivity [%]	Z/E
<b>Mo1@OSiPh<sub>3</sub></b>				
0.5 mol%	74	0.99	50	0.26
1.0 mol%	76	0.99	50	0.28
<b>Mo2@OSiPh<sub>3</sub></b>				
0.5 mol%	70	1.15	53	0.25
1.0 mol%	76	0.95	49	0.32
<b>Mo3@OSiPh<sub>3</sub></b>				
0.5 mol%	65	1.13	53	0.25
1.0 mol%	77	0.92	48	0.31
<b>Mo4@OSiPh<sub>3</sub></b>				
0.5 mol%	70	1.17	54	0.22
1.0 mol%	76	0.93	48	0.30

**General procedure for the RCM of  $\alpha,\omega$ -dienes with catalyst @ OMS/SBA-15 (GP-5).** The substrate was dissolved in  $C_6D_6$  (1.0 mL) and the corresponding SBA-15/OMS material containing the catalyst (12-50 mg, depending on the Mo content) was added. After 16 hours,  $^1H$  NMR data were acquired. Conversion, the MMC:O ratio and the selectivity were determined by integration of the corresponding signals.

**MMC with Mo1@OMS<sub>25A</sub>:** **4** (10.9 mg, 0.025 mmol, 1 eq.) was dissolved in  $C_6D_6$  (1.00 mL, 25 mM) and **Mo1@OMS<sub>25A</sub>** (46.8 mg, 0.5 mol-%) was added. The resulting mixture was stirred for 16 hours and subjected to  $^1H$  NMR spectroscopy. Overall conversion: 34%. MMC:O = 5.59 (selectivity = 85%).

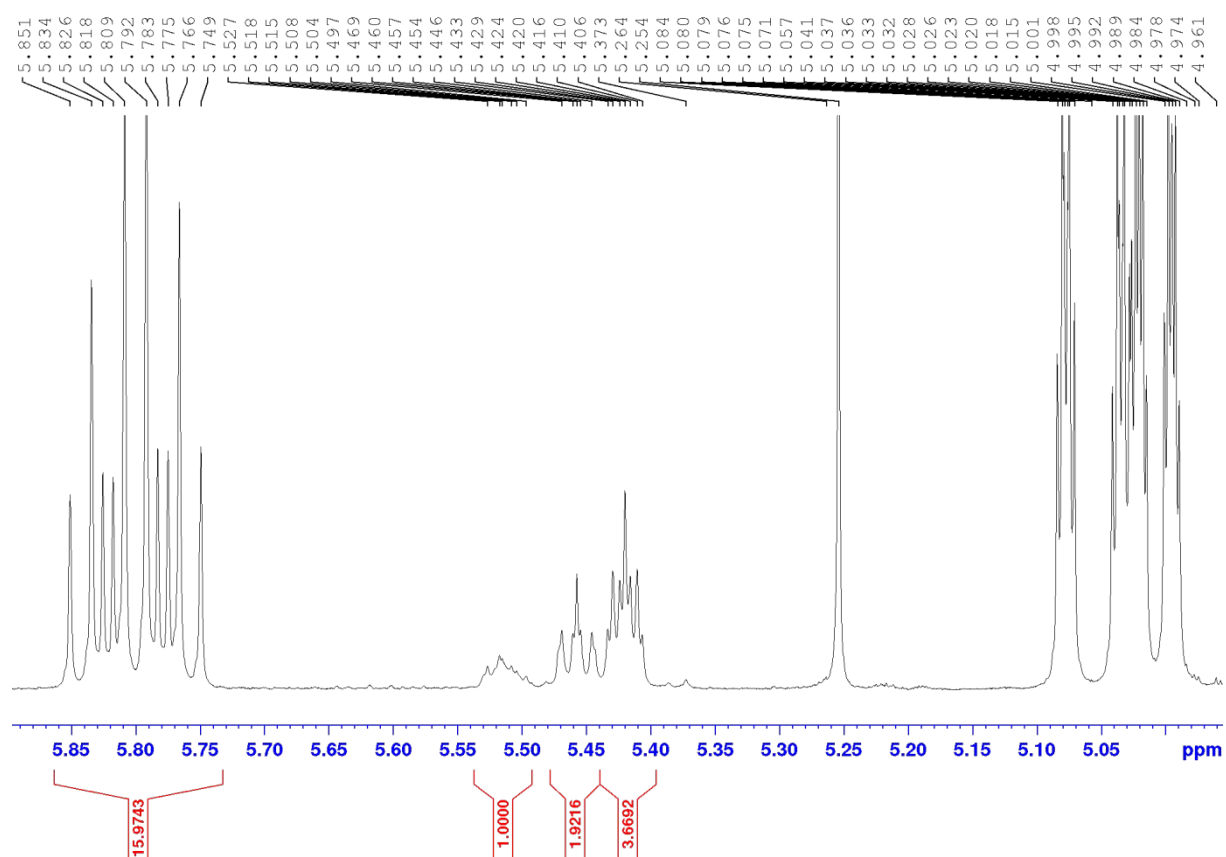


**Figure S19:**  $^1H$  NMR spectrum of the MMC reaction mixture of **4** with the homogeneous catalyst **Mo1@OMS<sub>25A</sub>** in  $C_6D_6$ . MMC:O = 5.59 (selectivity = 85%).

**MMC with Mo1@SBA-15<sub>50A</sub>:** **4** (10.9 mg, 0.025 mmol, 1 eq.) was dissolved in  $C_6D_6$  (1.00 mL, 25 mM) and **Mo1@SBA-15<sub>50A</sub>** (32.2 mg, 1.0 mol-%) was added. The resulting mixture was stirred for 16 hours and subjected to  $^1H$  NMR spectroscopy. Overall conversion: 21%. MMC:O = 3.30 (selectivity = 77%).

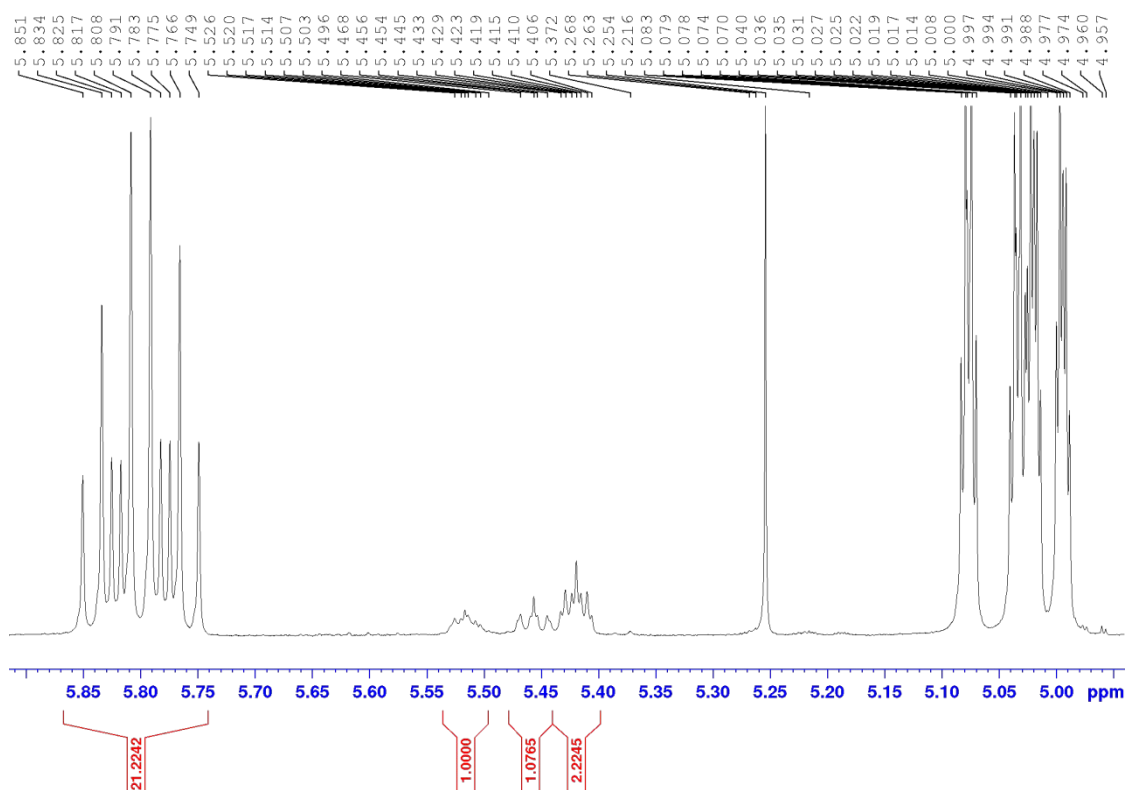


**Figure S20:**  $^1\text{H}$  NMR spectrum of the reaction mixture of the MMC of **4** with the homogeneous catalyst **Mo1@SBA-15<sub>50A</sub>** in  $\text{C}_6\text{D}_6$ . MMC:O = 3.30 (selectivity = 77%).

**MMC with Mo1@SBA-15<sub>62A</sub>:** **4** (10.9 mg, 0.025 mmol, 1 eq.) was dissolved in  $\text{C}_6\text{D}_6$  (1.00 mL, 25 mM) and **Mo1@SBA-15<sub>62A</sub>** (18.1 mg, 1.0 mol-%) was added. The resulting mixture was stirred for 16 hours and subjected to  $^1\text{H}$  NMR spectroscopy. Overall conversion: 50%. MMC:O = 2.47 (selectivity = 71%).

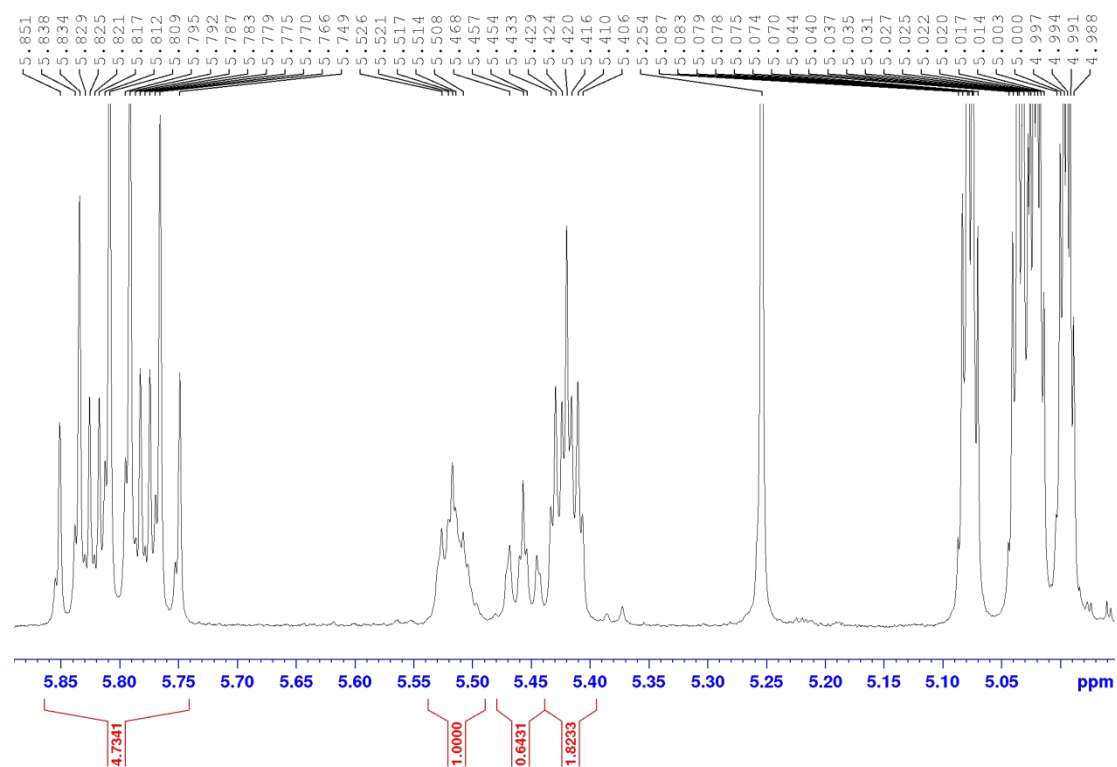


**Figure S21:**  $^1\text{H}$  NMR spectrum of the reaction mixture of the MMC of **4** with the homogeneous catalyst **Mo1@SBA-15**<sub>62A</sub> in  $\text{C}_6\text{D}_6$ . MMC:O = 2.47 (selectivity = 71%).

**Table S9:** Conversion, MMC:O ratio, selectivity and Z/E ratio for the RCM of substrate **1** by the action of **Mo1@OMS<sub>25A</sub>/SBA-15<sub>50A, 62A</sub>** – **Mo4@OMS<sub>25A</sub>/SBA-15<sub>50A, 62A</sub>** as determined by NMR.

Mesopore size	Conversion [%]	MMC:O	Selectivity [%]	Z/E
<b>Mo1@OMS/SBA-15</b>				
25 Å	34	5.22	84	0.81
50 Å	22	3.90	80	0.57
62 Å	41	3.10	76	0.45
<b>Mo2@OMS/SBA-15</b>				
25 Å	30	5.71	85	0.87
50 Å	28	3.83	79	0.52
62 Å	26	3.30	77	0.57
<b>Mo3@OMS/SBA-15</b>				
25 Å	10	5.12	84	0.96
50 Å	23	4.05	80	0.42
62 Å	43	3.48	78	0.42
<b>Mo4@OMS/SBA-15</b>				
25 Å	36	5.56	85	0.77
50 Å	14	3.91	80	0.85
62 Å	15	3.00	75	0.86

**Table S10:** Conversion, MMC:O ratio, selectivity and Z/E ratio for the RCM of substrate **2** by the action of **Mo1@OMS<sub>25A</sub>/SBA-15<sub>50A, 62A</sub>** – **Mo4@OMS<sub>25A</sub>/SBA-15<sub>50A, 62A</sub>** as determined by NMR.

Mesopore size	Conversion [%]	MMC:O	Selectivity [%]	Z/E
<b>Mo1@OMS/SBA-15</b>				
25 Å	26	4.69	82	0.52
50 Å	18	2.63	72	0.57
62 Å	40	2.26	69	0.38
<b>Mo2@OMS/SBA-15</b>				
25 Å	19	4.28	81	0.58
50 Å	27	2.78	74	0.38
62 Å	25	2.41	71	0.38
<b>Mo3@OMS/SBA-15</b>				
25 Å	7	3.65	78	0.63
50 Å	16	2.99	75	0.28
62 Å	39	2.75	73	0.20
<b>Mo4@OMS/SBA-15</b>				
25 Å	24	3.24	76	0.49
50 Å	25	2.49	71	0.61
62 Å	29	2.07	67	0.58

**Table S11:** Conversion, MMC:O ratio, selectivity and Z/E ratio for the RCM of substrate **3** by the action of **Mo1@OMS<sub>25A</sub>/SBA-15<sub>50A, 62A</sub>** – **Mo4@OMS<sub>25A</sub>/SBA-15<sub>50A, 62A</sub>** as determined by NMR.

Mesopore size	Conversion [%]	MMC:O	Selectivity [%]	Z/E
<b>Mo1@OMS/SBA-15</b>				
25 Å	21	39.87	98	0.66
50 Å	23	15.40	94	0.34
62 Å	32	14.28	93	0.26
<b>Mo2@OMS/SBA-15</b>				
25 Å	19	28.38	97	0.62
50 Å	27	19.44	95	0.34
62 Å	25	15.50	94	0.34
<b>Mo3@OMS/SBA-15</b>				
25 Å	4	15.37	94	0.72
50 Å	18	18.67	95	0.28
62 Å	32	16.54	94	0.21
<b>Mo4@OMS/SBA-15</b>				
25 Å	24	35.23	97	0.55
50 Å	16	16.59	94	0.57
62 Å	15	13.14	93	0.53

**Table S12:** Conversion, MMC:O ratio, selectivity and Z/E ratio for the RCM of substrate **4** by the action of **Mo1@OMS<sub>25A</sub>/SBA-15<sub>50A, 62A</sub>** – **Mo4@OMS<sub>25A</sub>/SBA-15<sub>50A, 62A</sub>** as determined by NMR.

Mesopore size	Conversion [%]	MMC:O	Selectivity [%]	Z/E
<b>Mo1@OMS/SBA-15</b>				
25 Å	31	5.59	85	0.67
50 Å	21	3.30	77	0.48
62 Å	50	2.47	71	0.35
<b>Mo2@OMS/SBA-15</b>				
25 Å	25	5.23	84	0.55
50 Å	37	3.50	78	0.39
62 Å	34	2.61	72	0.38
<b>Mo3@OMS/SBA-15</b>				
25 Å	5	4.13	81	0.56
50 Å	30	3.37	77	0.30
62 Å	51	2.52	72	0.29
<b>Mo4@OMS/SBA-15</b>				
25 Å	31	5.94	86	0.48
50 Å	28	3.34	77	0.61
62 Å	32	2.37	70	0.52

## Kinetics

**Table S13:** Conversion, MMC:O ratio, selectivity and Z/E ratio for the RCM of substrate **1** by the action of **Mo1@OSiPh<sub>3</sub>** (0.5 mol%) as determined by NMR.

Time [min]	Conversion [%]	MMC:O	Selectivity [%]	Z/E
10	4	1.54	61	0.15
16	9	1.53	60	0.15
22	14	1.54	61	0.18
28	18	1.54	61	0.20
40	22	1.65	62	0.30
52	34	1.65	62	0.30
64	41	1.45	60	0.27
100	50	1.36	58	0.29
130	53	1.31	57	0.32
160	56	1.26	56	0.35
960	71	0.96	49	0.45

**Table S14:** Conversion, MMC:O ratio, selectivity and Z/E ratio for the RCM of substrate **1** by the action of **Mo1@OSiPh<sub>3</sub>** (1.0 mol%) as determined by NMR.

Time [min]	Conversion [%]	MMC:O	Selectivity [%]	Z/E
7	20	1.61	62	0.29
14	34	1.59	61	0.27
21	38	1.59	61	0.27
28	42	1.59	61	0.31
70	50	1.47	60	0.31
147	58	1.37	58	0.33
960	69	0.92	48	0.52

**Table S15:** Conversion, MMC:O ratio, selectivity and Z/E ratio for the RCM of substrate **1** by the action of **Mo1@OMS<sub>25A</sub>** as determined by NMR.

Time [min]	Conversion [%]	MMC:O	Selectivity [%]	Z/E
15	11	5.87	85	1.09
30	14	6.09	86	1.08
60	17	5.98	86	1.07
150	22	6.05	86	0.97
960	34	5.22	84	0.81

**Table S16:** Conversion, MMC:O ratio, selectivity and Z/E ratio for the RCM of substrate **1** by the action of **Mo1@SBA-15<sub>50A</sub>** as determined by NMR.

Time [min]	Conversion [%]	MMC:O	Selectivity [%]	Z/E
15	6	3.54	78	1.10
30	8	3.11	76	0.85
60	12	3.39	77	0.74
150	15	3.72	78	0.65
300	16	3.76	79	0.64
960	22	3.90	80	0.57

**Table S17:** Conversion, MMC:O ratio, selectivity and Z/E ratio for the RCM of substrate **1** by the action of **Mo1@SBA-15<sub>62A</sub>** with substrate **1** as determined by NMR.

Time [min]	Conversion [%]	MMC:O	Selectivity [%]	Z/E
15	12	3.20	76	0.69
30	15	3.31	77	0.60
60	21	3.17	76	0.51
150	29	3.34	77	0.48
300	34	3.26	77	0.47
960	41	3.10	76	0.45

### Variation of Concentration

**Table S18:** Conversion, MMC:O, selectivity and *Z/E* ratio for the RCM of substrate **1** by the action of **Mo1@OSiPh<sub>3</sub>** (0.5 mol%) as determined by NMR at different substrate concentrations.

Concentration [mmol/L]	Conversion [%]	MMC:O	Selectivity [%]	<i>Z/E</i>
5	77	6.39	86	0.44
10	68	2.41	71	0.50
25	71	0.97	49	0.45
50	74	0.36	27	0.33
100	81	0.21	19	0.36

**Table S19:** Conversion, MMC:O, selectivity and *Z/E* ratio for the RCM of substrate **1** by the action of **Mo1@OSiPh<sub>3</sub>** (1.0 mol%) as determined by NMR at different substrate concentrations.

Concentration [mmol/L]	Conversion [%]	MMC.O	Selectivity [%]	<i>Z/E</i>
5	77	6.31	86	0.40
10	67	2.73	73	0.40
25	69	0.92	48	0.52
50	73	0.51	34	0.54
100	69	0.21	18	0.66

**Table S20:** Conversion, MMC:O, selectivity and *Z/E* ratio for the RCM of substrate **1** by the action of **Mo1@OMS<sub>25A</sub>** as determined by NMR at different substrate concentrations.

Concentration [mmol/L]	Conversion [%]	MMC:O	Selectivity [%]	<i>Z/E</i>
5	51	11.90	92	0.82
10	48	8.96	89	0.79
25	34	5.22	84	0.81
50	36	3.46	78	0.81
100	34	1.46	59	0.76

**Table S21:** Conversion, MMC:O, selectivity and Z/E ratio for the RCM of substrate **1** by the action of **Mo1@SBA-15<sub>50A</sub>** as determined by NMR at different substrate concentrations.

Concentration [mmol/L]	Conversion [%]	MMC:O	Selectivity [%]	Z/E
5	17	6.34	86	0.74
10	16	5.81	85	0.70
25	22	3.90	80	0.57
50	14	2.43	71	0.70
100	15	1.70	57	0.66

**Table S22:** Conversion, MMC:O, selectivity and Z/E ratio for the RCM of substrate **1** by the action of **Mo1@SBA-15<sub>62A</sub>** as determined by NMR at different substrate concentrations.

Concentration [mmol/L]	Conversion [%]	MMC:O	Selectivity [%]	Z/E
5	43	9.48	90	0.51
10	44	6.10	86	0.49
25	41	3.10	76	0.45
50	50	1.79	64	0.51
100	51	0.81	45	0.41

### Reactions Carried out Under Static Vacuum

**Table S23:** Conversion, MMC:O, selectivity and Z/E ratio **Mo1@OMS<sub>25A</sub>/SBA-15<sub>50A</sub>,<sub>62A</sub>** with substrate **1** determined by NMR.

Mesopore size [Å]	Conversion [%]	MMC:O	Selectivity [%]	Z/E
<b>Without Vacuum</b>				
25	34	5.22	84	0.81
50	22	3.90	80	0.57
62	41	3.10	76	0.45
<b>With Vacuum</b>				
25	36	5.92	85	1.00
50	36	3.63	78	0.58
62	88	2.55	72	0.56

## 9. MALDI-TOF Measurements

**Table S24:** Signal intensities and relative oligomer percentages for the RCM of **Mo1@OSiPh<sub>3</sub>** with **1**.

	Dimer	Trimer	Tetramer	Pentamer
Signal Intensity	7464	1336	151	22
Relative Percentage [%]	83.2	14.9	1.7	0.2

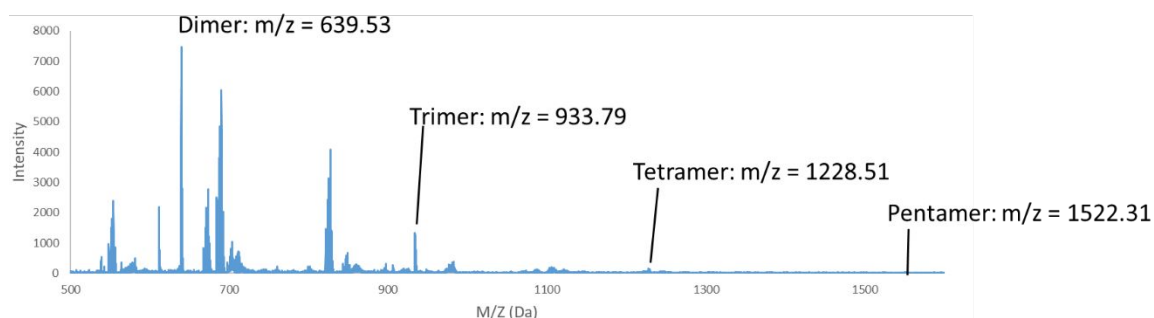


**Figure S22:** Representative MALDI-TOF spectrum of the products formed in the RCM of **1** using **Mo1@OSiPh<sub>3</sub>**.

**Table S25:** Signal intensities and relative oligomer percentages for the RCM of **Mo1@OMS<sub>25A</sub>** with **1**.

	Dimer	Trimer	Tetramer
Signal Intensity	5713	102	45
Relative Percentage [%]	97.5	1.7	0.8

**Table S26:** Signal intensities and relative oligomer percentages for the RCM of **Mo1@SBA-15<sub>50A</sub>** with **1**.

	Dimer	Trimer	Tetramer
Signal Intensity	3001	77	12
Relative Percentage [%]	97.1	2.5	0.4

**Table S27:** Signal intensities and relative oligomer percentages for the RCM of **Mo1@SBA-15<sub>62A</sub>** with **1**.

	Dimer	Trimer	Tetramer
Signal Intensity	50129	2723	95
Relative Percentage [%]	94.7	5.1	0.2

## 10. Spectra of Relevant Compounds

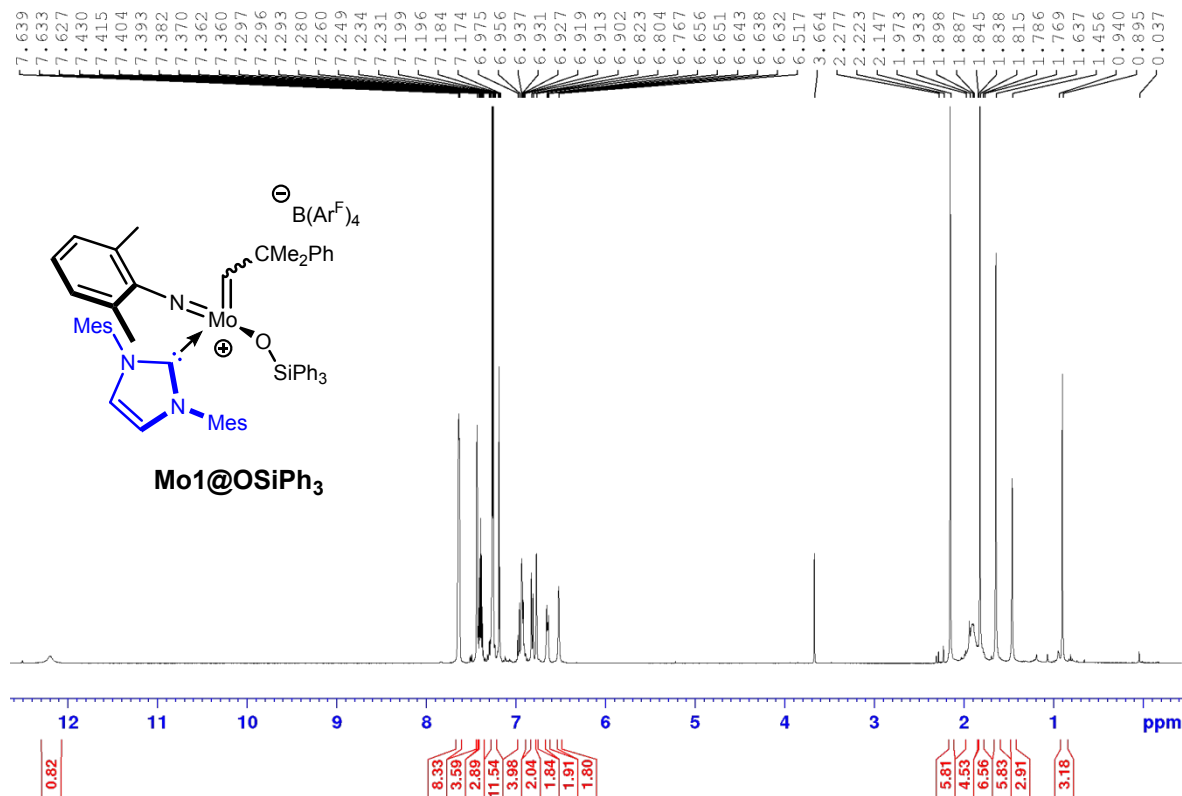


Figure S23: <sup>1</sup>H NMR (400 MHz, CDCl<sub>3</sub>) spectrum of Mo1@OSiPh<sub>3</sub>.

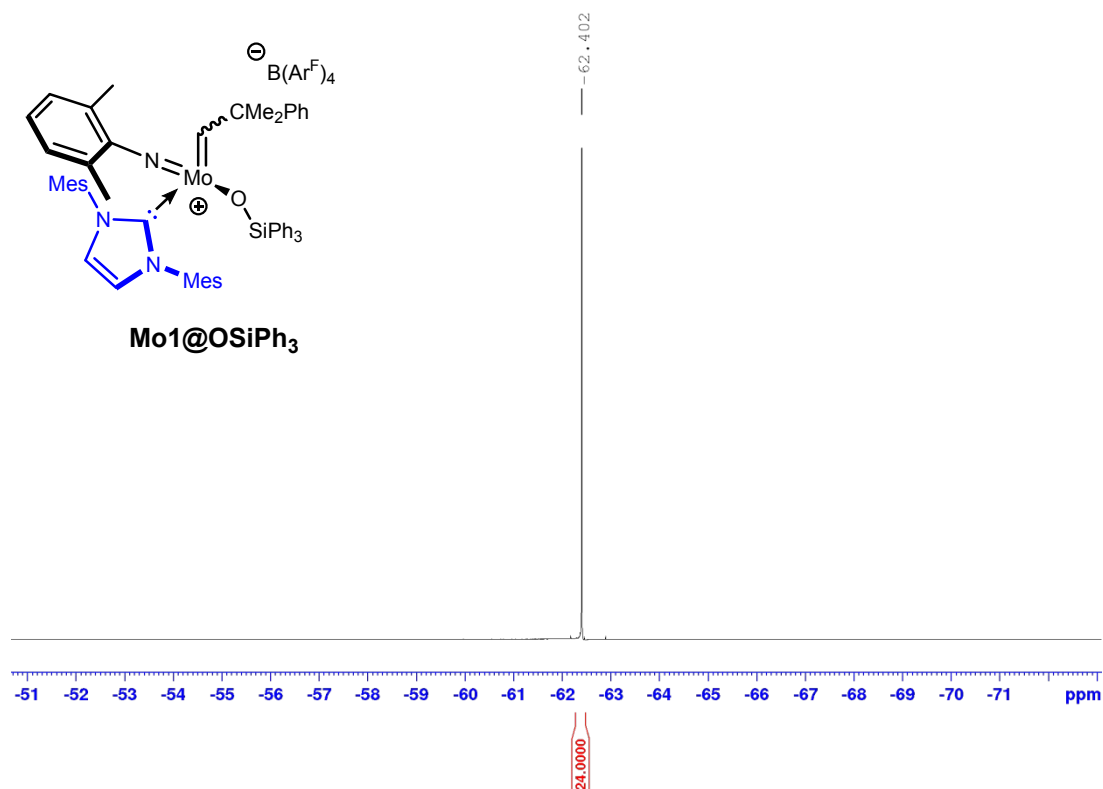


Figure S24: <sup>19</sup>F NMR (376 MHz, CDCl<sub>3</sub>) spectrum of Mo1@OSiPh<sub>3</sub>.

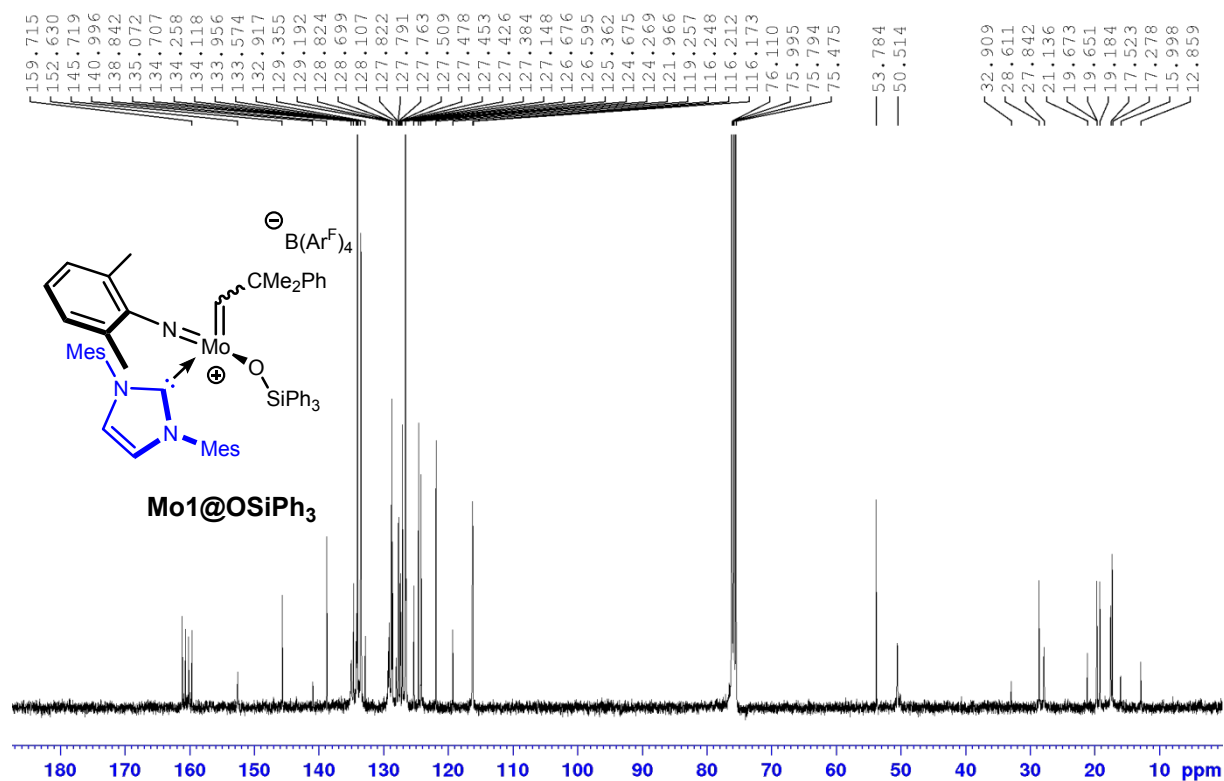


Figure S25:  $^{13}\text{C}$  NMR (101 MHz,  $\text{CDCl}_3$ ) spectrum of  $\text{Mo1@OSiPh}_3$ .

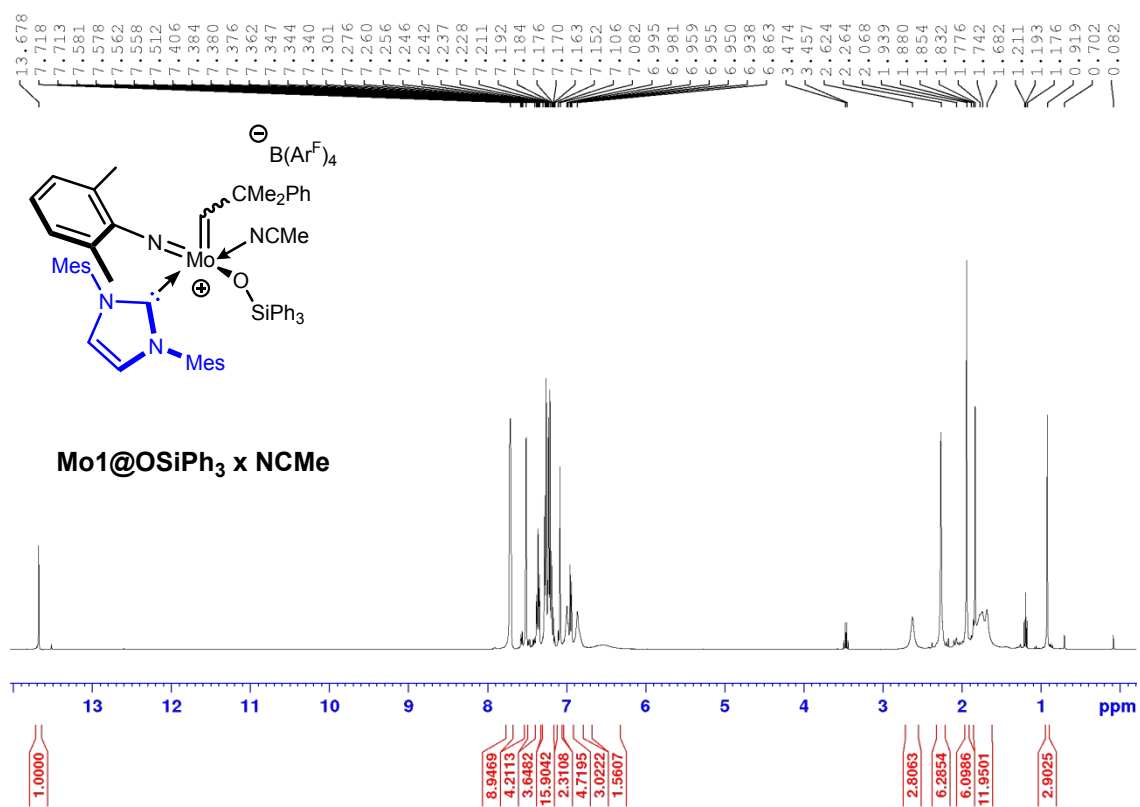
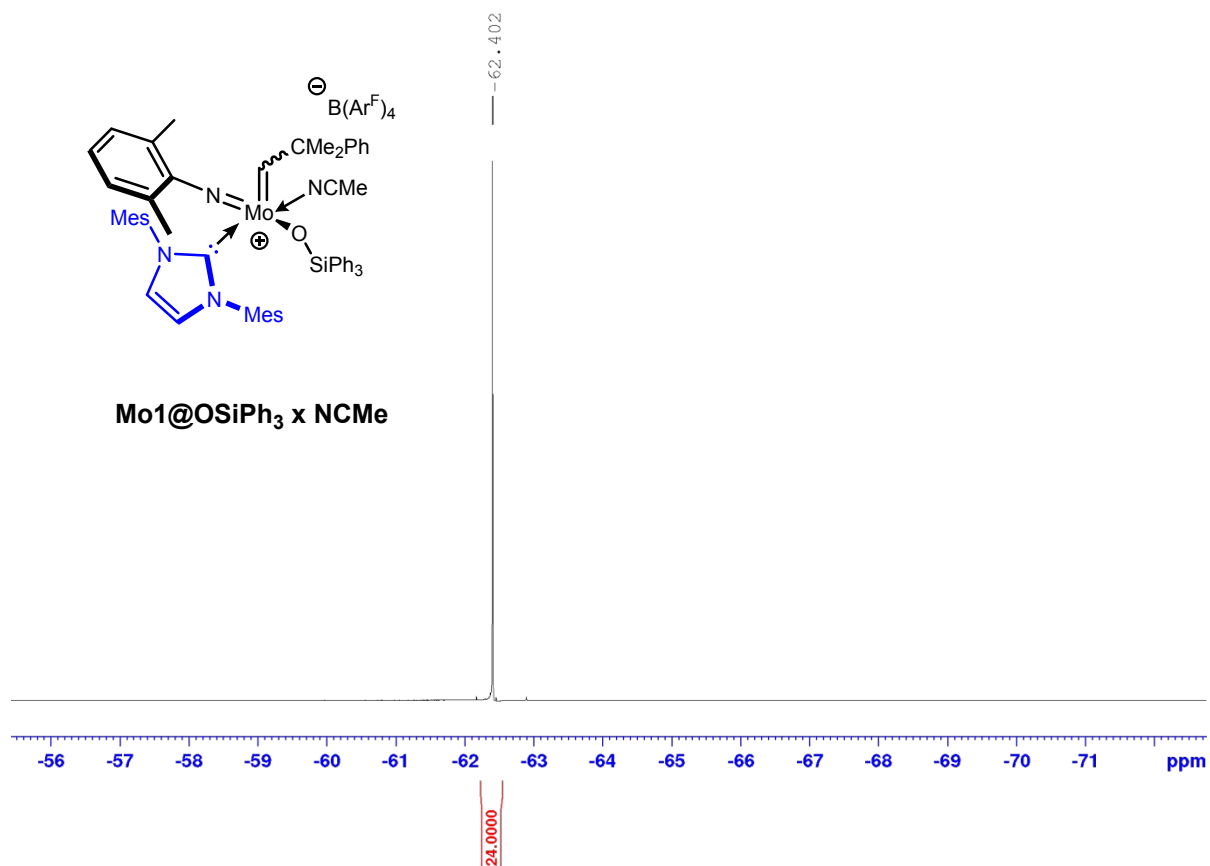
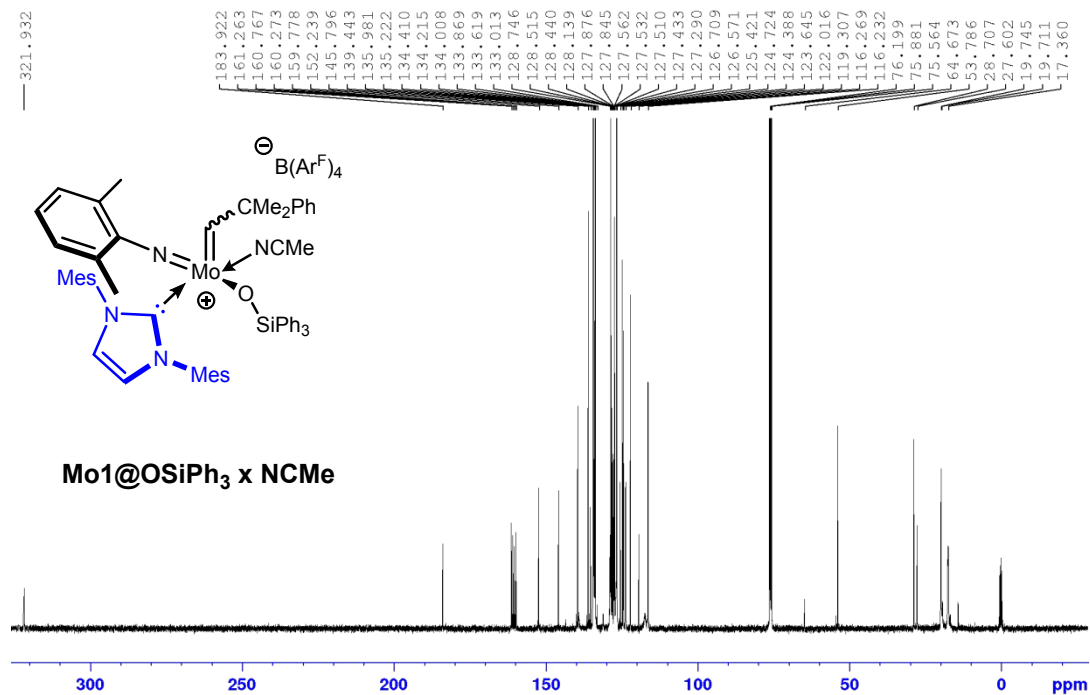


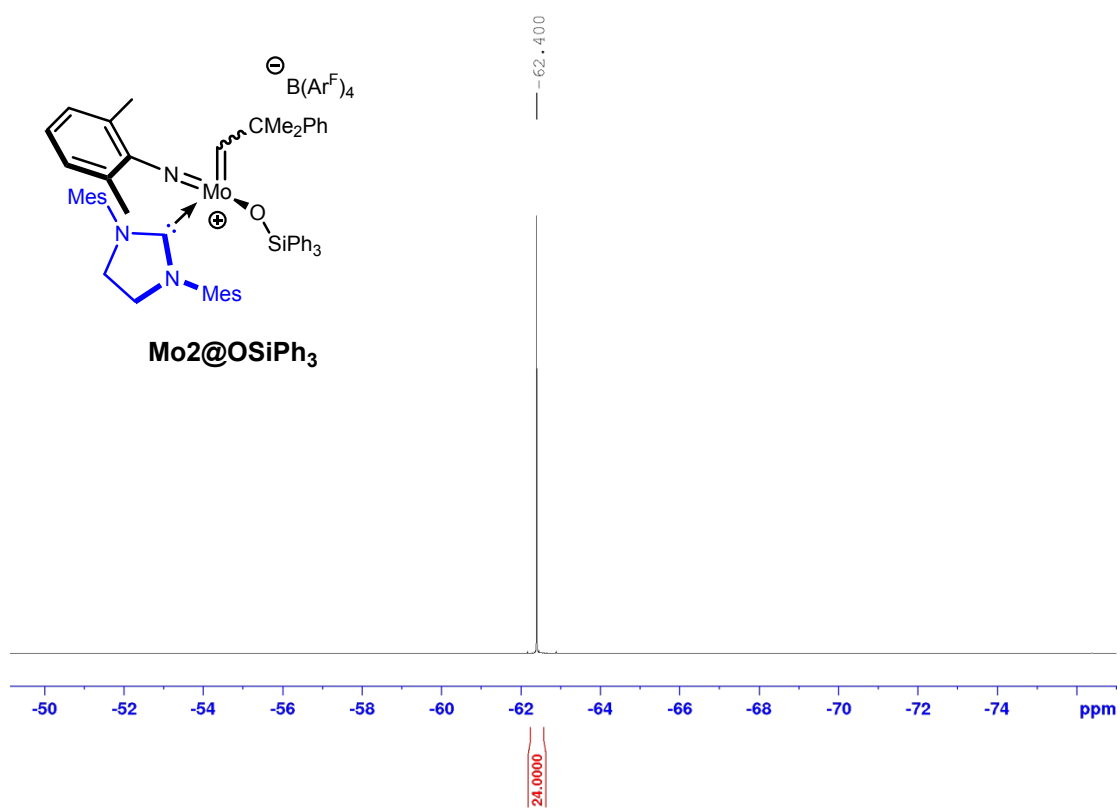
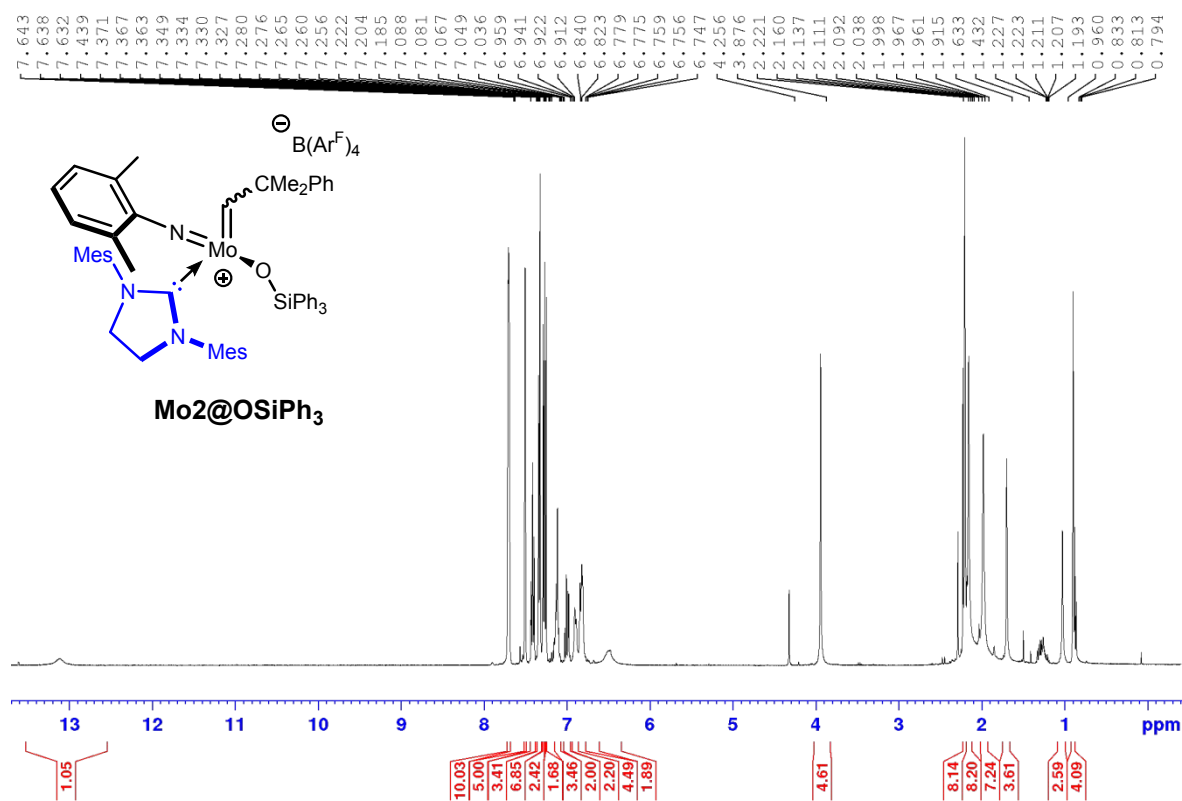
Figure S26:  $^1\text{H}$  NMR (400 MHz,  $\text{CDCl}_3 + \text{CD}_3\text{CN}$ ) spectrum of  $\text{Mo1@OSiPh}_3 \cdot \text{CH}_3\text{CN}$ .



**Figure S27:** <sup>19</sup>F NMR (376 MHz, CDCl<sub>3</sub> + CD<sub>3</sub>CN) spectrum of **Mo1@OSiPh<sub>3</sub> · CH<sub>3</sub>CN.**



**Figure S28:** <sup>13</sup>C NMR (101 MHz, CDCl<sub>3</sub> + CD<sub>3</sub>CN) spectrum of **Mo2@OSiPh<sub>3</sub> · CH<sub>3</sub>CN.**



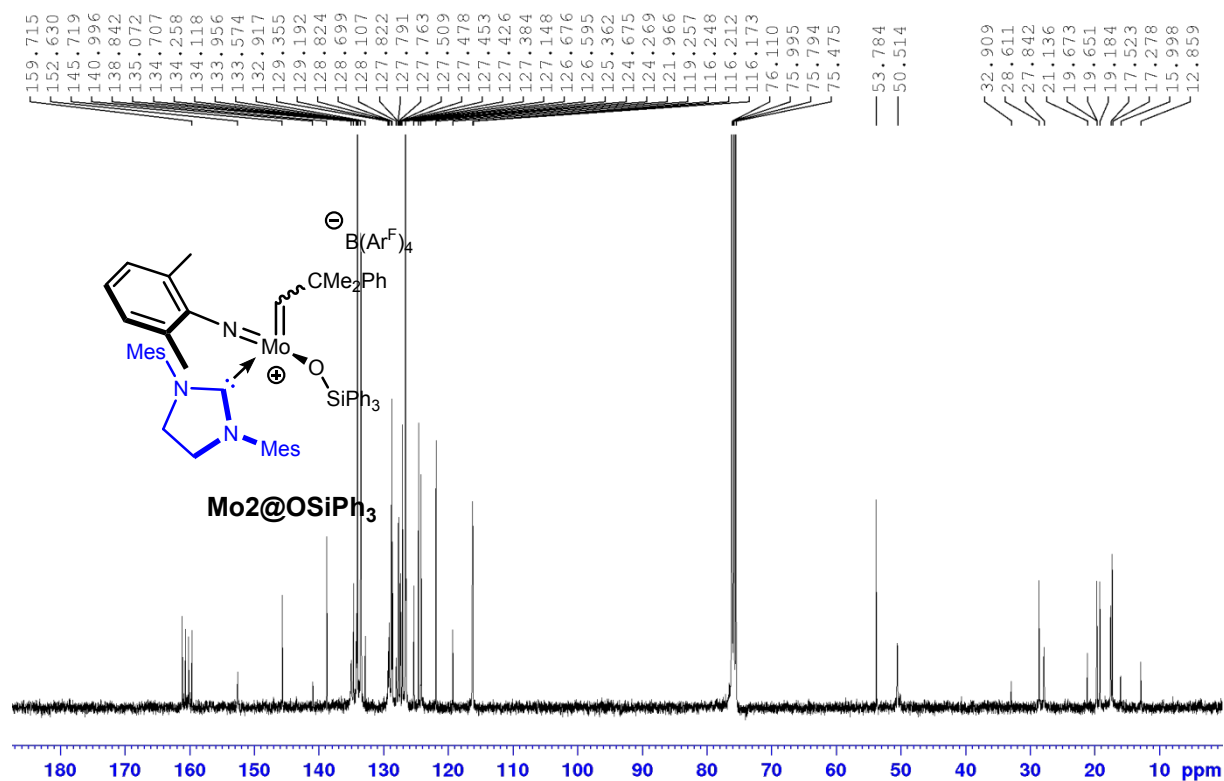


Figure S31:  $^{13}C$  NMR (101 MHz,  $CDCl_3$ ) spectrum of  $Mo_2@OSiPh_3$ .

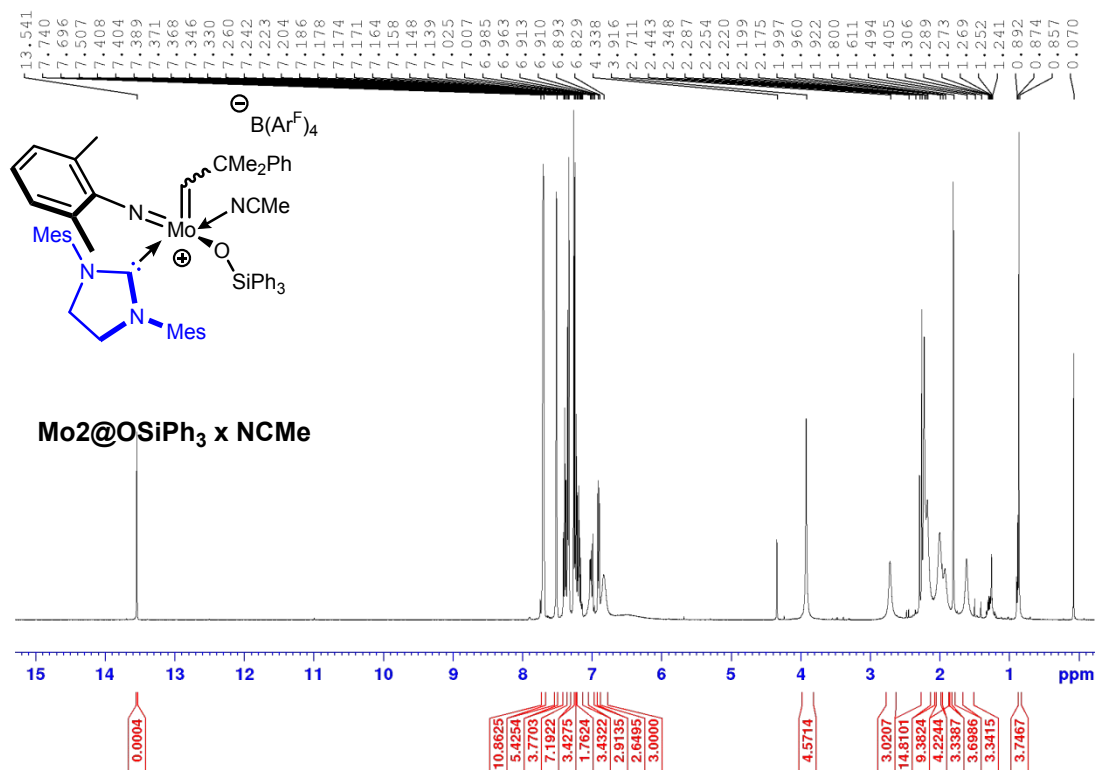
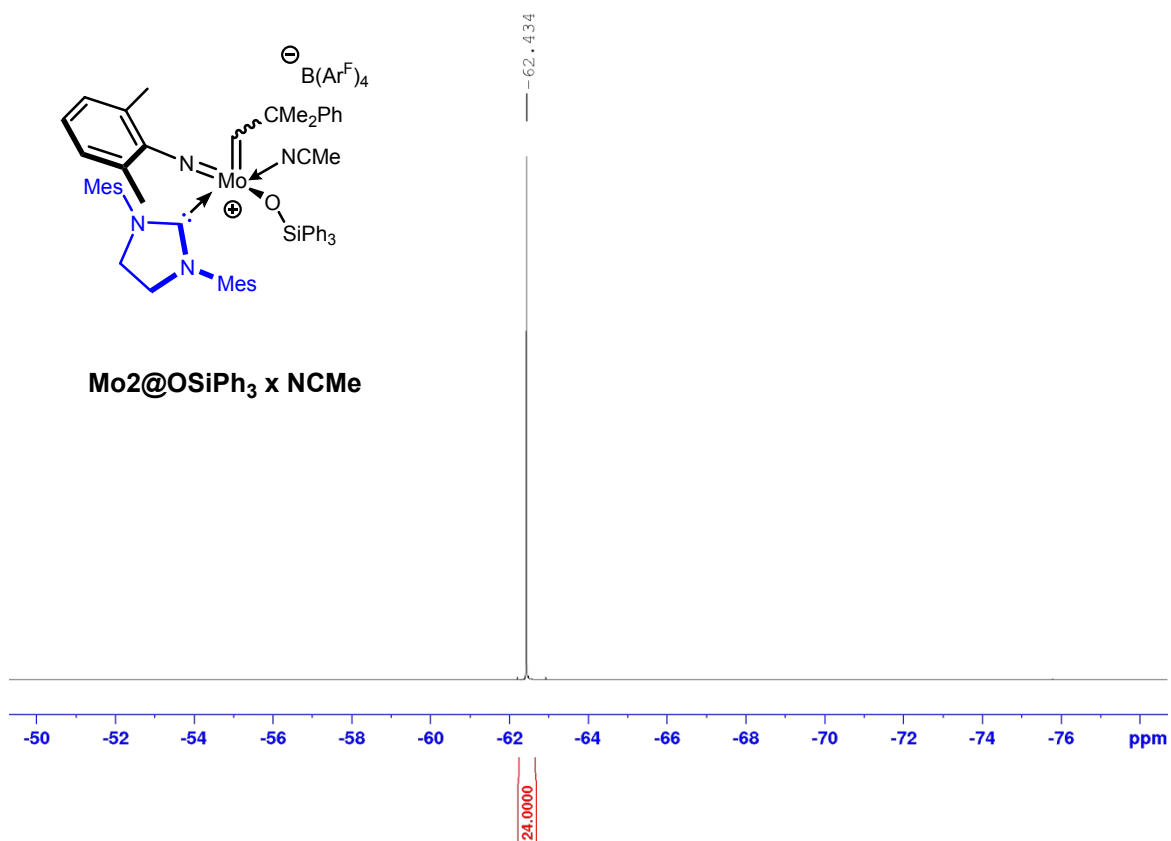
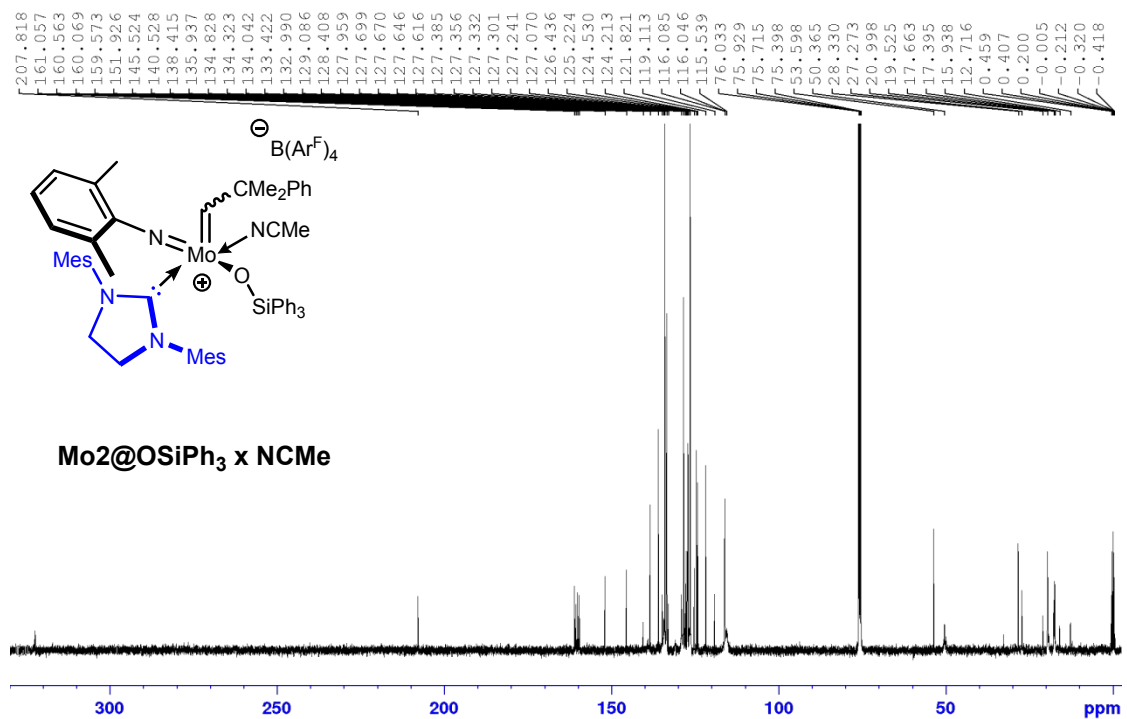


Figure S32:  $^1H$  NMR (400 MHz,  $CDCl_3 + CD_3CN$ ) spectrum of  $Mo_2@OSiPh_3 \cdot CH_3CN$ .



**Figure S33:**  $^{19}\text{F}$  NMR (376 MHz,  $\text{CDCl}_3 + \text{CD}_3\text{CN}$ ) spectrum of  $\text{Mo}_2@OSiPh_3 \cdot \text{CH}_3\text{CN}$ .



**Figure S34:**  $^{13}\text{C}$  NMR (101 MHz,  $\text{CDCl}_3 + \text{CD}_3\text{CN}$ ) spectrum of  $\text{Mo}_2@OSiPh_3 \cdot \text{CH}_3\text{CN}$ .

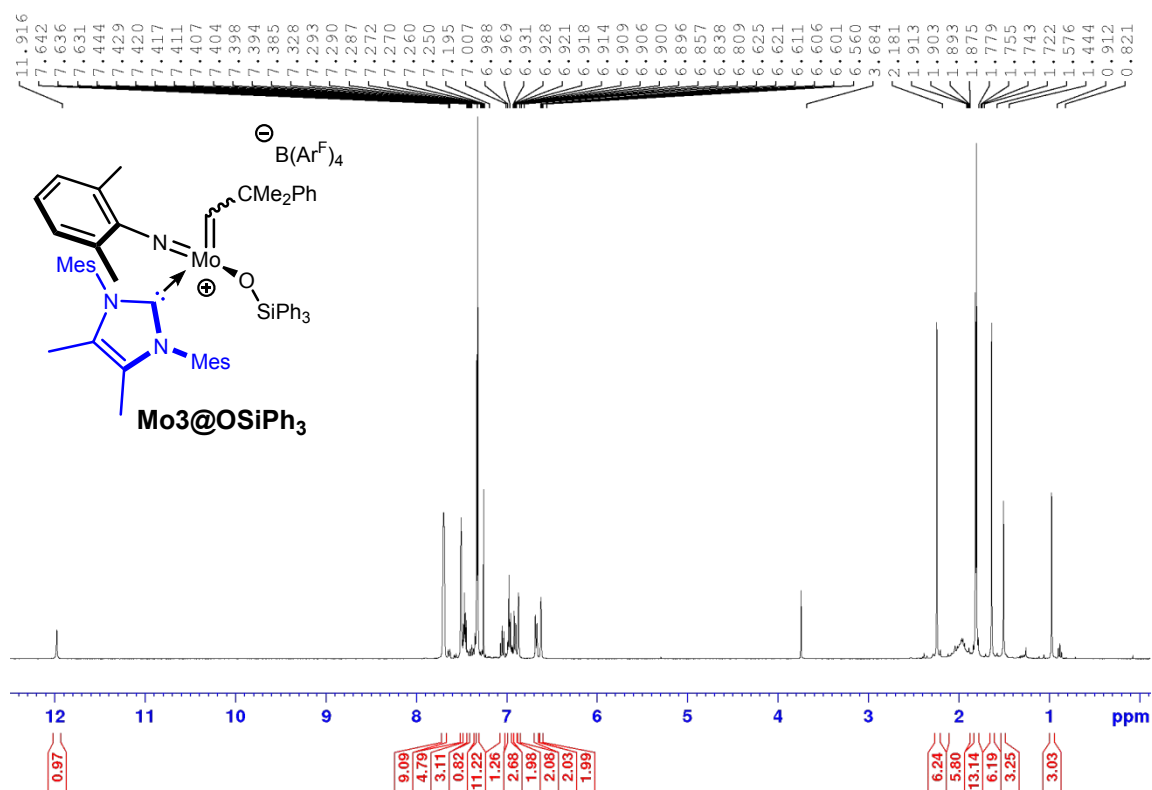


Figure S35: <sup>1</sup>H NMR (400 MHz, CDCl<sub>3</sub>) spectrum of **Mo3@OSiPh<sub>3</sub>**.

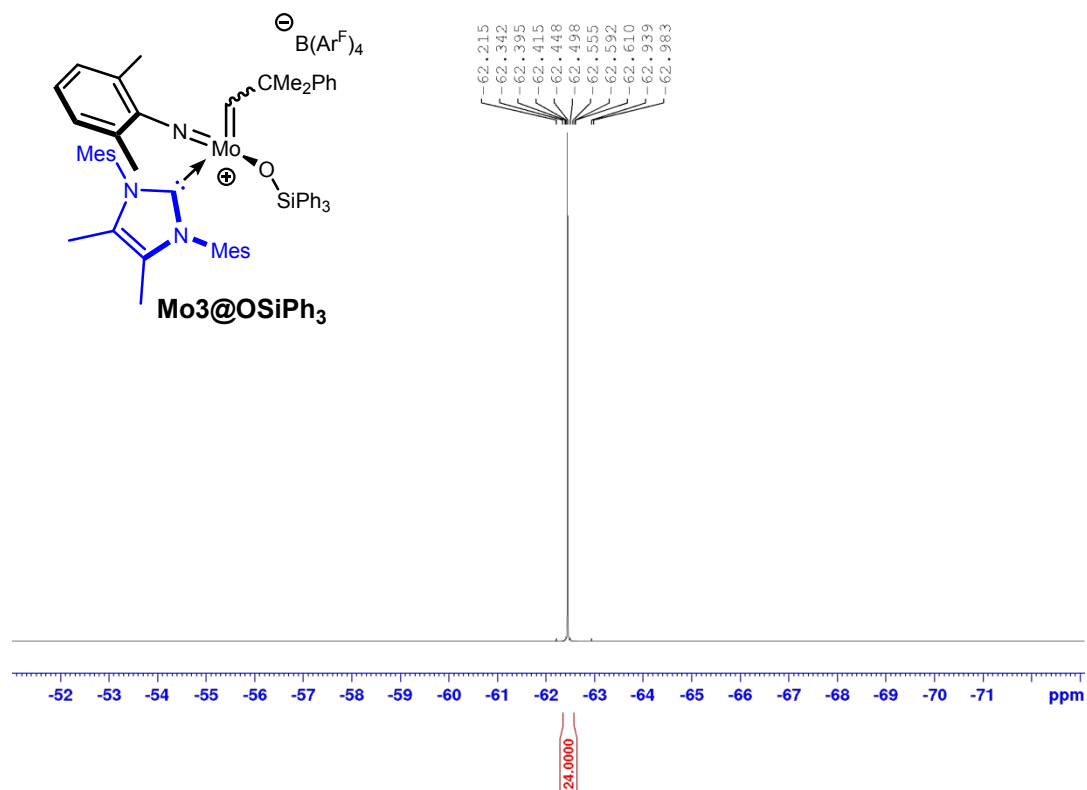
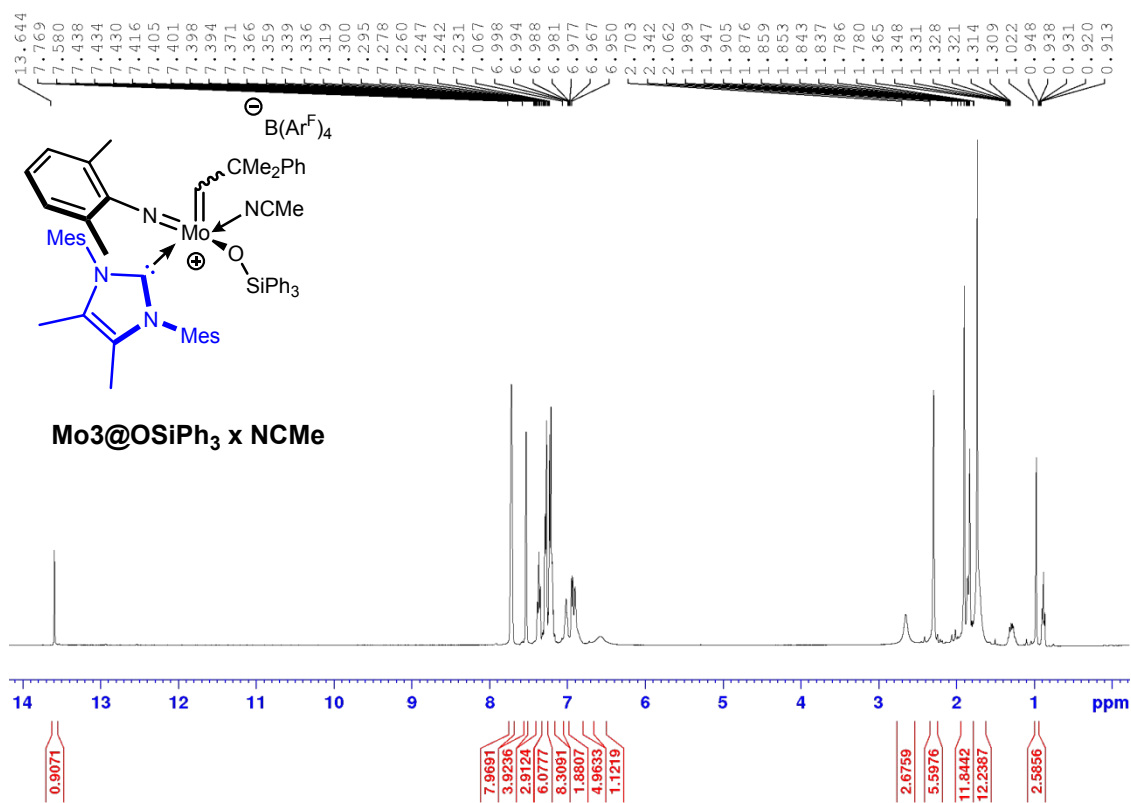
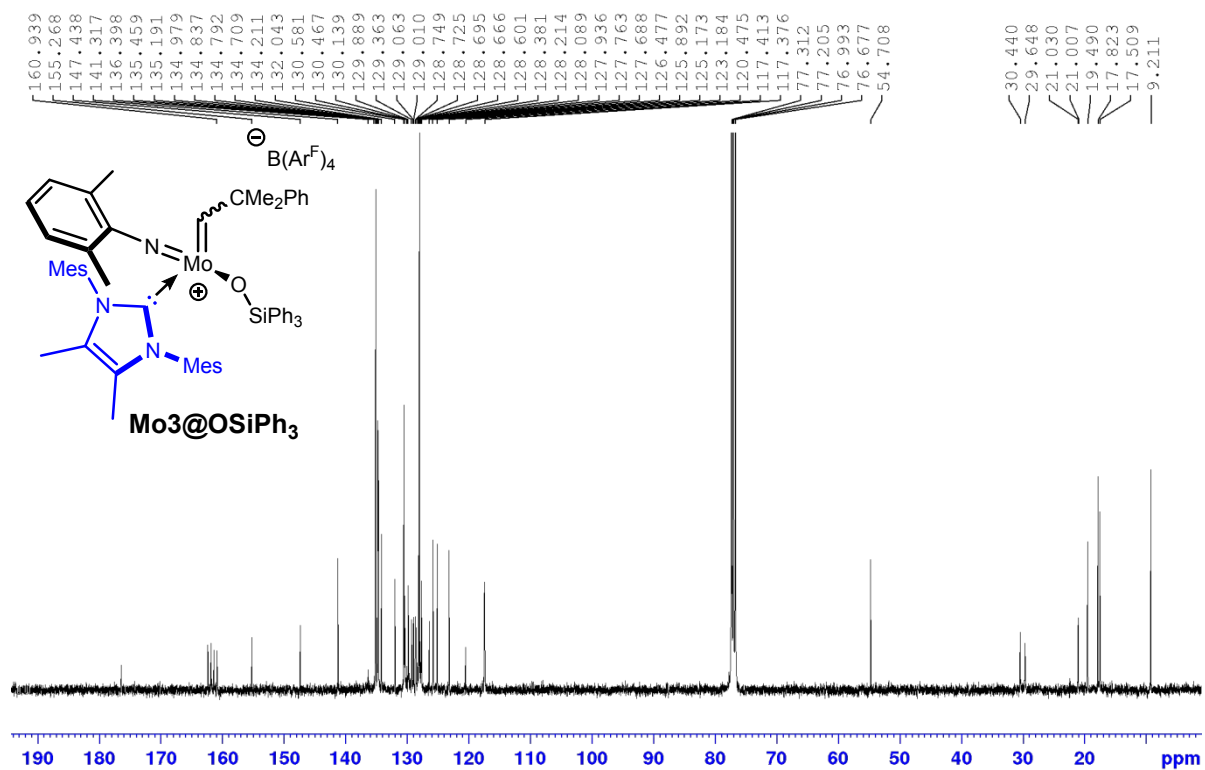
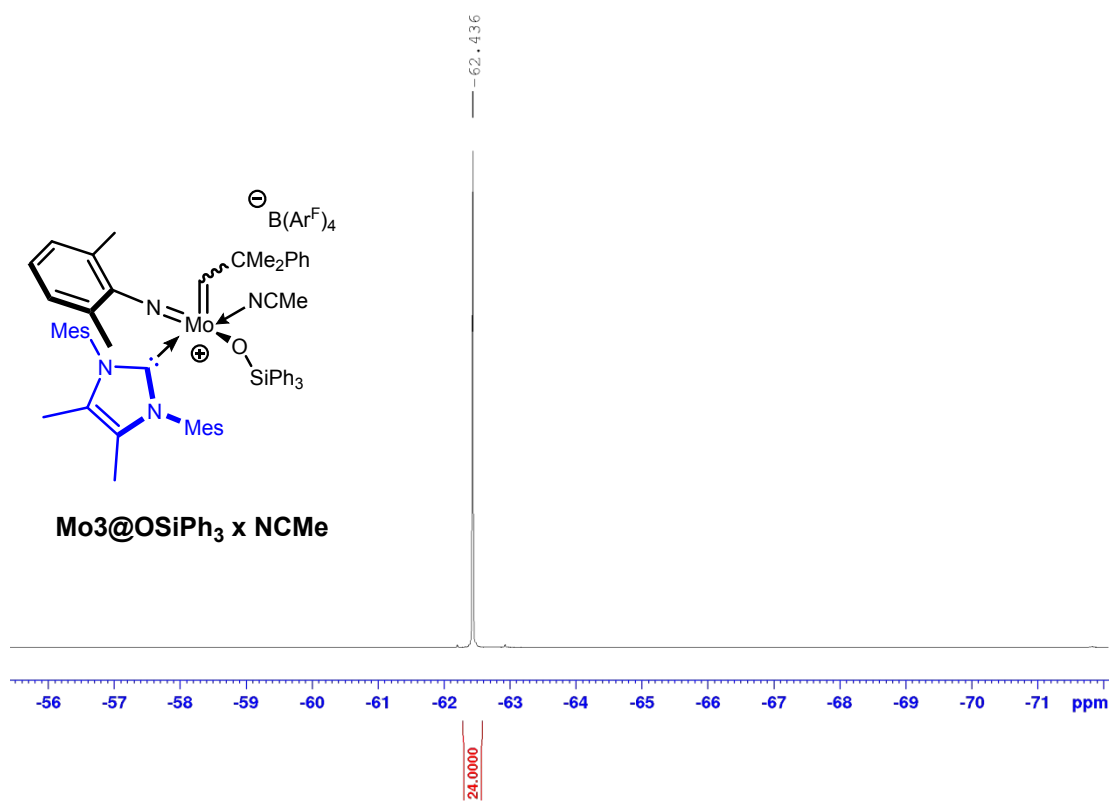
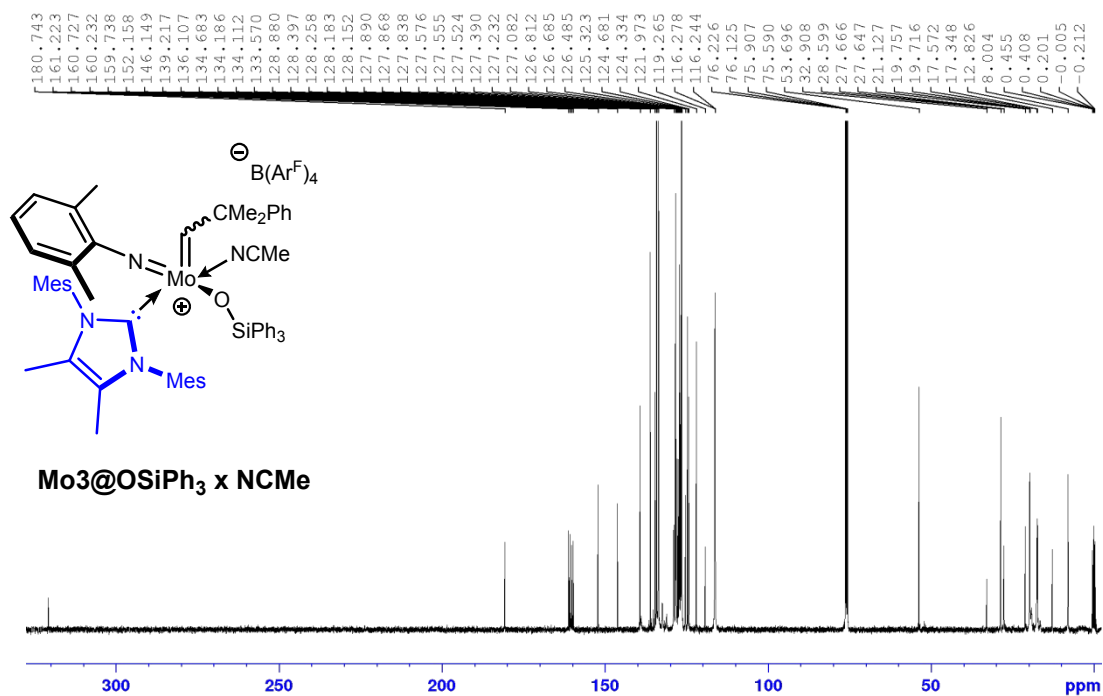


Figure S36: <sup>19</sup>F NMR (376 MHz, CDCl<sub>3</sub>) spectrum of **Mo3@OSiPh<sub>3</sub>**.





**Figure S39:**  $^{19}\text{F}$  NMR (376 MHz,  $\text{CDCl}_3 + \text{CD}_3\text{CN}$ ) spectrum of  $\text{Mo3@OSiPh}_3 \cdot \text{CH}_3\text{CN}$ .



**Figure S40:**  $^{13}\text{C}$  NMR (101 MHz,  $\text{CDCl}_3 + \text{CD}_3\text{CN}$ ) spectrum of  $\text{Mo3@OSiPh}_3 \cdot \text{CH}_3\text{CN}$ .

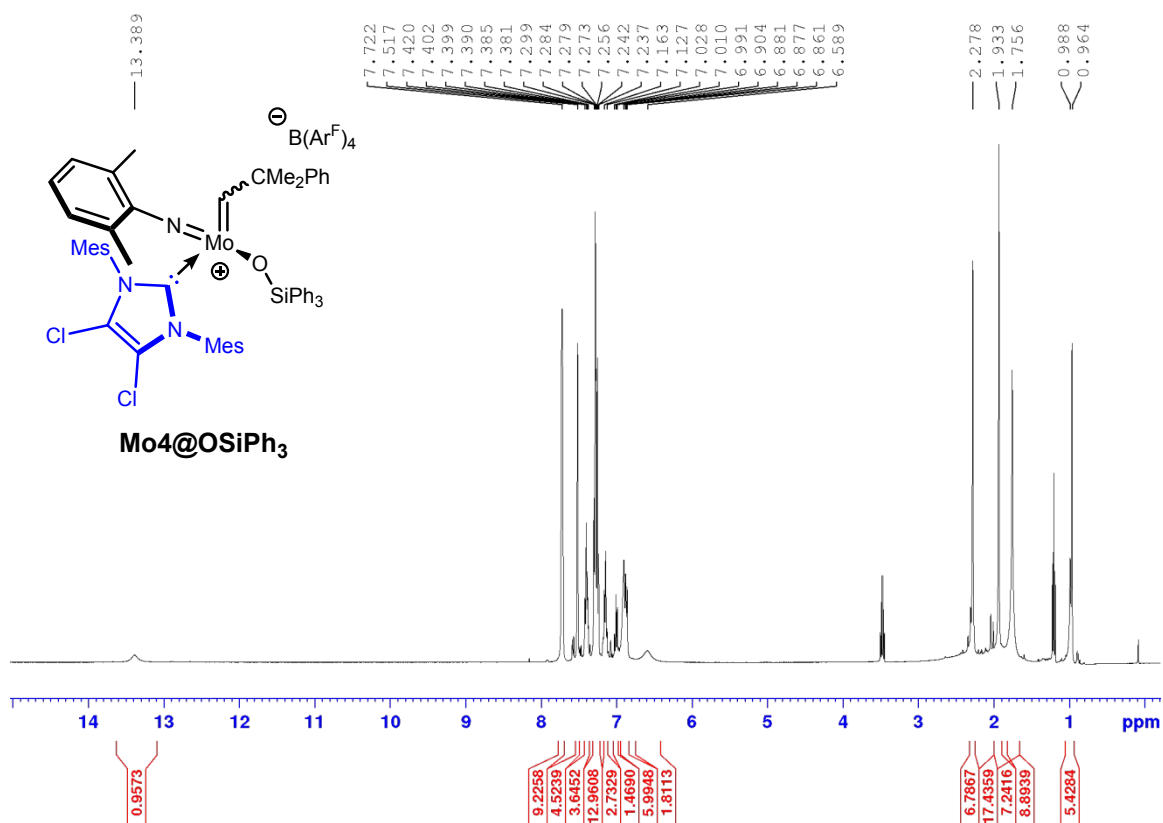


**Figure S41:** <sup>1</sup>H NMR (400 MHz, CDCl<sub>3</sub>) spectrum of **Mo4@OSiPh<sub>3</sub>**.

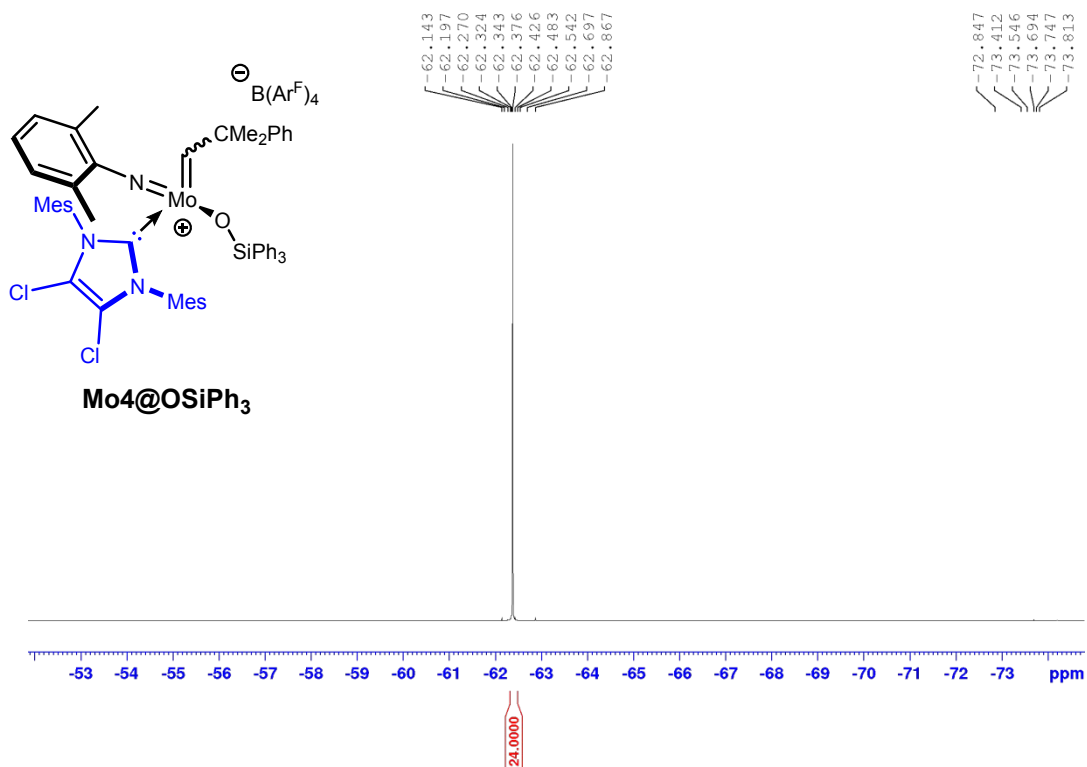


**Figure S42:** <sup>19</sup>F NMR (376 MHz, CDCl<sub>3</sub>) spectrum of **Mo4@OSiPh<sub>3</sub>**.

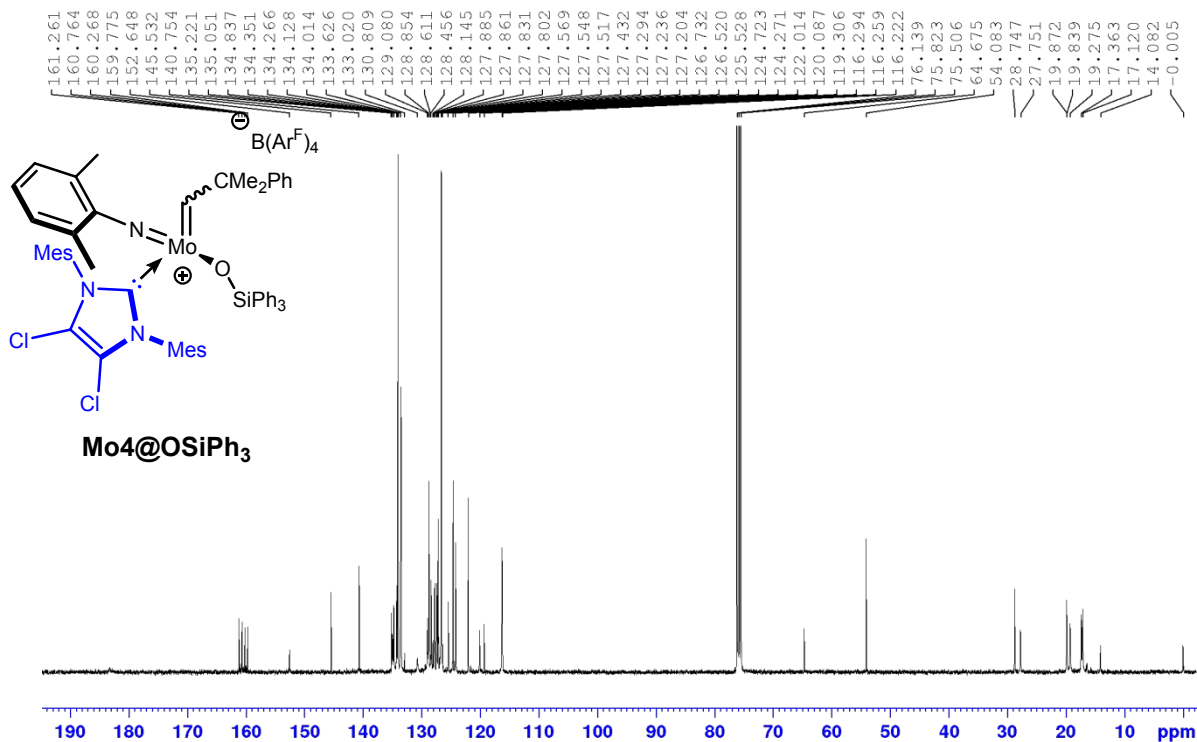


Figure S43: <sup>13</sup>C NMR (101 MHz, CDCl<sub>3</sub>) spectrum of **Mo4@OSiPh<sub>3</sub>**.

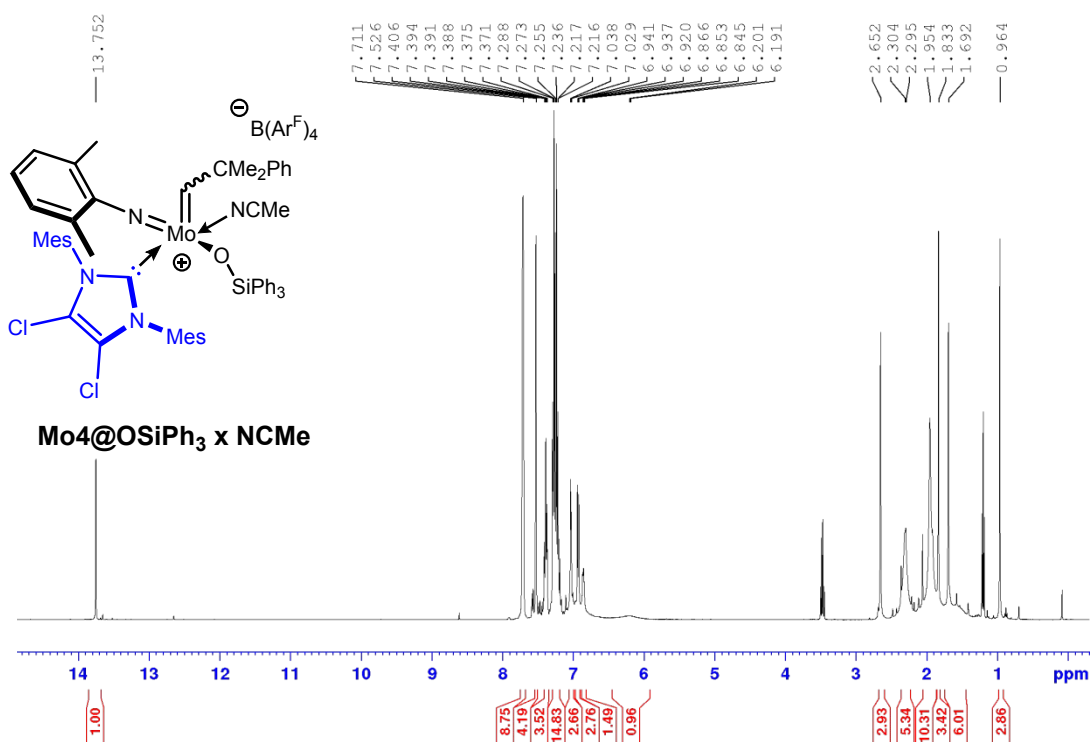
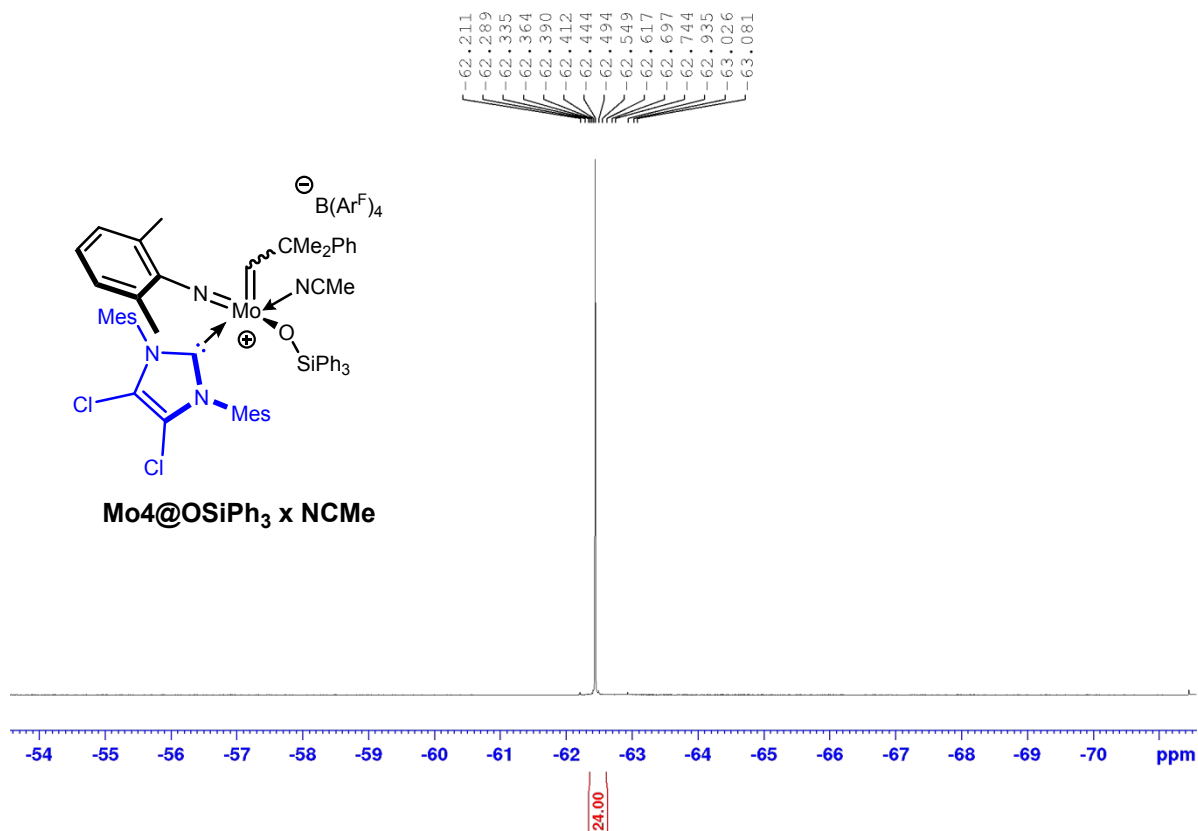
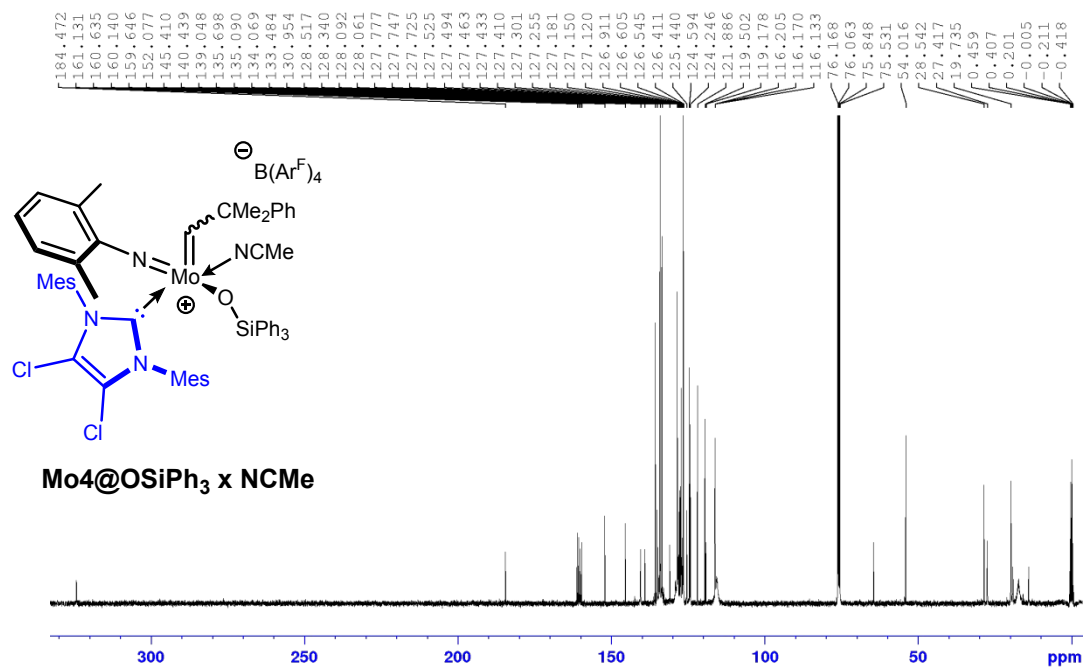


Figure S44: <sup>1</sup>H NMR (400 MHz, CDCl<sub>3</sub> + CD<sub>3</sub>CN) spectrum of **Mo4@OSiPh<sub>3</sub> · CH<sub>3</sub>CN**.



**Figure S45:**  $^{19}\text{F}$  NMR (376 MHz,  $\text{CDCl}_3 + \text{CD}_3\text{CN}$ ) spectrum of  $\text{Mo4@OSiPh}_3 \cdot \text{CH}_3\text{CN}$ .



**Figure S46:**  $^{13}\text{C}$  NMR (101 MHz,  $\text{CDCl}_3 + \text{CD}_3\text{CN}$ ) spectrum of  $\text{Mo4@OSiPh}_3 \cdot \text{CH}_3\text{CN}$ .

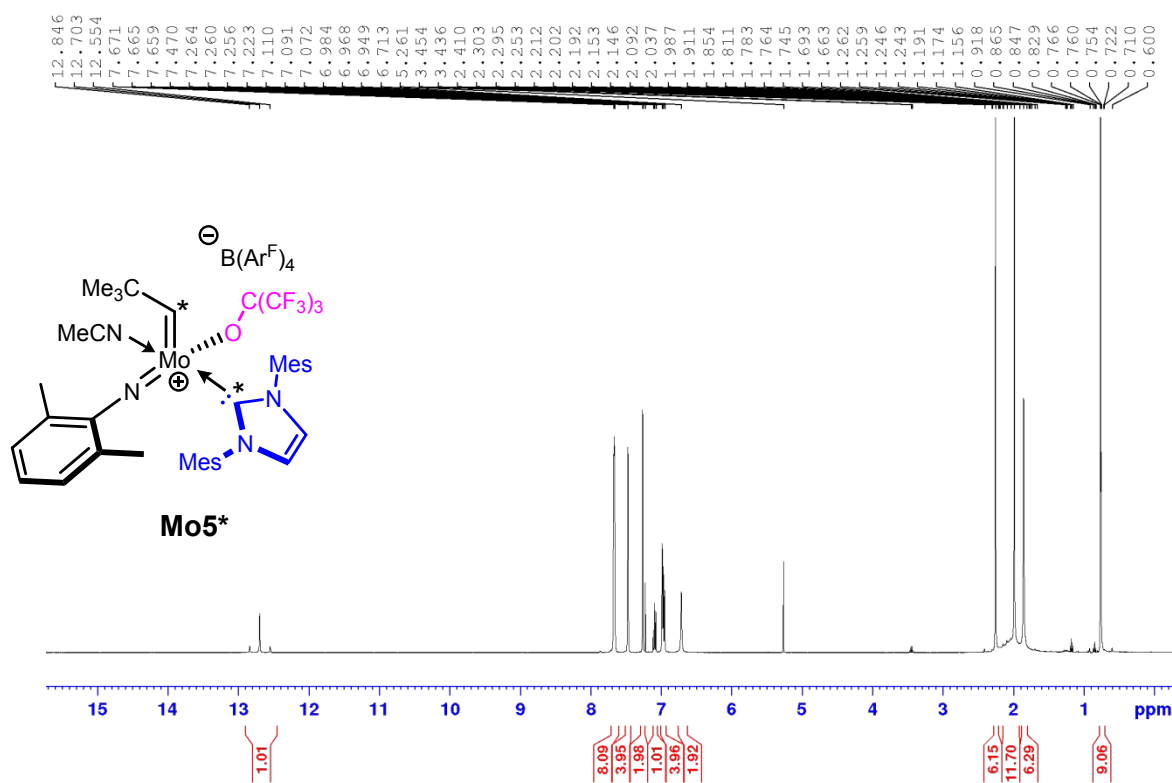


**Figure S47:  $^1\text{H}$  NMR (400 MHz,  $\text{CDCl}_3$ ) spectrum of **Mo5\***.**

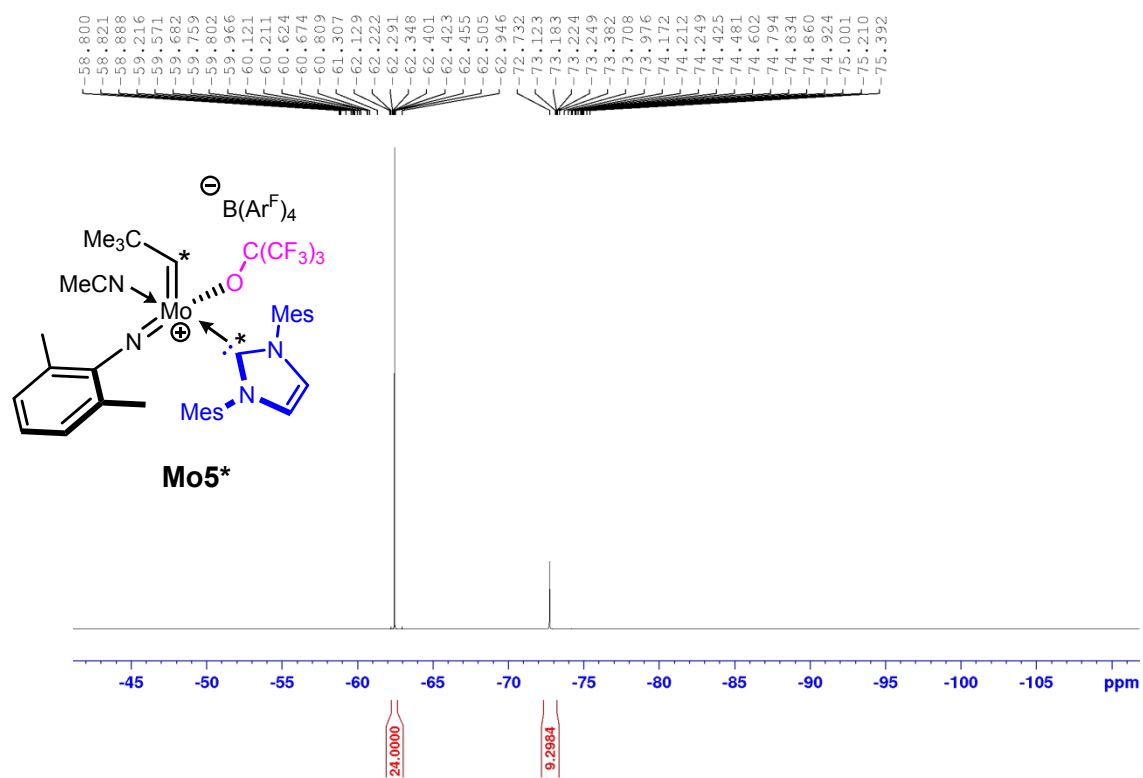


**Figure S48:  $^{19}\text{F}$  NMR (376 MHz,  $\text{CDCl}_3$ ) spectrum of **Mo5\***.**

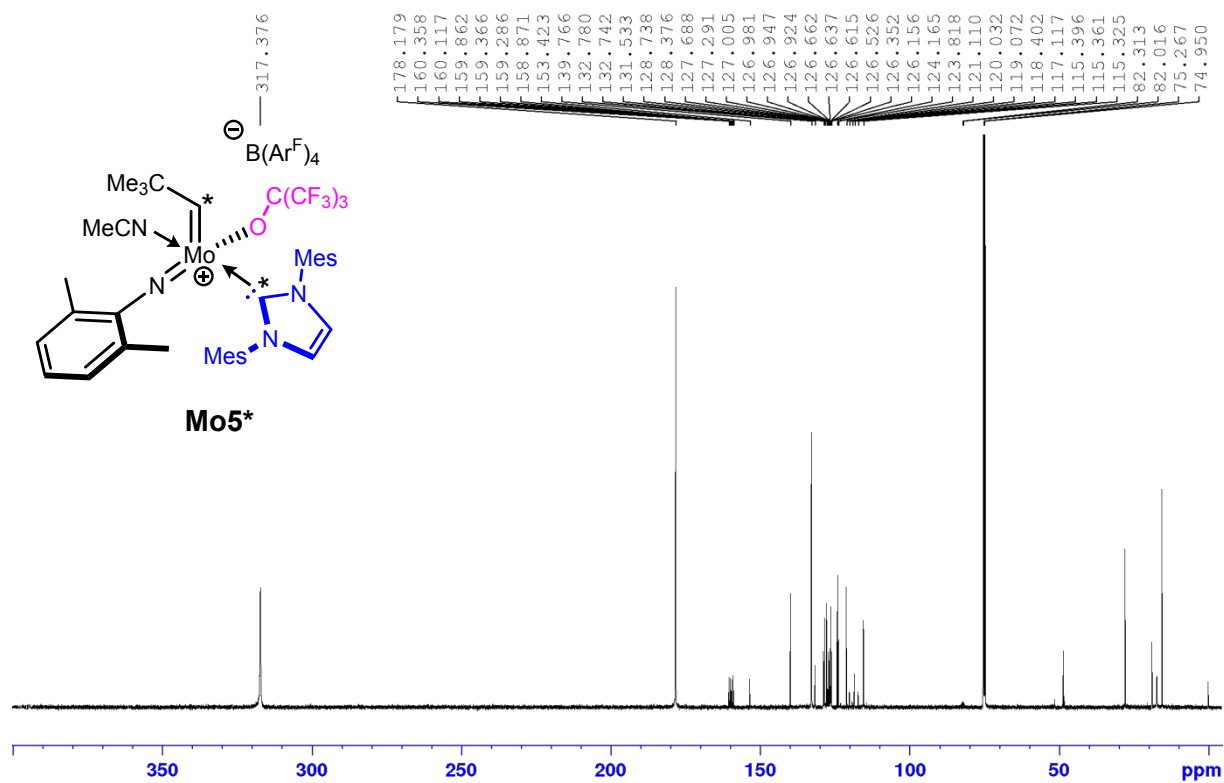


Figure S49:  $^{13}C$  NMR (101 MHz,  $CDCl_3$ ) spectrum of **Mo5\***.

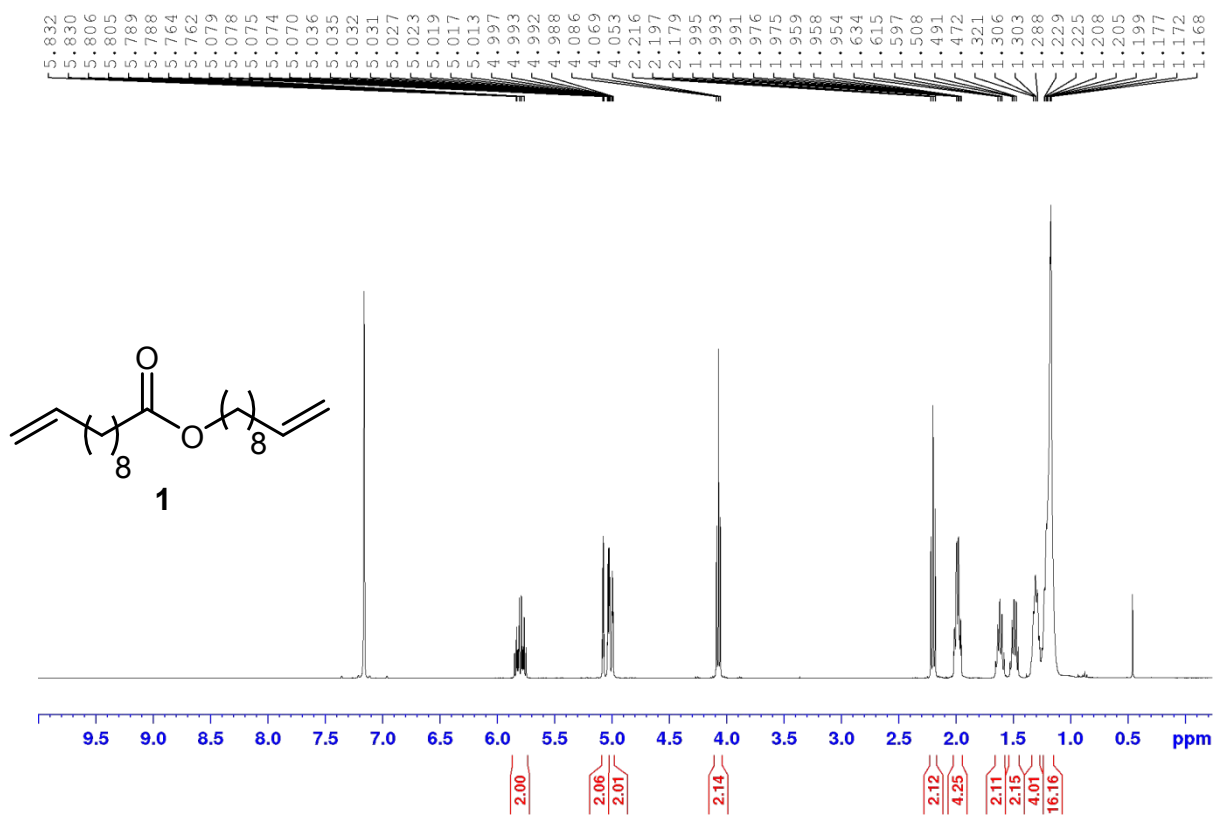


Figure S50:  $^1H$  NMR (400 MHz,  $C_6D_6$ ) spectrum of **1**.

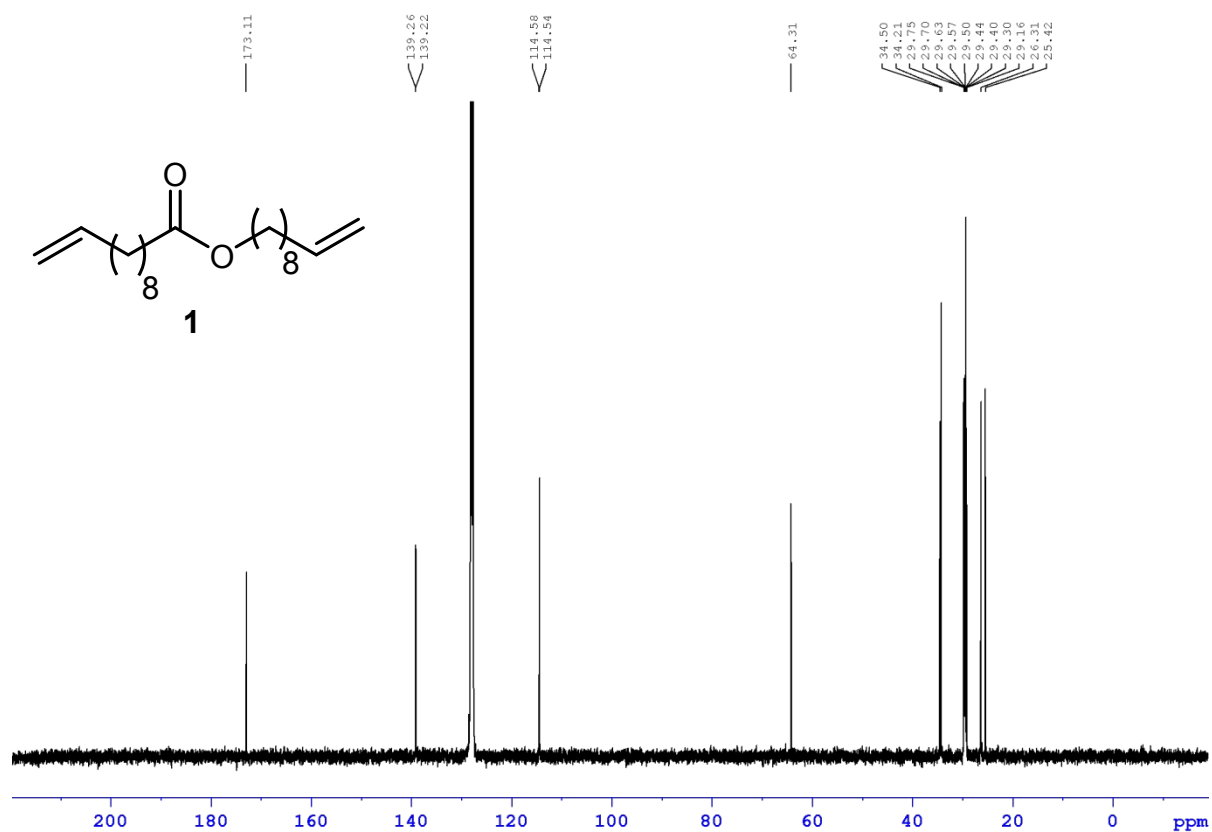


Figure S51:  $^{13}\text{C}$  NMR (101 MHz,  $\text{C}_6\text{D}_6$ ) spectrum of **1**.

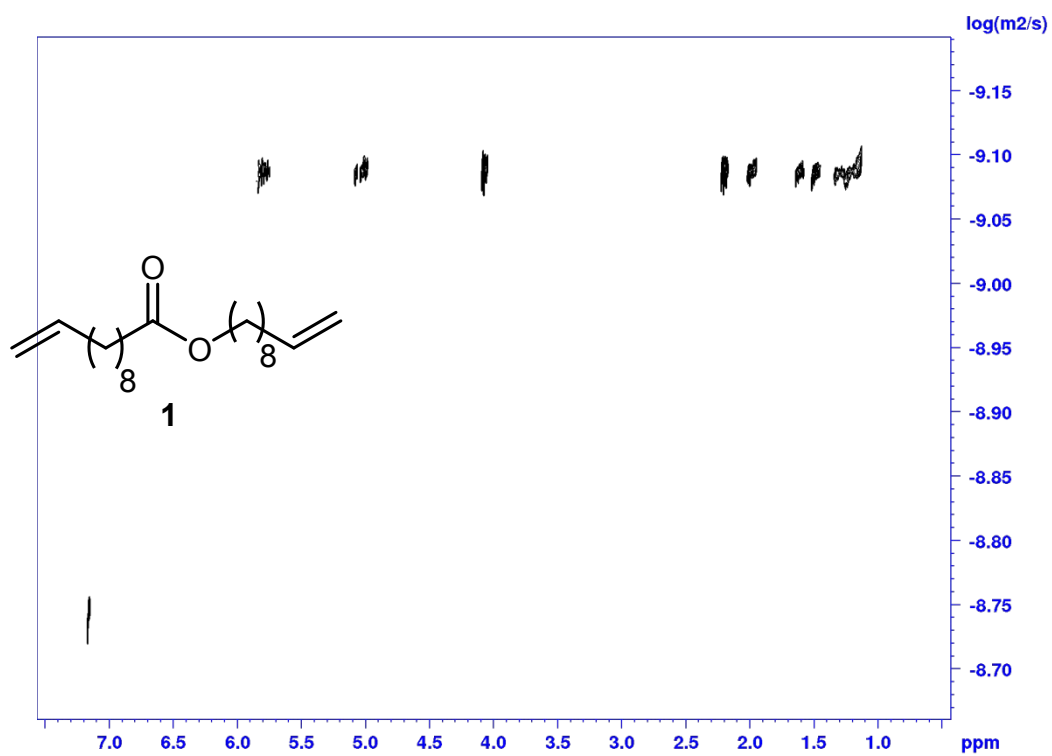


Figure S52: DOSY NMR (400 MHz,  $\text{C}_6\text{D}_6$ ) spectrum of **1**.

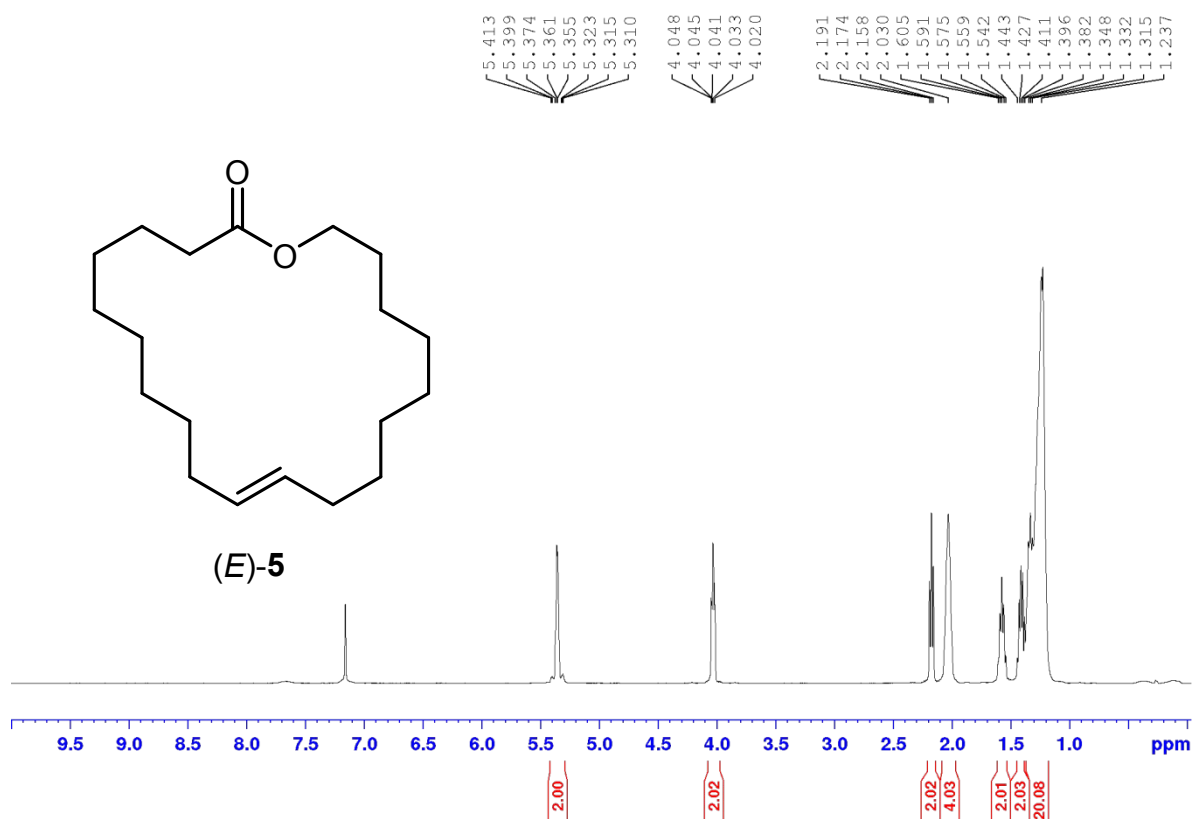


Figure S53: <sup>1</sup>H NMR (400 MHz, C<sub>6</sub>D<sub>6</sub>) spectrum of (E)-5.

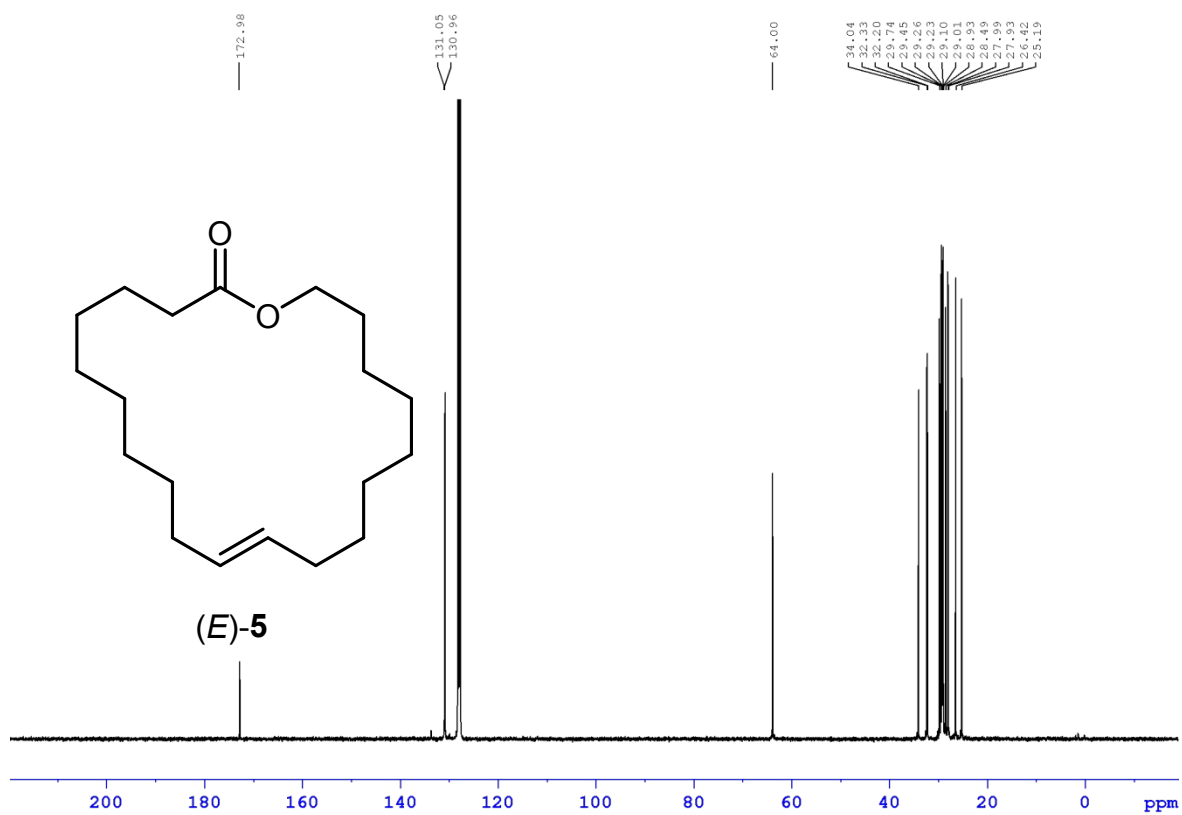


Figure S54: <sup>13</sup>C NMR (101 MHz, C<sub>6</sub>D<sub>6</sub>) spectrum of (E)-5.

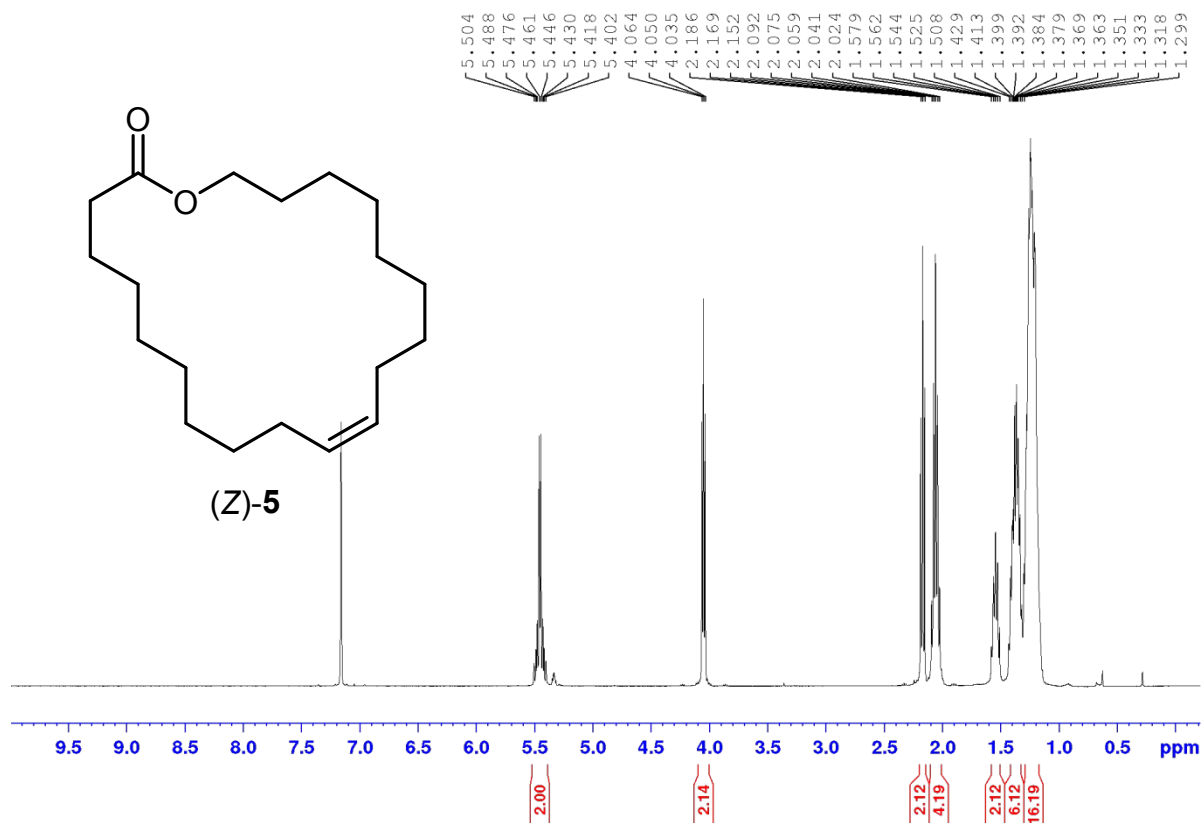


Figure S55: <sup>1</sup>H NMR (400 MHz, C<sub>6</sub>D<sub>6</sub>) spectrum of (Z)-5.

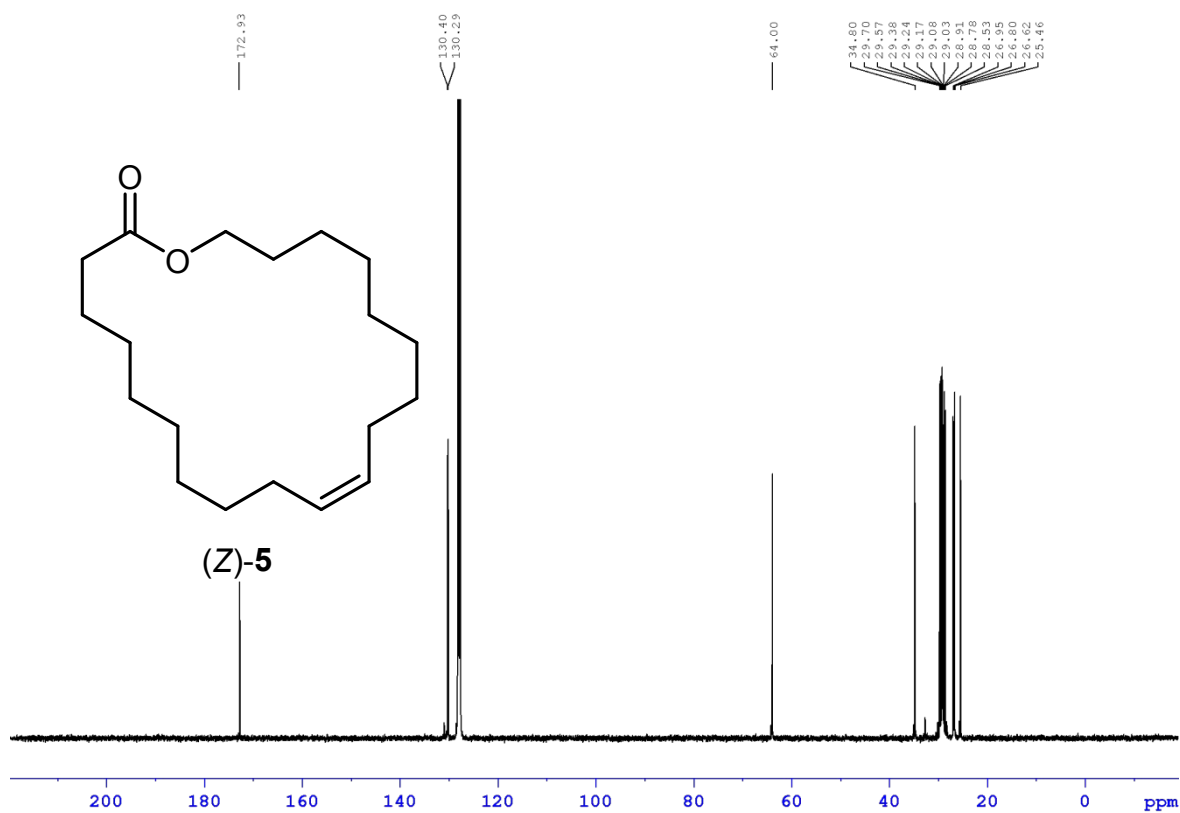
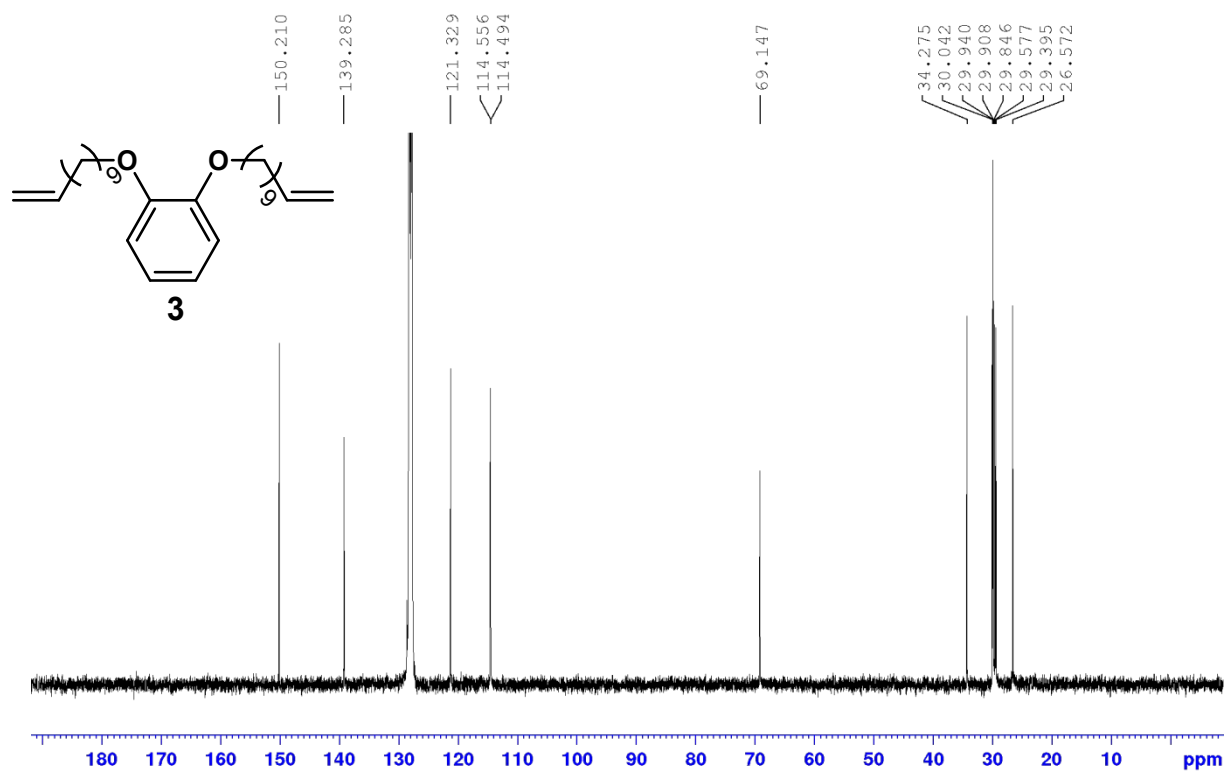


Figure S56: <sup>13</sup>C NMR (101 MHz, C<sub>6</sub>D<sub>6</sub>) spectrum of (Z)-5.









**Figure S63:**  $^{13}\text{C}$  NMR (101 MHz,  $\text{C}_6\text{D}_6$ ) spectrum of **3**.

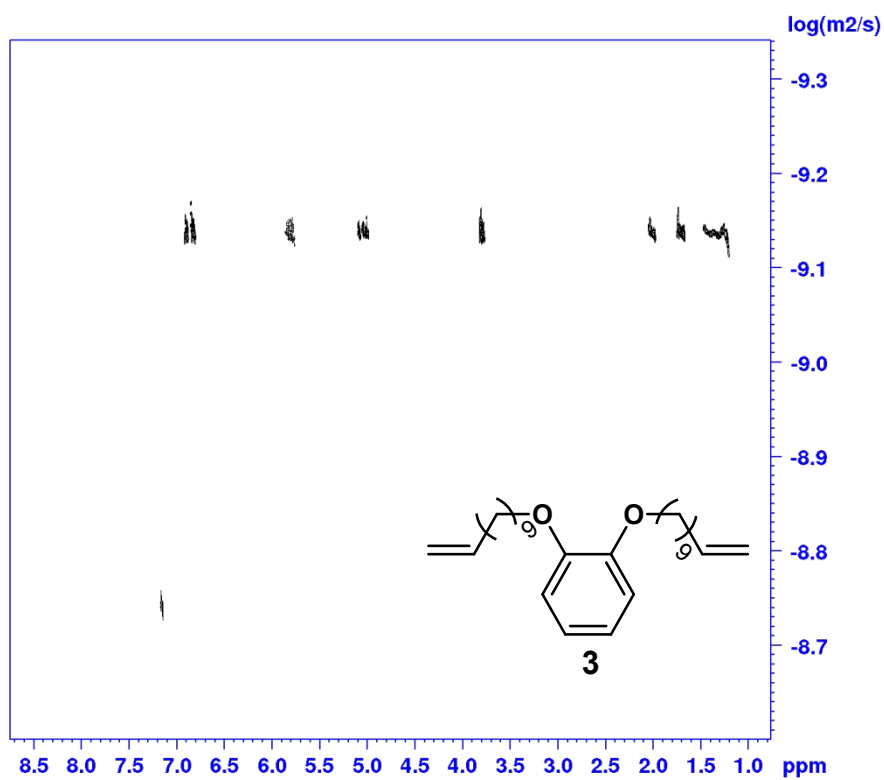


**Figure S64:** DOSY NMR (400 MHz,  $\text{C}_6\text{D}_6$ ) spectrum of **3**.

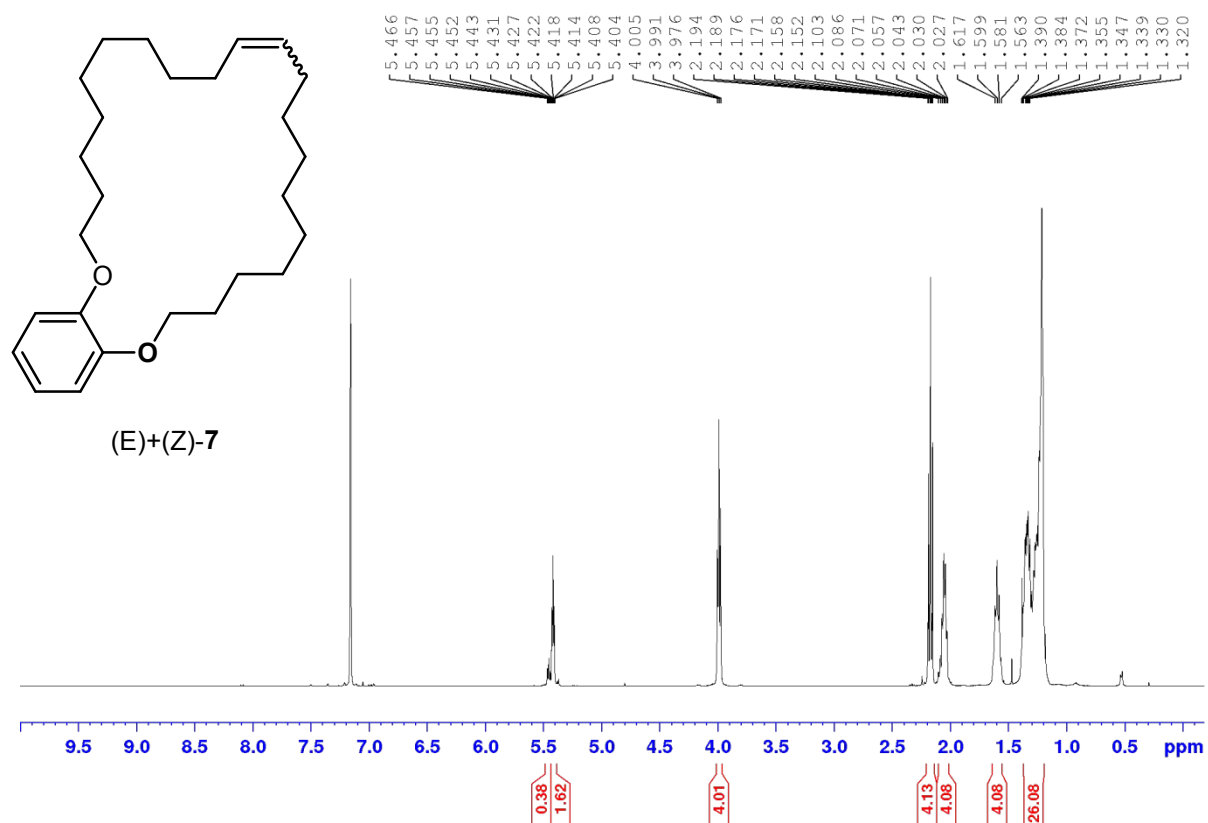


Figure S65:  $^1\text{H}$  NMR (400 MHz,  $\text{C}_6\text{D}_6$ ) spectrum of 7.

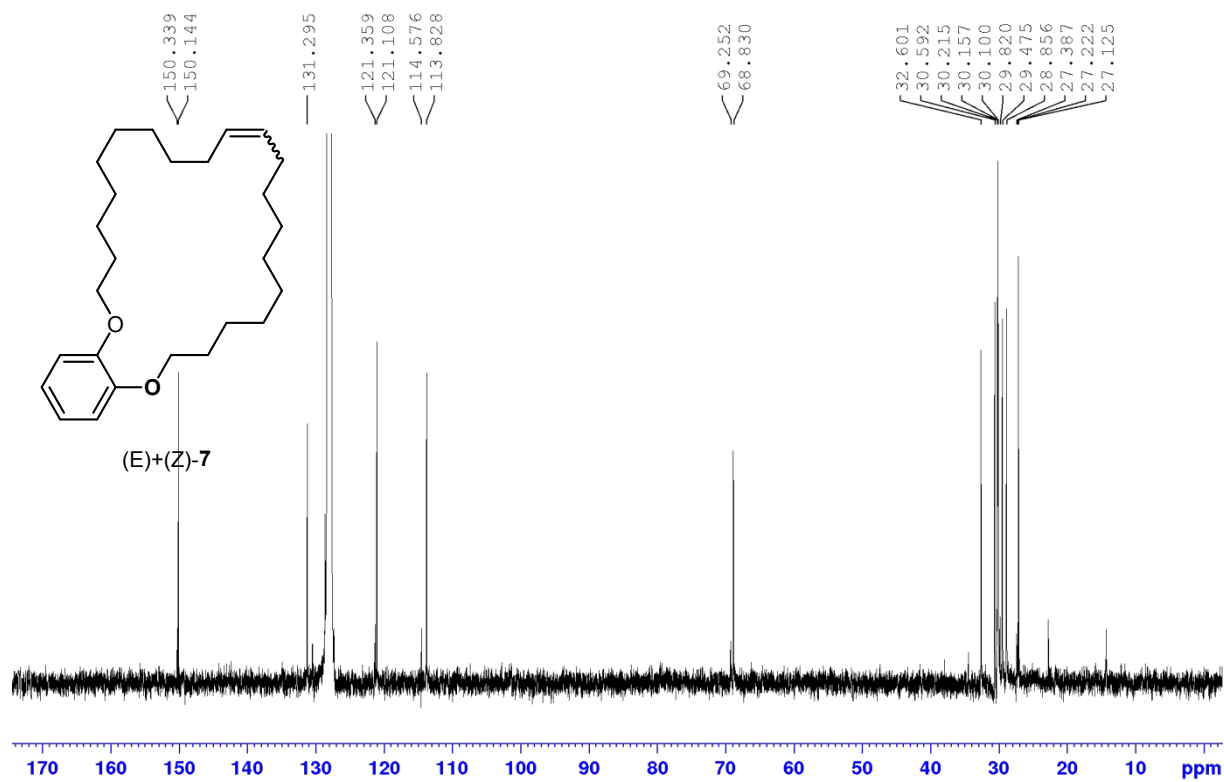


Figure S66:  $^{13}\text{C}$  NMR (101 MHz,  $\text{C}_6\text{D}_6$ ) spectrum of (E/Z)-7.

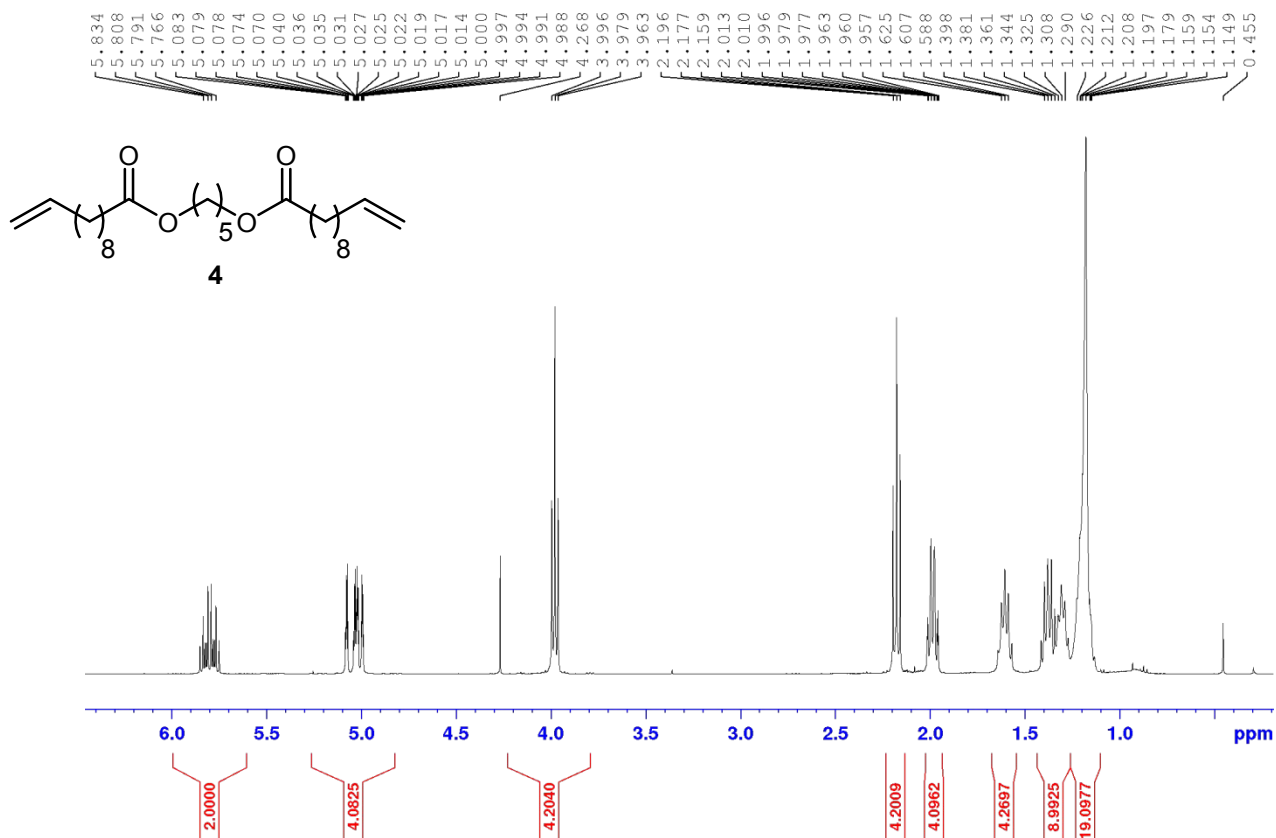


Figure S67: <sup>1</sup>H NMR (400 MHz, C<sub>6</sub>D<sub>6</sub>) spectrum of **4**.

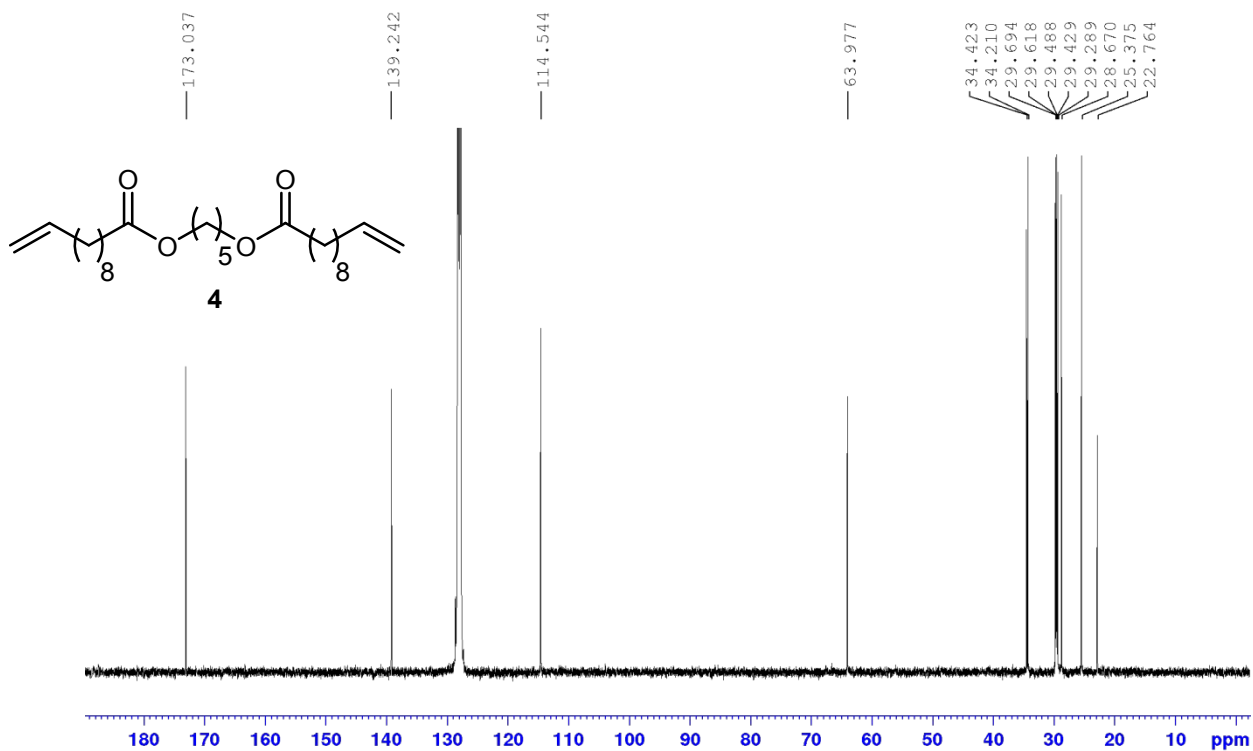
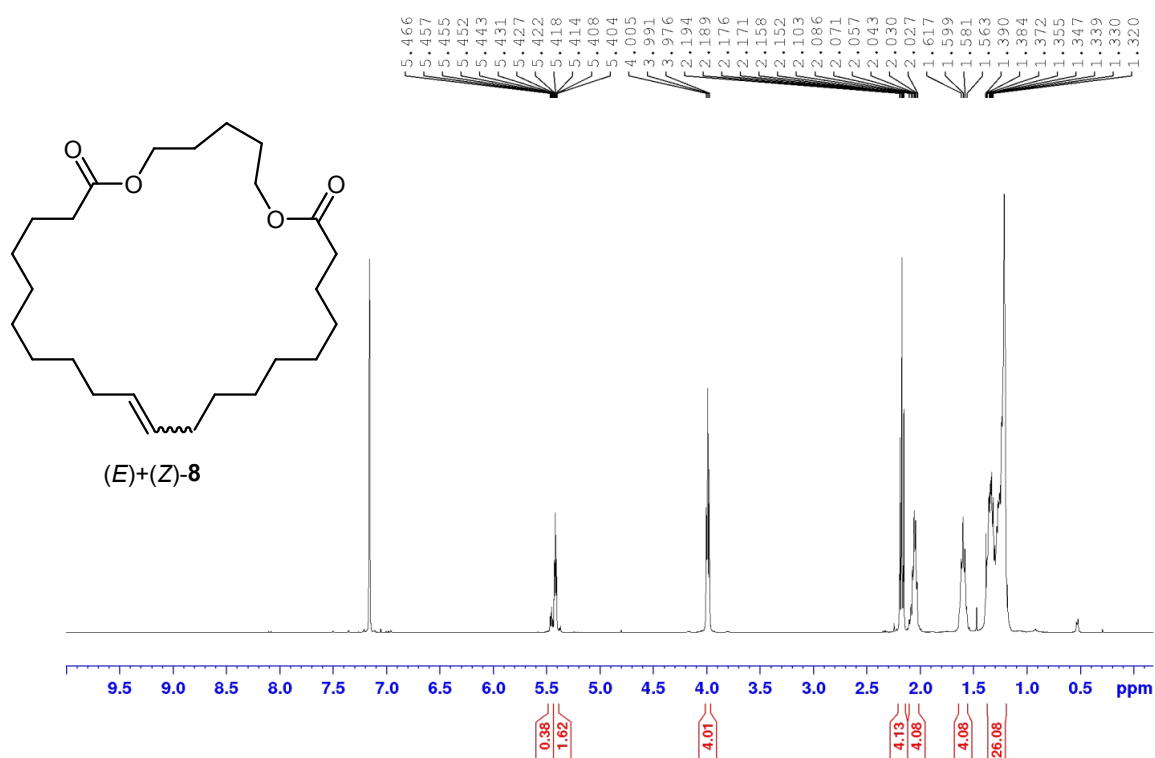
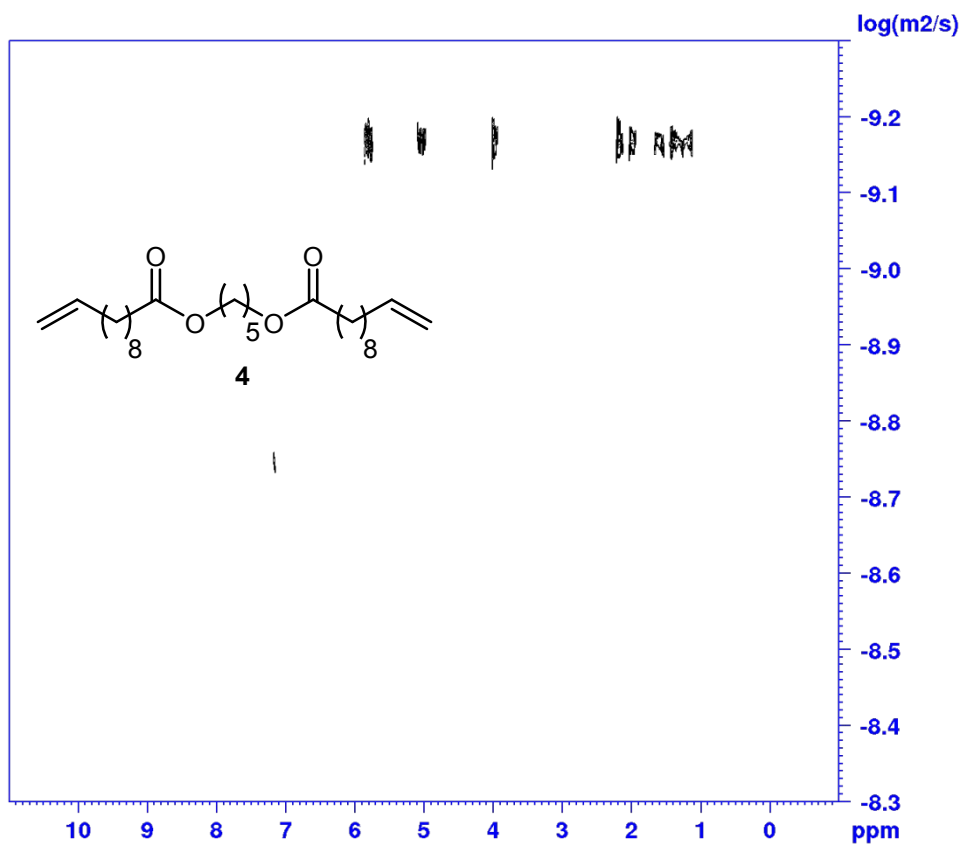
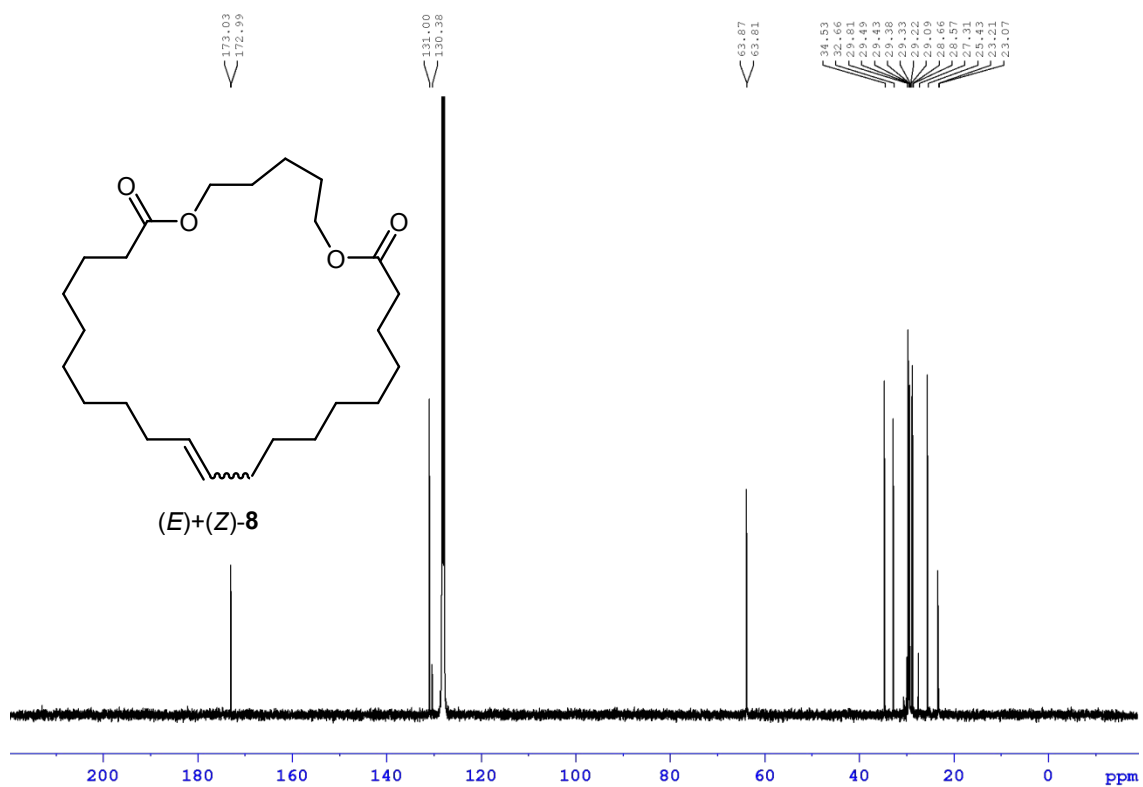


Figure S68: <sup>13</sup>C NMR (101 MHz, C<sub>6</sub>D<sub>6</sub>) spectrum of **4**.





**Figure S71:**  $^{13}\text{C}$  NMR (101 MHz,  $\text{C}_6\text{D}_6$ ) spectrum of *(E/Z)*-8.

## 11. Molecular Dynamics Simulations

### Generation of pore models

The pore models were used to study confinement effects with the goal to capture the size, the dominant geometry (cylinder) and the surface chemistry of the material used in the experimental study. The pore models target the experimental concept of pore-size selective immobilization of a well-defined organometallic catalyst present on the interior, but not on the exterior surface of a pore. The low residual hydroxylation of the experimental material was mimicked by converting redundant silanol groups to carbonyl-like terminal oxygen atoms (referred to SLO in Table S28), i.e., removing their ability to form hydrogen bonds with substrate and product molecules. This strategy was preferred over the use of siloxane bridges that appear somewhat artificial when based on the prescribed lattice positions of the Si atoms in the fixed  $\beta$ -cristobalite silica structure, whose distance is 5.07 Å and which become strongly solvent exposed upon the formation of a siloxane bridge.

The cylindrical mesopore models consisted of a 2.55, 5.03 or 6.24 nm-diameter pore carved through the (111)-face of a  $\beta$ -cristobalite silica block (8.10 nm  $\times$  7.89 nm  $\times$  10.08 nm ( $x \times y \times z$ )) along the z-direction, following procedures reported previously<sup>14-16</sup>. The residual silanol density on the inner pore surface was adjusted to 0.66, 1.02 or 1.25  $\mu\text{mol}/\text{m}^2$ . The cylindrical pore was flanked by two solvent reservoirs with the outer surface bearing a silanol density of 0.42, 0.38 or 0.42  $\mu\text{mol}/\text{m}^2$ . The outer surface was grafted uniformly and randomly with trimethylsilyl (TMS) groups with a density of 5.59, 4.94 or 4.90  $\mu\text{mol}/\text{m}^2$  to mimic experimental conditions, where the silanols on the external surface of the SBA-15 silica particles have been shielded by TMS groups. The 2.5, 5 and 6 nm pores were grafted with one, two and three molecules of catalyst **Mo1**, respectively. The properties of the generated pore models are listed in detail in Table S28.

**Table S28.** Properties of the cylindrical catalytic mesopore models generated by PoreMS<sup>16</sup> version 0.2.1 (<http://doi.org/10.5281/zenodo.4525195>).

Pore Diameter	2.5 nm		5.0 nm		6.2 nm	
	Interior	Exterior	Interior	Exterior	Interior	Exterior
Silica block xyz-dimensions (nm)	8.10; 7.89; 10.08		8.10; 7.89; 10.08		8.10; 7.89; 10.08	
Simulation box xyz-dimensions	8.10; 7.89; 24.08		8.10; 7.89; 21.08		8.10; 7.89; 20.08	
Pore drilling direction	z		z		z	
Pore diameter (nm)	2.55		5.03		6.24	
Surface roughness (nm)	0.08	0.00	0.08	0.00	0.08	0.00
Solvent reservoir z-dimension (nm)	7.00		5.50		5.00	
Pore volume (nm <sup>3</sup> )	51.40		200.19		307.70	
Solvent reservoir volume (nm <sup>3</sup> )	2x447.28		2x351.43		2x319.49	
Surface area (nm <sup>2</sup> )	80.67	2x58.79	159.20	2x44.03	197.37	2x33.36
Surface chemistry - Before Functionalization						
Number of single silanol groups	356	410	680	246	854	180
Number of geminal silanol groups	32	8	98	18	122	17
Number of siloxane bridges	0	61	0	79	0	66
Total number of OH groups	420	426	876	282	1098	214
Overall hydroxylation (μmol/m <sup>2</sup> )	8.65	6.02	9.14	5.32	9.24	5.33
Surface chemistry - After Functionalization						
Number of Mo1 groups	1	0	2	0	3	0
Mo1 density (μmol/m <sup>2</sup> )	0.02	0.00	0.02	0	0.03	0
Number of SLO groups	387	0	776	0	946	0
SLO density (μmol/m <sup>2</sup> )	7.97	0	8.10	0	7.95	0
Number of TMS groups	0	396	0	262	0	197
TMS density (μmol/m <sup>2</sup> )	0	5.59	0	4.94	0	4.90
Bonded-phase density (μmol/m <sup>2</sup> )	7.99	5.59	8.12	4.94	7.98	4.90
Number of residual OH groups	32	30	98	20	149	17
Residual hydroxylation (μmol/m <sup>2</sup> )	0.66	0.42	1.02	0.38	1.25	0.42

### Development of a force field for the catalyst

The single-crystal X-ray structure of catalyst **Mo1** was optimized using density functional theory (DFT) calculations as implemented in the TURBOMOLE program<sup>17, 18</sup>. The cationic model pre-catalyst and the B(Ar<sup>F</sup>)<sub>4</sub><sup>-</sup> counter anion were optimized separately within the resolution-of-the-identity (RI) approximation<sup>19-21</sup> using the PBE0<sup>22, 23</sup> hybrid DFT method and the def2-TZVP basis set<sup>24, 25</sup>. For Mo the def2-ECP effective core potential was used<sup>26</sup>. Empirical dispersion corrections in the form of Grimme's DFT-D3 version with Becke-Johnson damping (D3BJ)<sup>27, 28</sup> were included in all DFT calculations, following previous work<sup>29</sup>. During the structure optimizations, energies were converged to 10<sup>-7</sup> Ha and the maximum norm of the Cartesian gradient

to  $10^{-4}$  Ha/bohr. To proceed with the parametrization, most force-field parameters were taken from the GAFF force field<sup>25, 30</sup> if available, combined with bond lengths and equilibrium bond angles resulting from the DFT optimizations. Parameters assigned to describe the torsional profiles were assessed by simulating the cation or anion, respectively, in aqueous solution at infinite dilution and monitoring the structural stability, as the main goal of the catalyst force field is to keep the catalyst close to the crystal structure. For rotating trifluoromethyl groups rather small torsional barriers were assigned in accordance with the literature<sup>31</sup>. Lennard-Jones parameters for Mo are taken from Liu et al.<sup>32</sup> while parameters for B are taken from the DREIDING force field<sup>33</sup>, following previous work<sup>34</sup>. Partial atomic charges were calculated with the DDEC method<sup>35-37</sup> implemented in the DDEC6 program<sup>37</sup>.

### MD simulation details

The MD simulations were carried out with the GROMACS 2019.6 program package<sup>38</sup>. The silica frame was kept rigid during simulations. Lennard Jones parameters for Si, O and H atoms of the silica surface were taken from ref.<sup>39</sup> and partial atomic charges from ref.<sup>40</sup>. The GAFF force field was used for substrate, product and benzene molecules as well as for the non-Si atoms of the TMS groups<sup>25, 30</sup>. Each simulated pore system contained seven substrate molecules **4**, seven product molecules **8** and seven ethene molecules, corresponding to the situation of an initial substrate concentration of 25 mM and 50% conversion. The steepest descent method was used for energy minimization. Initial velocities were randomly assigned through a Maxwell-Boltzmann distribution. Equilibration was carried out for 50 ns, and the spatially dependent density and diffusion profiles were generated from a 1  $\mu$ s trajectory for the two larger pores and two 0.85  $\mu$ s trajectories for the smallest pore, one with the catalyst located in the center of the pore and one with two catalysts located close to the pore mouths. The equations of motion were integrated using the leap-frog scheme<sup>41</sup> with a time-step of 1 fs. A velocity-rescaling scheme<sup>42</sup> with a 2 ps-coupling constant was used to hold the temperature constant at 323.15 K. Prior to the production simulations, the number of benzene molecules in the simulation box was adjusted in a series of shorter preliminary simulation runs until the resulting density in the bulk phase reservoirs matched the density in a constant-pressure bulk-phase simulation of an equimolar 25 mM substrate/product mixture solution. The final number of benzene molecules in the simulation boxes was 5770 for the 2.5 nm pore, 5500 for the 5 nm pore and 5920 for

the 6 nm pore. The output frequency for the trajectory was set to 2 ps. Short-range electrostatic and Lennard-Jones interactions were evaluated up to a cut-off radius of 1.4 nm. Lennard-Jones parameters for unlike interactions were calculated using the Lorentz-Berthelot combining rules. Analytical dispersion corrections for the energy were included. Long-range electrostatic interactions were treated with the particle-mesh Ewald algorithm<sup>20, 43</sup>.

### **Input files**

We provide configuration files of the equilibrated pore systems, corresponding topologies and simulation parameter files via the Data Repository of the University of Stuttgart (DaRUS) under <https://doi.org/10.18419/darus-1752>. The material can be accessed via the private URL:

<https://darus.uni-stuttgart.de/privateurl.xhtml?token=a76a5840-99c4-48ad-8b5f-16092e64ce8f>

### **Trajectory analysis**

All analyses were carried out with the python package PoreAna version 0.2.0 (<http://doi.org/10.5281/zenodo.4738182>) which uses the chemfiles library (<http://doi.org/10.5281/zenodo.4540492>) as an adapter between the GROMACS output and the input to the analysis scripts.

### **Calculation of density profiles**

Density profiles shown in Figure S72 of the main text were calculated from the atom number density of the carbonyl oxygen and the vinylic carbon for the substrate and product molecules, respectively. The distance  $r$  was measured starting from the pore center ( $r = 0$ ) to the cylindrical silica surface from the  $x$  and  $y$  coordinates of the respective atom. For the calculation of distance-dependent profiles, the cylindrical pore was divided into 150 hollow cylinder bins in radial direction. Density profiles of substrate and product molecules were additionally calculated from the center of mass of a molecule for the calculation of the average pore diffusion coefficient (*vide infra*).

### Calculation of diffusion coefficient profiles

The local diffusion coefficient of substrate and product molecules in direction parallel to the silica surface (along the pore axis,  $z$ ) as a function of the radial distance  $r$  from the pore center was calculated from the slope of the mean squared displacement  $\Delta(r,t)$  over an observation interval of 4 – 20 ps, according to

$$\text{Equation S1: } D_{||}(r) = \frac{1}{2} \frac{d\Delta(r,t)}{dt}$$

$D_{||}(r)$  was determined with a bin size of 0.2 nm along  $r$ , allowing the molecules a shift of  $\pm 1$  bin around their initial bin determined by the radial coordinate.

### Calculation of the average pore diffusion coefficient

The average diffusion coefficient of substrate and product molecules in the cylindrical pores was calculated from the local diffusion coefficient and density profiles (of the center of mass of the respective species) by

$$\text{Equation S2: } \langle D_{||} \rangle = \frac{\sum_2^n \rho(r_i) D_{||}(r_i) A(r_i)}{\sum_2^n \rho(r_i) A(r_i)} \text{ with } A(r_i) = \pi(r_i^2 - r_{i-1}^2)$$

$A(r)$  describes the area of the circular bins along the radius  $r$  of the cylindrical pore, which is calculated by the areas determined for the largest and shortest radius,  $r_i$  and  $r_{i-1}$ , of each bin, respectively.

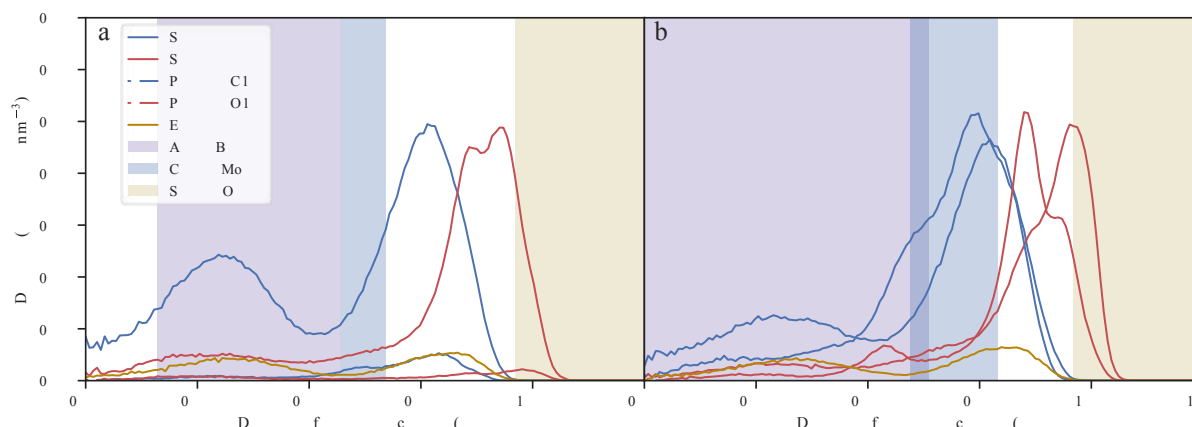


**Figure S72:** Radial number density profiles of the carbonyl oxygen (red) and vinylic carbon (blue) in the substrate (solid lines) and product (dashed lines) as well as of ethene (yellow) in the 2.5 nm pores obtained from a 0.85  $\mu$ s simulation in a model pore containing 1 catalyst in the center (a) or two catalysts close to the pore mouth (b). The shaded areas indicate the configurational space accessible by the boron atom (purple) of the anion, the molybdenum atom (blue) of the cation and the silanol oxygen (yellow).

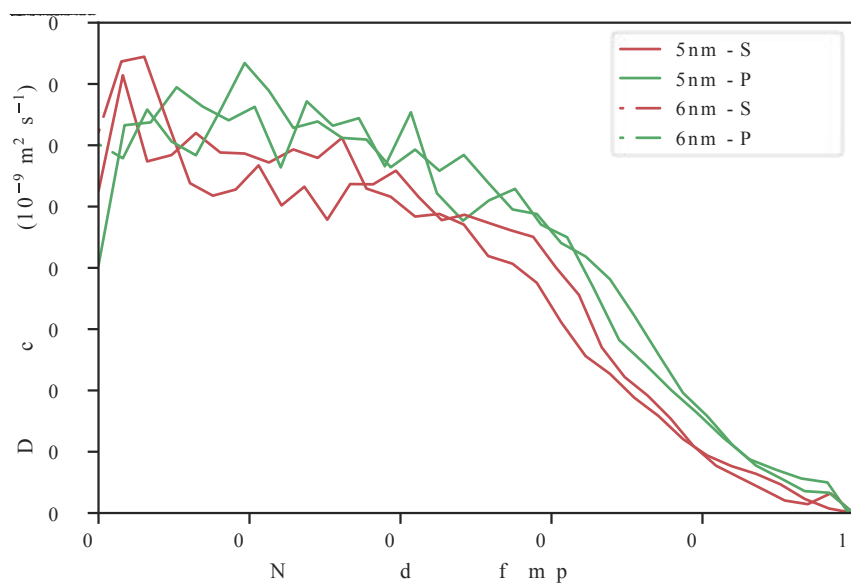


**Figure S73:** Radial dependence of the axial self-diffusion coefficient of substrate (red) and product molecules (green) in the 5 nm pore (solid lines) and the 6 nm pore (dashed lines). The radial distance  $r$  from the pore center (where  $r = 0$ ) is normalized by the effective pore radius, representing the region accessible to the substrate and product molecules. The mean diffusion coefficients are  $0.134 / 0.123$  and  $0.106 / 0.123 \times 10^{-9} \text{ m}^2/\text{s}$  for the substrate / product molecules in the 5 nm and 6 nm pore, respectively.

## 12. EXAFS

**Table S29:** EXAFS results for **Mo1**. N = number of scatterers (equivalent to the coordination number for single scattering in the 1<sup>st</sup> and 2<sup>nd</sup> shell),  $\sigma^2$  = Debye-Waller factor,  $R_{\text{eff}}$  = atomic distance from the model used (crystal structure), R +  $\Delta R$  - refined distances of scatterers.

Scattering Path	N	$\sigma^2$ [Å <sup>2</sup> ]	$R_{\text{eff}}$ [Å]	R + $\Delta R$ [Å]
Mo-N	0.8(1)	0.0033(3)	1.707	1.716(5)
Mo-C	0.9(1)	0.0011(3)	1.871	1.952(10)
Mo-O	0.9(1)	0.0013(6)	1.954	2.031(8)
Mo-C	1.1(1)	0.0013(4)	2.175	2.183(6)
Mo-C	0.8(1)	0.0018(5)	3.086	2.648(17)
Mo-N-C-N	1.4(1)	0.0067(9)	3.096	2.664(15)
Mo-N	3.4(3)	0.0058(5)	3.044	2.969(35)
Mo-O-C	3.6(2)	0.0022(8)	3.274	3.040(19)
Mo-C-C	2.2(4)	0.0030(9)	3.329	3.136(63)
Mo-N	3.9(7)	0.0064(6)	3.328	3.562(42)
Mo-C	2.2(4)	0.0022(6)	3.723	3.728(40)
Mo-F	1.7(2)	0.0020(12)	3.535	3.792(15)
Mo-F	1.5(4)	0.0021(13)	3.607	3.822(31)
Mo-O-N	15.1(7.3)	0.0029(7)	3.402	3.912(69)
Mo-C	2.2(7)	0.0025(7)	4.214	4.112(39)
Mo-O-C-O	5.7(2.2)	0.0044(17)	3.324	4.127(52)
Mo-C	1.2(3)	0.0025(7)	4.289	4.440(32)
Mo-C	2.0(7)	0.0028(8)	4.721	4.810(41)

**Table S30:** EXAFS results for **Mo1@SBA-15<sub>62A</sub>**.

Scattering Path	N	$\sigma^2$ [Å <sup>2</sup> ]	$R_{\text{eff}}$ [Å]	R + $\Delta R$ [Å]
Mo-N	1.0(1)	0.0014(3)	1.714	1.687(5)
Mo-C	1.1(2)	0.0039(10)	1.852	1.899(17)
Mo-O	0.9(1)	0.0018(10)	1.921	1.960(8)
Mo-C	1.1(3)	0.0046(12)	2.153	2.068(22)
Mo-C	2.5(5)	0.0068(18)	3.207	2.683(29)
Mo-C	3.4(5)	0.0066(17)	3.078	2.764(22)
Mo-N	3.0(3)	0.0026(6)	3.236	2.871(18)
Mo-N-C-N	4.7(4)	0.0086(22)	3.078	3.300(28)
Mo-Si	1.4(2)	0.0049(24)	3.223	3.227(35)
Mo-O	2.2(4)	0.0034(19)	3.535	3.600(28)
Mo-C	2.8(1.2)	0.0085(22)	4.006	3.771(49)
Mo-C-C	15.1(2.8)	0.0084(22)	4.221	4.303(19)
Mo-N-C	3.9(1.9)	0.0056(14)	4.030	4.328(47)
Mo-C	5.5(3.5)	0.0088(23)	4.145	4.528(58)

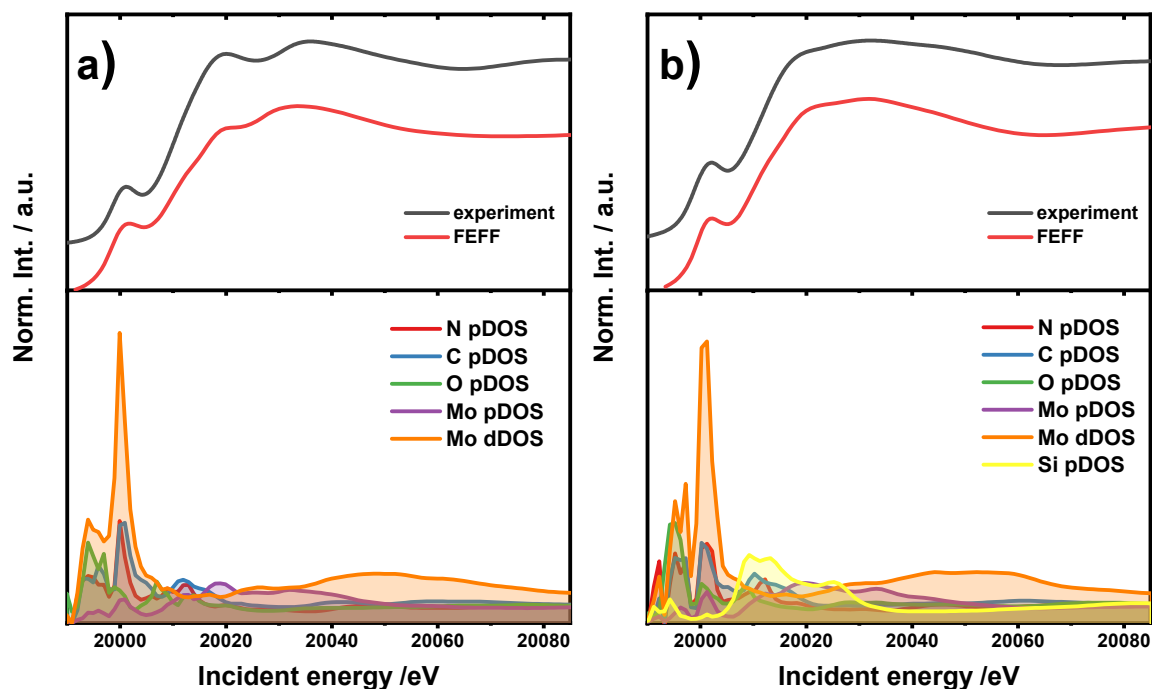


**Figure S74:** *Ab-initio* FEFF calculations for a) **Mo1** and for b) **Mo1@SBA-15<sub>62A</sub>**.

### EXAFS experimental details, fitting and *ab-initio* details

Mo-K edge EXAFS measurements were conducted on the P65 beamline, Petra III, Hamburg. Energy selection was conducted with a Si(111) double crystal monochromator; the energy resolution was around 1.4 eV at 20 keV. The beam spot size was 0.5 x 1 mm<sup>2</sup> and the total flux on the sample was 10<sup>12</sup> ph/s. Signal detection was conducted in the transmission mode using ionization chambers with partial pressures of 900 mbar Ar plus 100 mbar Kr and 340 mbar Ar plus 660 mbar Kr for I<sub>0</sub> and I<sub>1</sub> detection, respectively, all at room temperature. For beam focusing and higher harmonic rejections, Rh-coated mirrors were used. Data acquisition was performed in the continuous scanning mode and spectra were rebinned afterwards. Energy calibration was conducted at the first inflection point of the pure Mo XANES spectrum (20000 eV). To avoid radiation damage, each EXAFS spectrum was collected at a different sample position.

Initial normalization and data reduction were conducted with the Athena software; EXAFS fitting was performed with the Artemis package using the Multiple Scattering approach. The fitting procedures were done in an R-range of 1.0-4.0 Å and a k-range of 3.0 – 12.5 Å<sup>-1</sup>. *Ab-initio* calculations were conducted with the FEFF 9.6 software. Computations were done within the Full Multiple Scattering theory using muffin-tin

atomic potentials optimized in Self-Consistent Field (SCF) approach. The FMS and SCF radii were set to 7.0 Å. For both calculations, the Hedin-Lundquist exchange–correlation potential and final state rule core-hole screening were applied.<sup>44</sup> From the total DOS functions, occupied and unoccupied contributions were obtained by multiplication of each IDOS function by the arctangent step function broadened by the Mo 1s core-hole lifetime at the Fermi level given by FMS calculations. The experimental resolution of 1.4 eV was included in the calculations.

### 13. References

1. Fulmer, G. R.; Miller, A. J. M.; Sherden, N. H.; Gottlieb, H. E.; Nudelman, A.; Stoltz, B. M.; Bercaw, J. E.; Goldberg, K. I., NMR Chemical Shifts of Trace Impurities: Common Laboratory Solvents, Organics, and Gases in Deuterated Solvents Relevant to the Organometallic Chemist. *Organometallics* **2010**, *29* (9), 2176-2179.
2. Arduengo, A. J.; Dias, H. V. R.; Harlow, R. L.; Kline, M., Electronic stabilization of nucleophilic carbenes. *J. Am. Chem. Soc.* **1992**, *114* (14), 5530-5534.
3. Kinuta, H.; Tobisu, M.; Chatani, N., Rhodium-Catalyzed Borylation of Aryl 2-Pyridyl Ethers through Cleavage of the Carbon–Oxygen Bond: Borylative Removal of the Directing Group. *J. Am. Chem. Soc.* **2015**, *137* (4), 1593-1600.
4. Arduengo, A. J.; Davidson, F.; Dias, H. V. R.; Goerlich, J. R.; Khasnis, D.; Marshall, W. J.; Prakasha, T. K., An Air Stable Carbene and Mixed Carbene “Dimers”. *J. Am. Chem. Soc.* **1997**, *119* (52), 12742-12749.
5. Arduengo, A. J.; Goerlich, J. R.; Marshall, W. J., A stable diaminocarbene. *J. Am. Chem. Soc.* **1995**, *117* (44), 11027-11028.
6. Schowner, R.; Elser, I.; Benedikter, M.; Momin, M.; Frey, W.; Schneck, T.; Stöhr, L.; Buchmeiser, M. R., Origin and Use of Hydroxyl Group Tolerance in Cationic Molybdenum Imido Alkylidene N-Heterocyclic Carbene Catalysts. *Angew. Chem. Int. Ed.* **2020**, *59* (2), 951-958.
7. Benedikter, M.; Musso, J.; Kesharwani, M. K.; Sterz, K. L.; Elser, I.; Ziegler, F.; Fischer, F.; Plietker, B.; Frey, W.; Kästner, J.; Winkler, M.; van Slageren, J.; Nowakowski, M.; Bauer, M.; Buchmeiser, M. R., Charge Distribution in Cationic Molybdenum Imido Alkylidene N-Heterocyclic Carbene Complexes: A Combined X-ray, XAS, XES, DFT, Mössbauer, and Catalysis Approach. *ACS Catalysis* **2020**, *10* (24), 14810-14823.
8. Pucino, M.; Inoue, M.; Gordon, C. P.; Schowner, R.; Stöhr, L.; Sen, S.; Hegedüs, C.; Robé, E.; Tóth, F.; Buchmeiser, M. R.; Copéret, C., Promoting Terminal Olefin Metathesis with a Supported Cationic Molybdenum Imido Alkylidene N-Heterocyclic Carbene Catalyst. *Angew. Chem. Int. Ed.* **2018**, *57* (44), 14566-14569.
9. Marx, V. M.; Herbert, M. B.; Keitz, B. K.; Grubbs, R. H., Stereoselective Access to Z and E Macrocycles by Ruthenium-Catalyzed Z-Selective Ring-Closing Metathesis and Ethenolysis. *J. Am. Chem. Soc.* **2013**, *135* (1), 94-97.
10. Ziegler, F.; Teske, J.; Elser, I.; Dyballa, M.; Frey, W.; Kraus, H.; Hansen, N.; Rybka, J.; Tallarek, U.; Buchmeiser, M. R., Olefin Metathesis in Confined Geometries: A Biomimetic Approach toward Selective Macrocyclization. *J. Am. Chem. Soc.* **2019**, *141* (48), 19014-19022.
11. Song, S.-F.; Guo, Y.-T.; Wang, R.-Y.; Fu, Z.-S.; Xu, J.-T.; Fan, Z.-Q., Synthesis and Crystallization Behavior of Equisquential ADMET Polyethylene Containing Arylene Ether Defects: Remarkable Effects of Substitution Position and Arylene Size. *Macromolecules* **2016**, *49* (16), 6001-6011.
12. Jee, J.-E.; Cheong, J. L.; Lim, J.; Chen, C.; Hong, S. H.; Lee, S. S., Highly Selective Macrocycle Formations by Metathesis Catalysts Fixated in Nanopores. *J. Organomet. Chem.* **2013**, *78* (7), 3048-3056.

13. Bruckner, J. R.; Bauhof, J.; Gebhardt, J.; Beurer, A.-K.; Traa, Y.; Giesselmann, F., Mechanisms and Intermediates in the True Liquid Crystal Templating Synthesis of Mesoporous Silica Materials. *J. Phys. Chem. B* **2021**, *125* (12), 3197-3207.
14. Coasne, B.; Di Renzo, F.; Galarnau, A.; Pellenq, R. J. M., Adsorption of Simple Fluid on Silica Surface and Nanopore: Effect of Surface Chemistry and Pore Shape. *Langmuir* **2008**, *24* (14), 7285-7293.
15. Melnikov, S. M.; Hölzel, A.; Seidel-Morgenstern, A.; Tallarek, U., A Molecular Dynamics Study on the Partitioning Mechanism in Hydrophilic Interaction Chromatography. *Angew. Chem. Int. Ed.* **2012**, *51* (25), 6251-6254.
16. Kraus, H.; Rybka, J.; Hölzel, A.; Trebel, N.; Tallarek, U.; Hansen, N., PoreMS: a software tool for generating silica pore models with user-defined surface functionalisation and pore dimensions. *Molec. Simul.* **2021**, 1-11.
17. Ahlrichs, R.; Bär, M.; Häser, M.; Horn, H.; Kölmel, C., Electronic structure calculations on workstation computers: The program system turbomole. *Chem. Phys. Lett.* **1989**, *162* (3), 165-169.
18. Balasubramani, S. G.; Chen, G. P.; Coriani, S.; Diedenhofen, M.; Frank, M. S.; Franzke, Y. J.; Furche, F.; Grotjahn, R.; Harding, M. E.; Hättig, C.; Hellweg, A.; Helmich-Paris, B.; Holzer, C.; Huniar, U.; Kaupp, M.; Marefat Khah, A.; Karbalaei Khani, S.; Müller, T.; Mack, F.; Nguyen, B. D.; Parker, S. M.; Perlt, E.; Rappoport, D.; Reiter, K.; Roy, S.; Rückert, M.; Schmitz, G.; Sierka, M.; Tapavicza, E.; Tew, D. P.; van Wüllen, C.; Voora, V. K.; Weigend, F.; Wodyński, A.; Yu, J. M., TURBOMOLE: Modular program suite for *ab initio* quantum-chemical and condensed-matter simulations. *J. Chem. Phys.* **2020**, *152* (18), 184107.
19. Eichkorn, K.; Treutler, O.; Öhm, H.; Häser, M.; Ahlrichs, R., Auxiliary basis sets to approximate Coulomb potentials (Chem. Phys. Letters 240 (1995) 283-290). *Chem. Phys. Lett.* **1995**, *242* (6), 652-660.
20. Essmann, U.; Perera, L.; Berkowitz, M. L.; Darden, T.; Lee, H.; Pedersen, L. G., A smooth particle mesh Ewald method. *J. Chem. Phys.* **1995**, *103* (19), 8577-8593.
21. Eichkorn, K.; Weigend, F.; Treutler, O.; Ahlrichs, R., Auxiliary basis sets for main row atoms and transition metals and their use to approximate Coulomb potentials. *Theoretical Chemistry Accounts: Theory, Computation, and Modeling (Theor. Chim. Acta)* **1997**, *97* (1-4), 119-124.
22. Perdew, J. P.; Burke, K.; Ernzerhof, M., Generalized Gradient Approximation Made Simple. *Phys. Rev. Lett.* **1996**, *77* (18), 3865-3868.
23. Perdew, J. P.; Ernzerhof, M.; Burke, K., Rationale for mixing exact exchange with density functional approximations. *J. Chem. Phys.* **1996**, *105* (22), 9982-9985.
24. Weigend, F.; Ahlrichs, R., Balanced basis sets of split valence, triple zeta valence and quadruple zeta valence quality for H to Rn: Design and assessment of accuracy. *Phys. Chem. Chem. Phys.* **2005**, *7* (18), 3297.
25. Wang, J.; Wang, W.; Kollman, P. A.; Case, D. A., Automatic atom type and bond type perception in molecular mechanical calculations. *J. Molec. Graphics Modell.* **2006**, *25* (2), 247-260.
26. Andrae, D.; Häußermann, U.; Dolg, M.; Stoll, H.; Preuß, H., Energy-adjusted *ab initio* pseudopotentials for the second and third row transition elements. *Theoret. Chim. Acta* **1990**, *77* (2), 123-141.
27. Grimme, S.; Antony, J.; Ehrlich, S.; Krieg, H., A consistent and accurate *ab initio* parametrization of density functional dispersion correction (DFT-D) for the 94 elements H-Pu. *J. Chem. Phys.* **2010**, *132* (15), 154104.
28. Grimme, S.; Ehrlich, S.; Goerigk, L., Effect of the damping function in dispersion corrected density functional theory. *J. Comput. Chem.* **2011**, *32* (7), 1456-1465.
29. Kesharwani, M. K.; Elser, I.; Musso, J. V.; Buchmeiser, M. R.; Kästner, J., Reaction Mechanism of Ring-Closing Metathesis with a Cationic Molybdenum Imido Alkyldiene *<i>N</i>* - Heterocyclic Carbene Catalyst. *Organometallics* **2020**, *39* (17), 3146-3159.
30. Wang, J.; Wolf, R. M.; Caldwell, J. W.; Kollman, P. A.; Case, D. A., Development and testing of a general amber force field. *J. Comput. Chem.* **2004**, *25* (9), 1157-1174.

31. Polêto, M. D.; Rusu, V. H.; Grisci, B. I.; Dorn, M.; Lins, R. D.; Verli, H., Aromatic Rings Commonly Used in Medicinal Chemistry: Force Fields Comparison and Interactions With Water Toward the Design of New Chemical Entities. *Front. Pharmacol.* **2018**, *9*, 395.
32. Liu, J.; Zeng, J.; Zhu, C.; Miao, J.; Huang, Y.; Heinz, H., Interpretable molecular models for molybdenum disulfide and insight into selective peptide recognition. *Chem. Sci.* **2020**, *11* (33), 8708-8722.
33. Mayo, S. L.; Olafson, B. D.; Goddard, W. A., DREIDING: a generic force field for molecular simulations. *J. Phys. Chem.* **1990**, *94* (26), 8897-8909.
34. de Andrade, J.; Böes, E. S.; Stassen, H., Computational Study of Room Temperature Molten Salts Composed by 1-Alkyl-3-methylimidazolium Cations Force-Field Proposal and Validation. *The J. Phys. Chem. B* **2002**, *106* (51), 13344-13351.
35. Manz, T. A.; Sholl, D. S., Chemically Meaningful Atomic Charges That Reproduce the Electrostatic Potential in Periodic and Nonperiodic Materials. *J. Chem. Theory Comput.* **2010**, *6* (8), 2455-2468.
36. Manz, T. A.; Sholl, D. S., Improved Atoms-in-Molecule Charge Partitioning Functional for Simultaneously Reproducing the Electrostatic Potential and Chemical States in Periodic and Nonperiodic Materials. *J. Chem. Theory Comput.* **2012**, *8* (8), 2844-2867.
37. Manz, T. A.; Limas, N. G., Introducing DDEC6 atomic population analysis: part 1. Charge partitioning theory and methodology. *RSC Adv.* **2016**, *6* (53), 47771-47801.
38. Abraham, M. J.; Murtola, T.; Schulz, R.; Páll, S.; Smith, J. C.; Hess, B.; Lindahl, E., GROMACS: High performance molecular simulations through multi-level parallelism from laptops to supercomputers. *SoftwareX* **2015**, *1-2*, 19-25.
39. Coasne, B.; Fourkas, J. T., Structure and Dynamics of Benzene Confined in Silica Nanopores. *J. Phys. Chem. C* **2011**, *115* (31), 15471-15479.
40. Gulmen, T. S.; Thompson, W. H., Testing a Two-State Model of Nanoconfined Liquids: Conformational Equilibrium of Ethylene Glycol in Amorphous Silica Pores. *Langmuir* **2006**, *22* (26), 10919-10923.
41. Hockney, R. W., The potential calculation and some applications. *Methods Comput. Phys.* **1970**, *9*, 136.
42. Bussi, G.; Donadio, D.; Parrinello, M., Canonical sampling through velocity rescaling. *J. Chem. Phys.* **2007**, *126* (1), 014101.
43. Darden, T.; York, D.; Pedersen, L., Particle mesh Ewald: An  $N$ -log( $N$ ) method for Ewald sums in large systems. *J. Chem. Phys.* **1993**, *98* (12), 10089-10092.
44. Van Bokhoven, J. A.; Lamberti, C., *X-Ray Absorption and X-Ray Emission Spectroscopy : Theory and Applications*. Wiley-VCH: Weinheim, 2016.